Thermal Behaviour of Compressed Earth Blocks with Municipal Organic Waste Incorporation

Guilherme Lopes Gontijo

Dissertation presented to the School of Technology and Management of Bragança to obtain the Master Degree in Construction Engineering.

Work oriented by:

Débora Rodrigues de Sousa Macanjo Ferreira

Luís Manuel Ribeiro Mesquita

Conrado Rodrigues de Souza

June of 2020

Thermal Behaviour of Compressed Earth Blocks with Municipal Organic Waste Incorporation

Guilherme Lopes Gontijo

Dissertation presented to the School of Technology and Management of Bragança to obtain the Master Degree in Construction Engineering.

Work oriented by:

Débora Rodrigues de Sousa Macanjo Ferreira

Luís Manuel Ribeiro Mesquita

Conrado Rodrigues de Souza

June of 2020

ACKNOWLEDGMENT

Agradeço, do fundo do meu coração, à minha mãe Rita, ao meu pai Fábio e meu irmão Daniel. Por cada ensinamento, paciência, zelo, carinho, confiança e amor imensurável, hoje e sempre.

Agradeço aos meus demais familiares: tios, tias, primos, primas, avôs e avós, muito obrigado por cada ensinamento.

Agradeço aos professores Débora Ferreira, Luís Mesquita, Conrado Rodrigues e também à Eduarda Luso, pelas orientações que muitas vezes foram além do âmbito professional e muito contribuíram/contribuem para meu crescimento como ser humano.

Agradeço a cada um dos professores com os quais tive contato pela inspiração e conhecimento, e por me apresentarem à profissão mais nobre de uma sociedade. Em especial, agradeço profundamente ao professor Allbens, por enxergar em mim um potencial que nem eu mesmo conhecia.

Agradeço a cada uma das minhas amizades, do São Bentinho, do Santa Maria, do CEFET, de Bragança e da vida em geral, por tornarem a vida mais leve e alegre, tanto nos momentos difíceis quanto nos de lazer.

Agradeço ao CEFET, por investir em minha educação e confiar sempre em meu potencial. Especialmente aos profissionais da Secretaria de Relações Internacionais e do Departamento de Engenharia Civil.

Agradeço ao IPB, por consolidar esta etapa de formação da forma mais produtiva e prazerosa possível. Em especial, à Lurdes Cruz, à fenómenal Luísa Barreira, e a todos que me auxiliaram durante o último ano.

Je remercie également la famille Rabusseau et les professeurs Gaël Combe et Vincent Richefeu pour l'accueil et l'amitié en France.

ABSTRACT

Construction sector is one of the largest consumers of natural resources among human activities. Over the last years, with the increasingly interest for sustainable practices, the use of earth as a raw construction material re-emerged as a feasible way to reduce environmental impacts. In this scenario, compressed earth blocks (CEBs) arose as a construction technique with large sustainable potential, once they do not require cooking processes on their manufacture and due to the possibility of incorporation of fibres and wastes. This work aims to evaluate the incorporation of the organic fraction of municipal waste on CEBs, through its thermal properties and behaviour when subjected to fire situations. For such, a preliminary characterization of the CEBs to determine their porosity and bulk density was held. Subsequently, an evaluation of chemical aspects of the CEBs and its components was performed through thermogravimetric analyses. Thermal properties of the blocks were also calculated using transient methods. Finally, a CEBs panel was tested experimentally to evaluate criteria of integrity and insulation, and numerical simulations were held to provide a better understanding towards this phenomenon. The obtained results indicate that the incorporation of organic waste does not affect the capability of CEBs walls to accomplish fire safety criteria. Furthermore, the incorporated CEBs thermal properties still accomplish the minimums required by the standards and may also allow to reduce the heat transfer through building envelopes, which emphasize the sustainable feature of the blocks.

Key-Words: Compressed earth blocks, sustainable construction, organic wastes, fire resistance.

RESUMO

A construção civil é um dos setores de maior consumo de recursos naturais entre as atividades humanas. Nos últimos anos, com o crescente interesse por práticas sustentáveis, o uso de terra como matéria-prima construtiva ressurgiu como uma maneira viável de reduzir impactos ambientais. Nesse cenário, os blocos de terra compactados (BTCs) surgiram como uma técnica de construção com grande potencial sustentável, uma vez que não requerem processos de cozimento em sua fabricação e devido à possibilidade de incorporação de fibras e resíduos. O presente trabalho tem como objetivo avaliar a incorporação da fração orgânica de resíduos urbanos em BTCs, por meio de suas propriedades térmicas e comportamento quando submetido a situações de incêndio. Para tal, foi realizada uma caracterização preliminar dos BTCs para determinar sua porosidade e densidade aparente. Posteriormente, foi realizada uma avaliação dos aspectos químicos dos BTCs e seus componentes por meio de análises termogravimétricas. As propriedades térmicas dos blocos também foram calculadas usando métodos transientes. Finalmente, um painel feito em BTCs foi testado experimentalmente para avaliar os critérios de integridade e isolamento quando submetido a incêncios, e simulações numéricas foram realizadas para fornecer uma melhor compreensão desse fenômeno. Os resultados obtidos indicam que a incorporação de resíduos orgânicos não afetam a capacidade das paredes de BTCs em cumprir os critérios de segurança contra incêndio. Além disso, as propriedades térmicas dos BTCs com resíduo incorporado cumprem ainda os mínimos exigidos pelas normas e também podem permitir reduzir a transferência de calor através das envoltórias da construção, o que enfatiza a característica sustentável dos blocos.

Palavras-Chave: Blocos de terra compactados, construção sustentável, resíduos orgânicos, resistência ao fogo

Contents

CHAPTER 1 1
INTRODUCTION 1
1.1 General Concepts 1
1.2 Main Goals 2
1.3 Document Structure 2
CHAPTER 2 4
STATE OF KNOWLEDGE 4
2.1 Earth as a Construction Material 4
2.2 Earth Construction in Brazil 8
2.3 Compressed Earth Blocks (CEBs) 11
2.4 Incorporations on CEBs 14
2.4.1 Fibres on CEBS 15
2.4.2 Construction and Industrial Wastes on CEBs 17
2.4.3 Municipal Wastes on CEBs 20
2.4.3.1 Water Absorption 21
2.4.3.2 Durability 21
2.4.3.3 Compressive Strength at Ambient Temperature 22
2.4.3.4 Compressive Strength at High Temperatures 25
2.5 Thermal Properties of CEBs 26
2.5.1 Thermal Conductivity and Specific Heat 26
2.5.2 Thermogravimetric Analysis 30
2.5.2.1 Artificial Soil 30
2.5.2.2 Cement 31
CHAPTER 3 33
MANUFACTURE AND PROPERTIES OF THE CEBs 33
3.1 Materials used on the Manufacture of the CEBs 33
3.1.1 Soil 33
3.1.1.1 Sand 33
3.1.1.2 Kaolin 33
3.1.1.3 Soil Characterization 34
3.1.2 Cement 36
3.1.3 Municipal Waste 36
3.1.4 Water 38

3.2 Manufacture of the CEBs 38
3.3 Manufacture of Prism Specimens 42
3.4 Porosity and Bulk Density of the CEBs 43
3.4.1 Le Chatelier Flask 43
3.4.2 Picnometer Tests 46
3.5 Thermal Properties of the CEBs 47
3.5.1 Thermogravimetry 47
3.5.2 Transient Plane Source (TPS) Analyses 51
3.5.3 Guarded Hot Plate (GHP) Tests 53
CHAPTER 4 55
PANEL FIRE RESISTANCE TEST - PRESCRIPTIONS 55
4.1 Manufacture of the CEBs panel 55
4.2 Mortar 56
4.3 Instrumentation of the Panel 57
4.4 Data Acquisition System 61
4.5 Temperature of the Furnace 62
4.6 Test Prescriptions 63
4.7 Compressive Resistance of the Blocks 64
CHAPTER 5 65
EXPERIMENTAL RESULTS 65
5.1 Le Chatelier Flask 65
5.2 Picnometer Tests 66
5.3 Thermogravimetric Results 67
5.3.1 Artificial Soil 67
5.3.2 Cement 68
5.3.3 Municipal Waste 69
5.3.4 Compressed Earth Blocks 70
5.4 Transient Plane Source (TPS) Results 72
5.5 Guarded Hot Plate (GHP) Results 73
5.6 CEBs Panel - Thermocouples Analyses 74
5.7 Infrared Thermography (IR) 78
5.8 Compressive Resistance of the Blocks 79
CHAPTER 6 80
NUMERICAL ANALYSIS 80
6.1 3D Analysis of the CEBs Panel 80
6.2 2D Analysis of the CEBs 86

6.3 CFD Analysis of the CEBs 91
CHAPTER 7 97
CONCLUSIONS AND FUTURE WORKS 97
BIBLIOGAPHY 99
ANNEX A – COMPACTION OF THE BLOCKS 108
ANNEX B – TPS Results 110
ANNEX C – GHP Results 113

List of Tables

Table 1: Mass proportions of CEBs at Nepomuceno's work [37]. 20

Table 2: Water Absorption Values (adapted from [37]). 21

Table 3: Volume Variation and Mass Loss for CEBs after six cycles of accelerated aging [37].22

Table 4: Physical Properties of kaolin (adapted from [50]). 34

Table 5: Chemical properties of kaolin (adapted from [50]). 34

Table 6: Consistency Limits of the artificial soil (adapted from [37]). 35

Table 7: Cement characteristics [56]. 36

Table 8: Municipal waste composition (supplied by the company Resíduos do Nordeste). 37

Table 9: Quantity of each material per block. 39

Table 10: Quantity of each material per prism specimen. 42

Table 11: Bulk density of the prism specimens. 65

Table 12: Results of the Le Chatelier Flask tests. 65

Table 13: Average values obtained on Le Chatelier flask tests. 66

Table 14: Density of distilled water 66

Table 15: Density of the powders determined through picnometer tests. 67

Table 16: TPS analyses results. 72

Table 17: Compressive resistance of the blocks. 79

Table 18: Compaction pressure of the CEBs. 109

Table 19: Complete TPS results for specimens without incorporated waste. 111

Table 20: Complete TPS results for specimens with incorporated waste. 112

Table 21: Complete GHP results for specimens without incorporated waste. 113

Table 22: Complete GHP results for specimens with incorporated waste. 114

List of Figures

Figure 1: Parts of the Great Wall of China made on rammed earth [5], [6]..... 4

Figure 2: Manufacture of a rammed earth wall in Mumeno, Mozambique [4]..... 5

Figure 3: A residential building made in rammed earth, built in 1828, in Weilburg, Germany [2]..... 6

Figure 4: Manufacture process of adobe blocks. a) Demoulding [9]; b) Set to dry [9]. 7

Figure 5: Aspect of an Adobe Wall. a) During laying of the blocks [10]; b) Final aspect [10]..... 7

Figure 6: Components of a Tabique wall: a) Timber frame [12]. b) Timber frame covered by earth render [12]..... 8

Figure 7: Old Town Hall and Prison of the city of Ouro Preto (Minas Gerais), built in rammed earth and stones [16]. 9

Figure 8: Example of house in wattle and daub in Ivaporunduva (São Paulo), Brazil [18]..... 10

Figure 9: Example of a CEB CINVA-Ram press machine [23]. 11

Figure 10: Different types of CEBs: a) Solid block [25] b) Interlocking block [26]. 12

Figure 11: Embodied energy in different masonry materials manufacture (adapted from [28])..... 13

Figure 12: Krafterra fibres to be incorporated in the CEBs [32]..... 15

Figure 13: Cut Date-Palm fibres to be incorporated on the CEBs [35]..... 16

Figure 14: Banana fibres under chemically treatment to be incorporated on CEBs [36]..... 17

Figure 15: Plastic fibres to be incorporated on CEBs: a) from carry bags [40]; b) from plastic bottles [40]..... 19

Figure 16: Specimens submitted to cycles of accelerated aging: a) before; b) after [46]. 22

Figure 17: Mean compressive strength for the reference specimen and minimum values stablished by the standards [46]. 23

Figure 18: Compressive strength of saturated specimens compared to reference values [46]..... 24

Figure 19: Compressive strength of aged specimens compared to reference values [46]..... 25

Figure 20: Compressive strength of the three compositions at higher temperatures [46]..... 26

Figure 21: Influence of bulk density on: a) compressive strength and thermal conductivity; b) specific heat; of CEBs at 20ºC [38]..... 27

Figure 22: Influence of porosity on thermal conductivity of CEBs at 20ºC [51]..... 28

Figure 23: Influence of cement content on the thermal conductivity of CEBs at 20ºC for different bulk densities [52]. 29

Figure 24: Influence of stabilizer content on thermal conductivity of CEBs at 20ºC [53]. 30

Figure 25: Thermogravimetry (TG) results for kaolin-quartz mixtures [56]. 31

Figure 26: Thermogravimetry (TG) and differential thermogravimetry (DTG) for cement pastes with different ages on calcinated mass basis [57]. 32

Figure 27: Artificial soil grain curve [46]. 35

Figure 28: Proctor compaction of the artificial soil [46]. 36

Figure 29: Municipal waste to be incorporated into the CEBs. 38

Figure 30: Geometry of the blocks. 39

Figure 31: Materials prepared to be mixed in a mortar mixer. 40

Figure 32: a) Material being inserted in the mould. b) Mechanical press being used to demould a block. 41

Figure 33: Blocks during the cure process in humid chamber. 42

Figure 34: Manufacture of the prism specimen: a) compaction; b) demoulding. 43

Figure 35: Le Chatelier flask for density and porosity test [67] 44

Figure 36: Le Chatelier flask test. 46

Figure 37: Picnometer test 47

Figure 48: Aspect of the waste after milling. 48

Figure 49: Basic analytic mill used for milling the waste and CEBs samples. 49

Figure 50: TG/DTG instrument Netzsch TG 209 F3 Tarsus 50

Figure 51: Samples on vacuum chamber before thermogravimetry tests. 50

Figure 56: Kapton-insulated sensor used on TPS analyses [81]. 52

Figure 57: Specimens during TPS analysis. 52

Figure 58: Schematic of a Guarded Hot Plate apparatus [83]. 53

Figure 59: Lambda-Messtechnik® λ-Meter EP500e Guarded Hot Plate apparatus 54

Figure 38: CEBs panel during its execution 56

Figure 39: Mortar test specimens moulded during panel manufacture. 57

Figure 40: Position of the thermocouples on the panel. 58

Figure 41: a) TH thermocouple placed inside the hole of the block; b) TM thermocouple positioned to monitor mortar temperatures. 59

Figure 42: a) TD thermocouple overlaid with plasterboard; b) TB thermocouple inserted in a drilling hole and filled with mortar 60

Figure 43: View of the instrumentalized panel from its unexposed surface. 61

Figure 44: Data Acquisition System used to monitor temperatures during fire test. 62

Figure 45: ISO 834-1 curve [71]. 62

Figure 46: Thermocouple installed to monitor the ambient temperature at the laboratory during fire test. 63

Figure 47: Infrared Camera monitoring the temperature of the unexposed surface of the panel. 64

Figure 52: Thermogravimetric analysis of the artificial soil. 68

Figure 53: Thermogravimetric analysis of the cement. 69

Figure 54: Thermogravimetric analysis of the municipal organic waste. 70

Figure 55: Thermogravimetric analyses of the CEBs with and without incorporated waste. 71

Figure 60: Average GHP results: a) specimens without waste; b) specimens with waste. 74

Figure 61: Time-temperature evolution on the unexposed surface of the panel (TDs). 75

Figure 62: Time-temperature evolution inside the blocks (TBs). 76

Figure 63: Time-temperature evolution inside the block holes (THs). 77

Figure 64: Time-temperature evolution in the mortar (TM). 77

Figure 65: Infrared thermograph diagrams of CEBs wall panel. 79

Figure 66: 3D CEBs panel model on Ansys 80

Figure 67: Boundary conditions applied on the 3D panel simulation. 82

Figure 68: Thermal properties of the CEBs and mortar used on 3D simulations: a) specific heat; b) thermal conductivity; c) specific mass [1]. 84

Figure 69: Gradients of temperature obtained on 3D simulation [1]. 85

Figure 70: Comparison between the results obtained on the experimental and 3D numerical models of the panel [1] 86

Figure 71: 3D sketch of the block designed for the 2D simulations. 87

Figure 72: Boundary conditions used on the 2D transient thermal simulation. 88

Figure 73: Thermal properties of the air used on 2D simulations: a) specific heat; b) thermal conductivity; c) specific mass [90]..... 89

Figure 74: Comparison between the results obtained on the experimental and 3D numerical models of the panel. 90

Figure 75: Temperature gradient on the adjacencies of the block holes on the 2D simulation..... 91

Figure 76: CEB model and mesh sketched for CFD simulation. 92

Figure 77: Gradient of temperature (a) and current of convection (b) inside the CEB holes at 1800s. 93

Figure 78: Gradient of temperature (a) and current of convection (b) inside the CEB holes at 3600s. 94

Figure 79: Gradient of temperature (a) and current of convection (b) inside the CEB holes at 5400s. 95

Figure 80: Gradient of temperature at the end of the CFD simulation..... 96

Acronyms

AASHTO	American Association of State Highway and Transportation Officials
ABNT	Brazilian Association of Technical Standards
ANN	Artificial Neural Network
ASTM	American Society for Testing and Materials
BC	Before Christ
CDW	Construction and Demolition Wastes
CEBs	Compressed Earth Blocks
DIN	German Standard
DTG	Differential Thermogravimetric Analysis
EN	European Standard
GB/T	Chinese Standard
GHP	Guarded Hot Plate
IPA	Isopropyl Alcohol
IPB	Polytechnic Institute of Bragança
ISO	International Standard
LNEC	National Laboratory for Civil Engineering
NP	Portuguese Standard
SC	Clayey Sand
SEM	Scanning Electron Microscopy
TG	Thermogravimetric Analysis
TPS	Transient Plane Source
UNE	Spanish Standard

CHAPTER 1

INTRODUCTION

1.1 General Concepts

Over the last century construction methods using earth as a raw material have been falling into disuse, especially in developed countries. Wrongly associated with an image of poverty and underdevelopment, and in consequence of technological advances, traditional building techniques were gradually replaced by the use of concrete, steel, plaster, among other materials.

In contrast to this modernization, the search for sustainable building solutions has been intensified and gained prominence in both the industrial and governmental policies. In this scenario, construction solutions that use soils have proved to be of great value, due, for example, to their low associated CO_2 emission and their ability to return to nature after their life-cycle. These include compressed earth blocks, also known as CEBs or soil-cement blocks. CEBs arise as a result of the refinement of modern block making techniques, and are moulded using moisture-compacted soil at specific pressures and often added cement in order to enhance their mechanical properties.

Earth is an abundant, recyclable, reusable, non-combustible, non-toxic raw material with significant thermal properties, which makes it highly versatile for sustainable building solutions. However, features as high variability and heterogeneity, in addition to the scarcity of quality controls in manufactured applications, make its properties to be considered as non-standardized, which causes difficulties to spread techniques and standards on international scales [1].

In order to further expand the sustainable character of CEBs, additions of wastes have been incorporated into their composition. Therefore, it is of essential to understand how it behaves in order to maximize the use of its thermal and mechanical properties.

1.2 Main Goals

The present work aims to contribute at the understanding of the thermal behaviour of compressed earth blocks (CEBs) with waste incorporation. For such, the main goals are:

• Evaluate the influences of waste incorporation on the thermal properties of compressed earth blocks;

• Develop a CEBs panel to perform fire resistance tests according to the Eurocode prescriptions;

• Develop a numerical model for simulation through Finite-Elements-Method (FEM) of the CEBs panel under fire situations;

• Compare the results obtained in the experimental and the simulation tests regarding the CEBs behaviour when submitted to fire situations.

1.3 Document Structure

The present work is divided in 7 chapters. Chapter 1 presents the subject and contextualizes the approaches used throughout the research, as well as the sought objectives.

Chapter 2 presents a review of the produced works and the scientifically disseminated knowledge in recent years regarding compressed earth blocks. It also elucidates the results obtained in other works that sought to analyse incorporations on CEBs. Besides, this chapter provides a brief background about thermal properties of the CEBs.

Chapter 3 shows the components used for the manufacture of the CEBs and their properties. Besides, it elucidates the process of manufacture of the CEBs and of the specimens used on experimental tests. This chapter also explains the experimental tests performed to characterize the blocks.

Chapter 4 describes how the CEBs panel was manufactured, and technical information about the experimental fire test performed on the panel.

Chapter 5 presents the obtained results on the experimental tests described on Chapters 3 and 4.

Chapter 6 contains the procedures adopted for numerical simulation of the studied phenomenon. In addition to the descriptions, it also presents the parameters used to simulate the heat transfer forms and boundary conditions applied to bodies in Finite Element Method (FEM) analysis and the obtained results.

Chapter 7 contains the conclusions obtained from the work and recommendations for future works on the field.

CHAPTER 2

STATE OF KNOWLEDGE

2.1 Earth as a Construction Material

There is no consensus about when humanity began to use earth as a building material. According to Minke (2006), the earliest known uses of earth as a building material date back more than 9,000 years ago. Buildings made of adobe blocks dating from 6,000 to 8,000 BC still exist in current territory of Turkmenistan [2]. According to Berge (2009), the oldest examples of earth-based blocks date from around 7,500 BC and can be found on the banks of the Tigris River [3].

Even though it is not known exactly when earth was first used as a building material, it is assumed that earth constructions began with the first agricultural societies, dating from 12,000 to 7,000 years BC [4]. There are several cases of earthen constructions executed thousands of years ago that still exist, i.e. the Great Wall of China (Figure 1), built about 4,000 years ago originally on rammed earth (and later covered with bricks and stones, resulting on its current appearance) and the core of the Pyramid of the Sun, in Teotihuacan - Mexico, made up of approximately 2 million tons of rammed earth. Nowadays, a considerable fraction of the world's population live in earthen constructions [2].

Figure 1: Parts of the Great Wall of China made on rammed earth [5], [6].

Different techniques using earth as a raw material were developed around the globe, depending on geomorphological characteristics of each locality and features required by users. Below, some of the main building techniques using it are presented:

- **Rammed Earth**: consists of a monolithic construction system that uses compacted moistened soil inside structures (usually made of timber). It is mostly common in regions where there is no abundant water, and it is widespread on a global scale. Rammed earth constructions can be found in several UNESCO World Heritage buildings, throughout the seven continents. As a consequence of its widespread diffusion, there are several techniques and methods of performing rammed earth constructions, using for example manual or mechanized compaction processes and different laying techniques [7], [8]. Figure 2 presents the manufacture of a rammed earth wall. Figure 3 shows a building made in rammed earth, built in 1828, in Weilburg, Germany.

Figure 2: Manufacture of a rammed earth wall in Mumeno, Mozambique [4].

Figure 3: A residential building made in rammed earth, built in 1828, in Weilburg, Germany [2].

- **Adobe**: Consists of a constructive technique of simple manufacture and execution, which makes it quite common in old buildings, many still inhabited today. In their manufacture, normally timber moulds are used to shape the blocks, which are demoulded while still fresh and then set for drying at room temperature. The blocks can be made in different sizes and shapes, depending on the characteristics of the used soil and the technique that will be used to lay the blocks [4]. Adobe blocks require soils with high plasticity and percentage of clay, which justifies the common use of this technique in places where there is plenty of water. Due to the shrinkage in the soil due to its high clay contents, it is common for adobe blocks to crack during the drying period. To avoid this phenomenon, it is usual to reinforce the blocks with straw or other vegetable fibres. The laying of the adobe blocks is similar to conventional ceramic ones. In order to obtain a better connection between materials, it is common to use earth-based mortar, which avoids the appearance of cracks or detachment of the material [7]. Figure 4 and Figure 5 show the manufacture process of adobe blocks and the aspect of an adobe wall, respectively.

a) b)

Figure 4: Manufacture process of adobe blocks. a) Demoulding [9]; b) Set to dry [9].

a) b)

Figure 5: Aspect of an Adobe Wall. a) During laying of the blocks [10]; b) Final aspect [10].

- **Tabique:** consists of a technique in which bamboo or timber are used to build a structure that is covered with earth render by both sides simultaneously [11]. Together with rammed earth and adobe blocks, it is one of the most used earth building techniques in Portugal. The earth render on tabique walls may assume a structural role, but its main function is to help in the protection and preservation of the timber structure. It can be constituted of local earth, with or without lime additions [12]. Figure 6 shows the components of a Tabique wall.

a) b)

Figure 6: Components of a Tabique wall: a) Timber frame [12]. b) Timber frame covered by earth render [12].

2.2 Earth Construction in Brazil

The use of earth as a raw construction material emerged in Brazil with the arrival of the Portuguese in 1500, and thereafter of the Africans, once there are no evidences of its use by the local civilizations. Ever since, techniques such as adobe and rammed earth were widely used in the colonial period due to its large availability and simplicity to handle and appropriation. These techniques were commonly used not only to build houses but also churches and governmental buildings, being associated to other raw materials (such as wood, straws, and stones) according to the characteristics of different areas of the country [13]–[15]. Figure 7 shows the Old Town Hall and Prison of the city of Ouro Preto (State of Minas Gerais, in the southeast of Brazil), built in 1785 using rammed earth and stones [16].

Figure 7: Old Town Hall and Prison of the city of Ouro Preto (Minas Gerais), built in rammed earth and stones [16].

During the colonial period (which dated from 1500 to 1822), rammed earth or adobe blocks were commonly used on the external structure of the houses, and tabique or wattle and daub were used on internal partitions. However, at the end of the nineteenth and beginning of the twentieth century, after the Industrial Revolution in Brazil, earth construction techniques were replaced by mass-produced manufactured materials (such as bricks), due to their greater durability and agility of construction. Similarly as occurred in developed countries, earth constructions where considered rudimentary and associated to poverty, which led to a considerable reduction on their use [14], [15].

In Brazil, earth construction has also been strongly associated to the spread of Chagas disease, which contributed to the disuse of these techniques. Chagas disease is an infection transmitted by insect vectors which can live in gaps and cracks in all kind of walls. Once in Brazil, mainly in northeast region, commonly low-income people live in houses built using wattle and daub technique, which often do not receive the proper maintenance, these houses were associated to the proliferation of the vector and consequently of the disease [17]. Figure 8 shows an example of a low-income house built in wattle and daub in Ivaporunduva (State of São Paulo) [18].

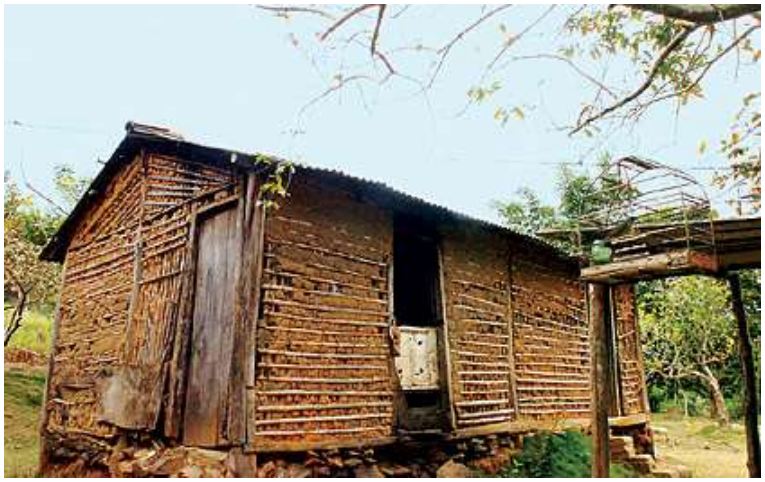

Figure 8: Example of house in wattle and daub in Ivaporunduva (São Paulo), Brazil [18].

Over the last years, due to the crescent interest on a more sustainable construction, Brazil faces the challenge of a change of paradigm concerning earth techniques. For this purpose, in 1970, the Brazilian institutions Centre for Research and Development (CEPED) and the Technological Research Institute (IPT) elaborated the first recommendations of the country for buildings with earth. In the decade of 1980, the Brazilian Association of Technical Standards (ABNT) published standards concerning earth construction techniques, mostly associated to the use of compressed earth blocks (CEBs). However, some of these standards lack for revisions and updates, considering the recent technologic advances in this field [19], [20].

Since 2006, Brazil is part of the PROTERRA, an Iberic American network that aims the dissemination and promotion of earth architecture in Latin America. Also, in the Brazilian construction scope there is Rede Terra Brasil, which is another network that promotes the use of earth construction techniques and organises every two years an event named Terra Brasil, to discuss technological innovations and to spread these techniques [15], [19].

Over the last years, according to Nito and Amorim (2010) the use of earth as a raw construction material in brazil occurs in three different fronts. The first is related to individual production and own initiative developed by permaculture and sustainability. The second is the production of housing, by governmental and non-governmental organizations which work in cooperation with communities. The third concerns to companies that are integrating these techniques to their scope of activities, however they still require a more social acceptability regarding earth constructions [21].

2.3 Compressed Earth Blocks (CEBs)

Compressed earth blocks, also known as CEBs, emerge as an evolution of the adobe technique, and consist of blocks made by the mechanical compression of confined soils into moulds. The compaction of the blocks is performed by mechanical means, eliminating voids with greater efficiency and consequently reducing their porosity. CEBs usually present greater durability and mechanical resistance when compared to adobe blocks [4].

The first experiments involving compressed earth blocks probably date from the eighteenth century, but only in the twentieth century the first mechanical presses were designed, using heavy lids to apply loads into the moulds. However, only after the mechanical press called CINVA-Ram (Figure 9), developed by engineer Raul Ramirez in Bogota, Colombia, compressed earth blocks started to be used in large scale for architectural and structural purposes [22].

Figure 9: Example of a CEB CINVA-Ram press machine [23].

Compressed earth blocks can be used either for structural purposes, thus acting as supporting masonry, or even serve as sealing masonry in structures made of reinforced

concrete, steel or timber, for instance. Since these blocks can be made in different shapes, they can be moulded into solid or perforated prisms (like ceramic or concrete blocks) that can be layer with mortar or can be interlocked (thus eliminating or drastically reducing the use of mortar joints) [4], [24]. To illustrate, Figure 10 shows a solid CEB and an interlocking CEB.

a) b)

Figure 10: Different types of CEBs: a) Solid block [25] b) Interlocking block [26].

Nowadays, CEBs are the most widely used earth construction technique in the world. However, the execution of dwellings made of CEBs is still uncommon in Portugal, which tends to change due to its associated sustainable feature, besides its better performance when compared to adobe blocks, for instance [7], [23].

In order to improve characteristics such as strength, durability and granulometric aspects of the blocks, it is usual to stabilize the soil by adding other components. The most used stabilizers are lime, fly ash and cement. Cement stabilized blocks are also called soil-cement blocks [2].

Among the main advantages of the CEBs, it can be highlighted [4], [22], [27], [28]:

- The use of mechanical presses represents a real improvement of CEBs when compared to other earth blocks, mainly in the consistency of quality at the end of the fabrication process. This quality enhances the social acceptability of earth construction methods;
- The possibility of standardization in the fabrication process of blocks makes it easier to elaborate standards and regulations. Thus, minimum performance

requirements can be stated guaranteeing the blocks architectural and structural capacity;

- CEBs can be made with intern holes, allowing the addition of reinforcements to the structure (such as steel) or the passage of pipes and wires (hydraulic, electrical, cabling) without need of later cuts in the masonry;
- CEBs present a good adaptability when used in renovation of constructions built on traditional techniques that relies on the use of small masonry elements (such as fired bricks, stones or blocks). This feature, associated to the low cost of production, makes CEBs an important technological resource to the socioeconomic development of the building sector;
- The manufacturing process of the blocks is easily to be assimilated and reproduced, without need of a highly specialized labour in its manufacture;
- CEBs promote the use of local raw materials, decreasing production costs. This aspect, when analysed at a social level, reduces the costs of popular housing, as well as improves the socialization and autonomy of a people, once it stimulates self-construction.
- Low embodied energy and CO_2 associated, since the blocks do not require any fire process in their manufacture (Figure 11);

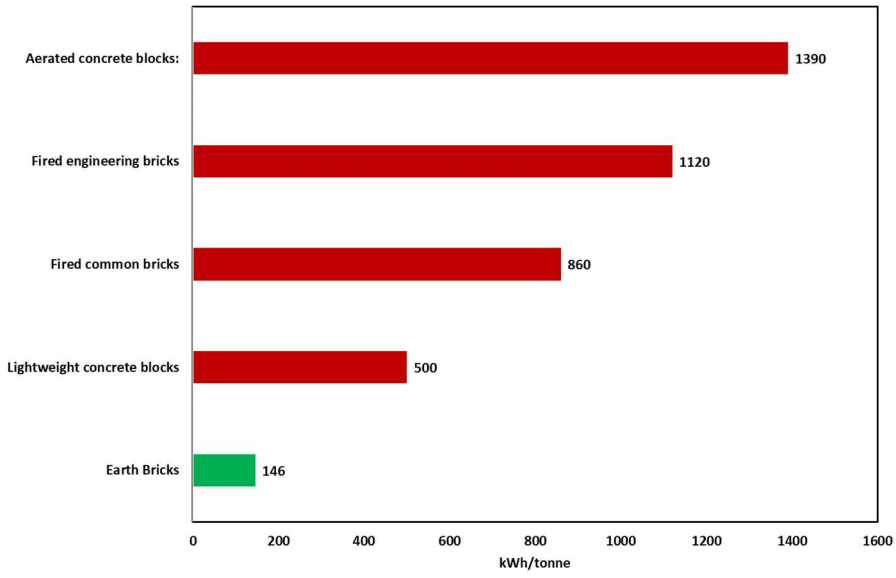

Figure 11: Embodied energy in different masonry materials manufacture (adapted from [28]).

However, despite the qualities of the CEBs, just as all other building techniques it also presents limitations and disadvantages. A few of them are listed below [23], [29]–[31]:

- Constructions made in CEBs present a scarce response at seismic loads (when not properly reinforced);
- Low tensile strength, which restrains its use to situations of exclusive or major compression efforts (e.g. bearing walls, domes and vaults). This aspect also restrains its use in situations of large free-spans and high buildings;
- CEBs presents low resistance to abrasion and impact (when not properly reinforced);
- In the same way as other earthen building techniques, CEBs are commonly considered as non-standard materials;
- Sub-stabilization or over-stabilization can both lead to a bad quality product and increase costs of CEBs.
- Low acceptability in social opinion. Like other earthen building techniques, CEBs are often considered as second class or lower building materials;

Due to the aspects listed above, earth as a building material lacks institutional acceptability in most countries and consequently building codes and performance standards still require development.

2.4 Incorporations on CEBs

Stabilization of soils has provided great enhances in CEBs performance, including improvements in resistance and durability. Since these gains, scientific community concentred huge efforts in the incorporation of materials (such as industrial wastes, organic materials and by-products) in the composition of CEBs, in order to maximize even more its sustainable feature. The aggregation of new materials in the composition of CEBs represents a feasible way to both reduce the use of conventional materials in the blocks (as cement) and to ensure usability to materials that were at once discarded. This section aims to present researches about incorporations on CEBs done over the last years.

2.4.1 Fibres on CEBS

Although the addition of fibres is very common in traditional earth construction methods (mainly on adobe blocks), Rigassi (1985) reported that fibres were incompatible to the compression process of CEBs, because of their high elasticity [22]. More recent works have shown the opposite, in which incorporated fibres increased mechanical behaviour of compressed earth blocks.

Blocks with the addition of kraft paper fibres from discarded cement bags, called Krafterra, were studied by Buson (2009, 2010, 2012). The incorporated CEBs presented better performance when compared to those without the composite. CEBs with Krafterra have shown better results regarding simple and diagonal compressive strength, shrinkage and fire resistance. However, the addition of Krafterra increased water absorption rates. In order to keep the water absorption on acceptable levels, Aloe Vera sap was also added to the composition of the CEBs [32]–[34]. Figure 12 presents the fibres incorporated on the CEBs in these works.

Figure 12: Krafterra fibres to be incorporated in the CEBs [32].

Villamizar *et al* (2012) analysed the influence of coal-ash and cassava peels on the engineering properties of CEBs. The work investigated the possibility of using coal-ash and cassava peels as non-traditional stabilizers, hence avoiding the use of cement or other binders. Although the authors concluded that engineering properties of the incorporated CEBs were not satisfactory, coal-ashes (in doses below 10%) increased compressive and flexural strengths of the blocks. Cassava peels increased considerably the dry strength of the blocks, which is useful to reduce scraps due to handling problems of the CEBs [25].

Taallah *et al* (2014) investigated mechanical properties and hygroscopicity behaviour of CEBs filled by date-palm fibres, as shown on Figure 13. In the work, blocks were

manufactured with soil stabilized with cement, crushed sand and date-palm fibres and compressed at 3 different static loads (1.5 MPa, 5 MPa and 10 MPa). The results show that date-palm fibres impact on tensile strength was unfavourable, because of their very high-water absorption, by heterogeneity or distribution and low adhesion with the matrix. However, the best results for dry compressive strength occurred at the CEB with 0.05% of fibre content, 8% of cement content and compaction pressure of 10 MPa. At other compaction pressures, the fibre incorporation has shown adverse effect on the CEB's properties. The swelling of the blocks increased with decreases of cement content and increases of date-palm fibre content [35].

Figure 13: Cut Date-Palm fibres to be incorporated on the CEBs [35].

The work of Mostafa and Uddin (2015) investigated the influence of the incorporation of banana fibres into CEBs, as shown on Figure 14. Banana fibres are available worldwide as agricultural waste and present properties such as low density, low cost, high tensile strength and are also fire and water resistant. The study analysed the addition of 6 different lengths of fibres in the CEBs compositions, which were compared to CEBs without any incorporations. Before being incorporated into the blocks, banana fibres were chemically treated in sodium hydroxide (NaOH) solution in order to enhance mechanical bonding and the amount of cellulose exposed on the fibre surface. Blocks with the fibres presented results about 70% higher in compressive strength and 80% higher on flexural strength than those without any additions. CEBs with banana fibre also presented gradual rupture, while those without it showed sudden rupture [36].

Figure 14: Banana fibres under chemically treatment to be incorporated on CEBs [36].

The possibility of incorporating rice production by-products in CEBs have been studied as well. Gapuz and Ongpeng (2018) analysed the possibility of adding rice straws (combined with cement) as CEB stabilizer using an Artificial Neural Network (ANN). The work studied compressive strength of CEBs under uniaxial tests at an age of 7 and 28 days. The conclusion was that any rice fibre content, when combined to 10% or more of cement, achieved at least 2.5MPa (which is the minimum required by the standard used for comparisons in the work) [37].

Tran *et al* (2018) have studied the influence of adding cornsilk fibres in the CEBs composition. The work analysed the incorporation of 3 different percentages of cornsilk in the block's composition. Also, different quantities of cement and different times of curing were investigated. The work revealed that CEBs with cornsilk fibres presented higher values of compressive and splitting tensile strength, mainly at early ages and with low cement contents. For the optimum fibre content (from 0.25% to 0.5%) the blocks presented results 177% and 88% higher for compressive strength and splitting tensile strength, respectively, when compared to the conventional ones [38].

2.4.2 Construction and Industrial Wastes on CEBs

For sustainable development, there is a need to use industrial by-products and construction and demolition waste materials (CDW), which are available in large scale and require proper disposal.

Acchar *et al* (2014) have studied the possibility of incorporating fired ceramic wastes as binary or ternary binders (also with hydrated lime and cement) on CEBs. In the research,

clay-based mixtures containing from 2% of 5% weight of ceramic rubble were prepared and analysed. Different percentages of conventional binders (hydrated lime and cement) were investigated as well (6%, 8%, 10% and 12% of total weight). The specimens were characterized in terms of microstructure through Scanning Electron Microscopy (SEM), compressive strength, water absorption and wear resistance. The results demonstrated that the waste can be incorporated into CEBs without degradation of typical properties. According to the authors, using about 2% of total weight of hydrated lime and 2% of ceramic rubble is a feasible way to reduce the cement content and still reach the expected CEB performance in terms of compressive strength and wear resistance [39].

Subramaniaprasad *et al* (2014, 2015) analysed the possibility of incorporating plastic wastes into CEBs. Fibres of plastic carry bags (pick-up bags) and plastic bottles were made by chopping these materials into small lengths with almost the same width (2 to 3 mm), as shown on Figure 15. One of the works investigated the influence of the incorporation of the wastes in the sorption characteristics of the blocks, with different percentages of cement (5%, 10% and 15%), different lengths of fibre (1 and 2 cm) and different percentages of fibres (0.1% and 0.2%). The results showed that fibres addition increases water absorption, and that the water absorption increases with fibre lengths. Fibres addition also increase absorption capacity, mainly at lower percentage and with smaller fibres. Increasing the amount of fibres and the fibre's length, the absorption capacity of the blocks reduces (for smaller values than those obtained without fibres) [40].

The authors also investigated the influences of adding these wastes in the tensile strength of the CEBs. At this research, different loading pressures (from 1.5 MPa to 7.5 MPa), different amounts of cement (7.5%, 10% and 15%), different lengths of fibre (1 and 2 cm) and different percentages of fibre (0.1% and 0.2%) were analysed. The results showed that the fibre addition helps the blocks to achieve given tensile strength at lower cement contents and that the tensile strength increases with the increase of the length of the plastic fibres. From the failure pattern, the authors concluded that the fibre reinforcement also improved ductility of the blocks. Both types of fibres performed in similar way, but carry bags fibres showed better performance than plastic bottle ones [41].

a) b)

Figure 15: Plastic fibres to be incorporated on CEBs: a) from carry bags [40]; b) from plastic bottles [40].

Nagaraj and Shreyasvi (2017) investigated the possibility of using iron mine spoil waste on the composition of CEBs. In the work, three different percentages of waste incorporation were analysed (30%, 40% and 50% of total mass), all of them with 6% of cement, 2% of lime and the remaining of quarry dust. The same amounts of waste were also studied with 8% of cement, 2% of lime and the remaining percentage of quarry dust. Results showed that all the specimens water absorption rates were below 15% at 30 days (the maximum stablished by the Indian standard IS: 1725-2013, used for comparison). As to the wet compression strength, all the blocks manufactured with 8% of cement presented resistance above 3.5 MPa at 60 days (the minimum stablished by the Indian standard IS: 3495-part1-1992, used for comparison). The higher wet compression strength were obtained for 40% of waste incorporation, thus suggesting an optimal value [42]–[44].

The work of França *et al* (2018) analysed the incorporation of limestone residues from the processing of marble into CEBs composition. The authors prepared specimens with 3 different percentages of limestone residues (30%, 40% and 50%) to the soil-cement mixture and analysed physical, chemical and mineralogic aspects. The studied parameters were water absorption rates and compressive strength. To assess the durability, a few specimens were subjected to a process of accelerated degradation and then tested for compressive strength. After the tests, all the fracture surfaces were analysed through Scanning Electron Microscopy (SEM). The results verified the feasibility of adding limestone residues into the CEBs, revealing a superior performance at the water absorption and compressive strength of the incorporated blocks. CEBs with 30% of

limestone residue presented the best results, since increasing the percentage of waste was evident an increase in water absorption and a decrease in mechanical resistance. The degraded blocks presented a significant increase in strength when compared to the corresponding non-degraded blocks [45].

2.4.3 Municipal Wastes on CEBs

In order to develop a feasible way to use municipal wastes generated by human activities, researches have been done to analyse the potentiality of incorporating this kind of residues into CEBs.

Nepomuceno (2018) investigated the possibility of using the organic fraction of municipal wastes to build compressed earth blocks [46]. The present work is a continuation of Nepomuceno's work, since its objective is to complement the thermal characterization of these blocks, beyond analysing how a wall panel of them behave when subjected to fire conditions. This subdivision is destined to present the stage of knowledge around CEBs with municipal waste incorporation at the beginning of the present work. Here, some of the results obtained by Nepomuceno, which will be widely further used, are introduced.

In order to assess the influences made by the waste incorporation on the CEBs, an artificial soil was used in the blocks. The artificial soil consisted in a mixture of kaolin and sand. Hence, three different compositions of CEBs were analysed, and the obtained results were compared to a reference specimen, built only with the artificial soil (composed by 70% of kaolin and 30% of sand). The three compositions were stabilized with cement and incorporated with municipal waste and in one of them silica fume was also added (which, due to filler presence, generates physical and chemical effects on the cement matrix). The proportions of materials are presented in Table 1.

Table 1: Mass proportions of CEBs at Nepomuceno's work [46].

	Soil		Residue	Cement	Silica	Unit
	Sand	Kaolin		(to the soil/soil	+ residue mass)	
Soil	70	30	-	-	-	%
SC_{10}	70	30	-	10	-	%
$SC_{10}R_{20}$	63.32	33.92	2.76	10	-	%
$SC_{10}R_{20}Si$	63.32	33.92	2.76	9	1	%

The work analysed each of the compositions testing cylindrical specimens for the following parameters: water absorption, durability (submitting blocks to accelerated aging) and compressive strength at ambient temperature and at high temperatures (100º C, 200º C, 400º C and 600º C). The results are presented below.

2.4.3.1 Water Absorption

Water absorption values for all the compositions were analysed at 7 and 28 days of cure and compared to the stablished by Brazilian standard NBR 8491:2012 [47], which prescribes a maximum value for individual measures of 22% and a maximum average value of 20%. Table 2 shows the obtained results.

Table 2: Water Absorption Values (adapted from [46]).

Composition	Time of cure								Unit
	7 days				28 days				
	Value 1	Value 2	Value 3	**Mean Value**	Value 1	Value 2	Value 3	**Mean Value**	
SC_{10}	10.97	11.89	11.50	**11.45**	9.02	8.91	9.51	**9.15**	%
$SC_{10}R_{20}$	13.34	12.29	12.49	**12.71**	12.12	12.43	12.38	**12.31**	%
$SC_{10}R_{20}Si$	12.72	12.68	12.07	**12.49**	13.33	13.17	13.47	**13.33**	%

From Table 2 one can see none of the compositions presented values above the maximum stablished by the standard. Thus, as regards to water absorption, the incorporation of municipal organic waste does not prevents the use of the CEBs [46].

2.4.3.2 Durability

In order to assess the durability of the compositions, cylindrical specimens were subjected to six cycles of accelerated aging. To evaluate the durability of the blocks after the cycles, parameters were compared to regulatory requirements prescribed by Spanish standard UNE 41410 [48], by German standard DIN 18945 [49] and by Brazilian standard NBR 13554:2012 [50]. These parameters were volume variation, mass loss and visual analysis, as presented on Table 3. Figure 16 shows the specimens before and after the accelerated aging cycles.

Table 3: Volume Variation and Mass Loss for CEBs after six cycles of accelerated aging [46].

Composition	Volume Variation	Mass Loss	Unit
SC_{10}	1.00	10.35	%
$SC_{10}R_{20}$	0.63	8.80	%
$SC_{10}R_{20}Si$	0.53	11.15	%

a) b)

Figure 16: Specimens submitted to cycles of accelerated aging: a) before; b) after [46].

Spanish standard stablishes only visual criteria to evaluate specimen's behaviour. As can be seen in Figure 16, none of the compositions showed cracks, swellings, cuts, erosion nor efflorescence, hence accomplishing the prescriptions of this standard. Comparing the results shown in Table 3 with the limits stablished by Brazilian standard, only composition $SC_{10}R_{20}$ meets the requirement of mass loss (which shall be smaller than 10%). In relation to the German standard, all specimens comply with the limits imposed for use in internal walls or protected external walls (mass loss smaller than 15%). If the blocks are meant to be used in exposed to weather purposes, none of the compositions meets the requirement of German standard (maximum mass loss of 5%) [46], [48]–[50].

Compressive strength of the aged specimens was also evaluated and will be analysed on section 2.4.3.3.

2.4.3.3 Compressive Strength at Ambient Temperature

Nepomuceno evaluated the compressive strength behaviour of the three compositions for ambient temperature of three different kind of samples: saturated specimens, aged specimens (which were subjected to accelerated aging as described in section 2.4.3.2) and

reference specimens (which were kept at the humid chamber for 7, 14 and 28 days and then tested for simple compression).

The results obtained for the reference specimens are shown in Figure 17. These results were used for comparison both with the other specimen and with the minimum values prescribed by Spanish standard UNE 41410, by German standard DIN 18945 and by Brazilian standard NBR 8491:2012. Even the lowest value obtained still accomplish the stablished by the three standards, being classified as CEB 2 by UNE 41410 and as class of strength 2 according to DIN 18945 [46]–[49].

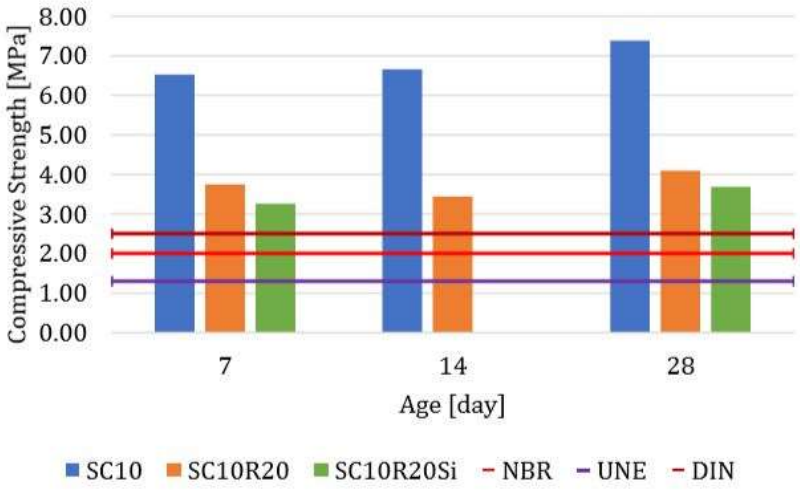

Figure 17: Mean compressive strength for the reference specimen and minimum values stablished by the standards [46].

Two saturated specimens of each composition (named T1 and T2) were tested for compressive strength. The results are presented and compared to the reference ones in Figure 18. Even that the results are lower than the obtained for the reference specimens, all the compositions still accomplish the minimum required by all the three standards.

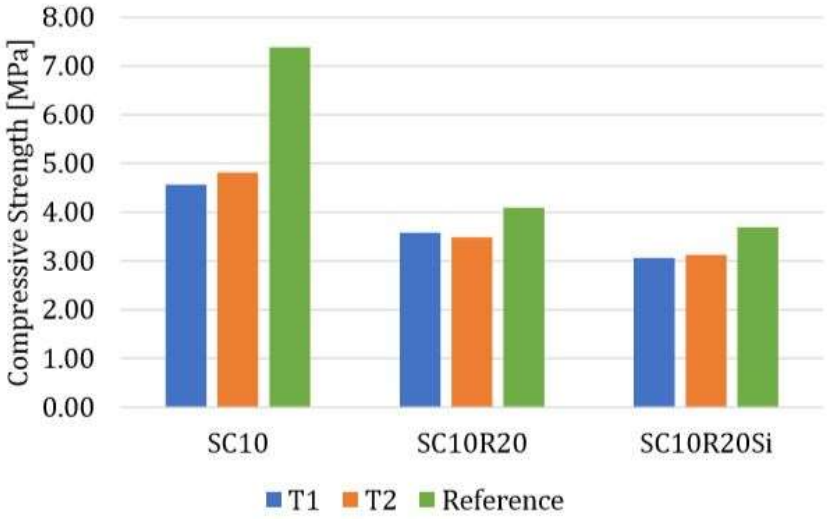

Figure 18: Compressive strength of saturated specimens compared to reference values [46].

In order to complement the evaluation of the durability of the CEBs with municipal organic waste incorporation, simple compressive strength tests were carried out on the aged specimens. The results are presented in Figure 19 and also compared to the reference values. As can be seen, after the cycles of aging an increase in the compressive resistance of the CEBs is noticed. Nepomuceno reports that this may be a consequence of the heating which the CEBs are submitted in the aging process, since increases were also noticed in the compressive resistance of the specimens at high temperatures, as will be presented in section 2.4.3.4. Analysing the compressive strength presented by the aged blocks, the composition with lowest average fits in the highest class of strength of the UNE 41410 (CEB3) and the class of strength 4 according to the DIN 18945 [46], [48], [49].

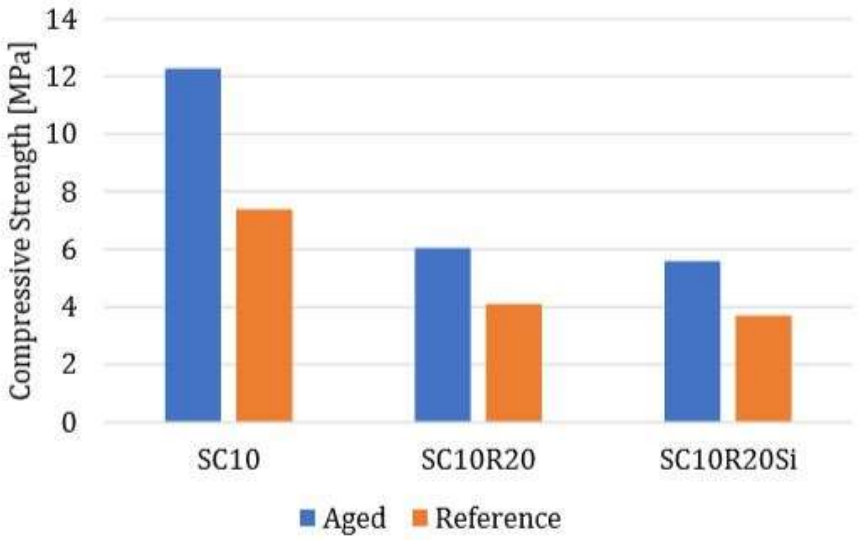

Figure 19: Compressive strength of aged specimens compared to reference values [46].

2.4.3.4 Compressive Strength at High Temperatures

Specimens of each of the three compositions were tested for compressive strength at 100ºC, 200ºC, 400ºC and 600ºC, as presented in Figure 20. The results show an increase in the compressive strength at all the compositions when submitted to heating, with major values for the highest analysed temperature. From ambient temperature to 100ºC, the specimens did not present elevations on their compressive resistance, but at 200ºC all the values showed an increase. This suggests the occurrence of chemical reactions in this interval of temperature responsible for the enhancement of this property. As expected, the CEBs with waste incorporation presented lower compression resistance than the reference specimen for all the temperatures [46].

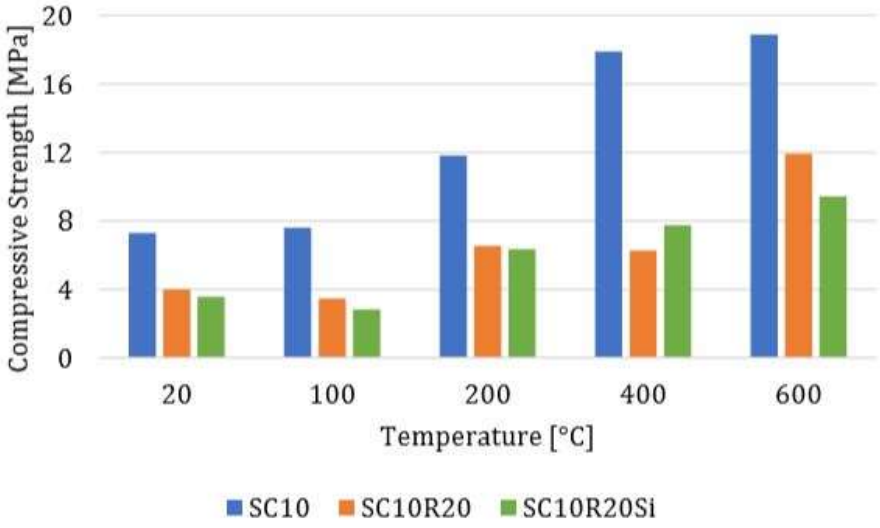

Figure 20: Compressive strength of the three compositions at higher temperatures [46].

2.5 Thermal Properties of CEBs

In order to assess the behaviour of structures made of CEBs when submitted to fire situations is essential to understand its thermal properties. This section aims to present the state of knowledge about CEBs thermal characteristics according to researches.

2.5.1 Thermal Conductivity and Specific Heat

CEBs are made from compressed earth and are consequently porous. Heat transfers inside the blocks occurs in different ways, namely conduction in solid, liquid and gas fractions and convection and radiation in the porous fraction. Additionally, endothermic and exothermic reactions are present due to water and cement presence. An equivalent thermal conductivity should consider all these heat mechanisms, but for CEBs there is a lack of information of thermal properties varying with temperature [1].

According to Mansour *et al* (2016) compaction pressure of the CEBs plays an important role on the bulk density of the blocks, which impacts directly on their thermal and mechanical performance. In order to obtain blocks with higher compressive strength, CEBs are commonly executed with high compaction pressure (and consequently high bulk density). However, a higher compaction pressure implies in higher thermal conductivity, as shown in Figure 21. Thus, Mansour *et al* suggest that the use of an optimal value for the bulk density would lead to blocks with a considerable mechanical

performance and allow to reduce transferred heat through building envelopes made of CEBs. This optimal value may vary in function of the compressive strength required by the context of use of the blocks [51].

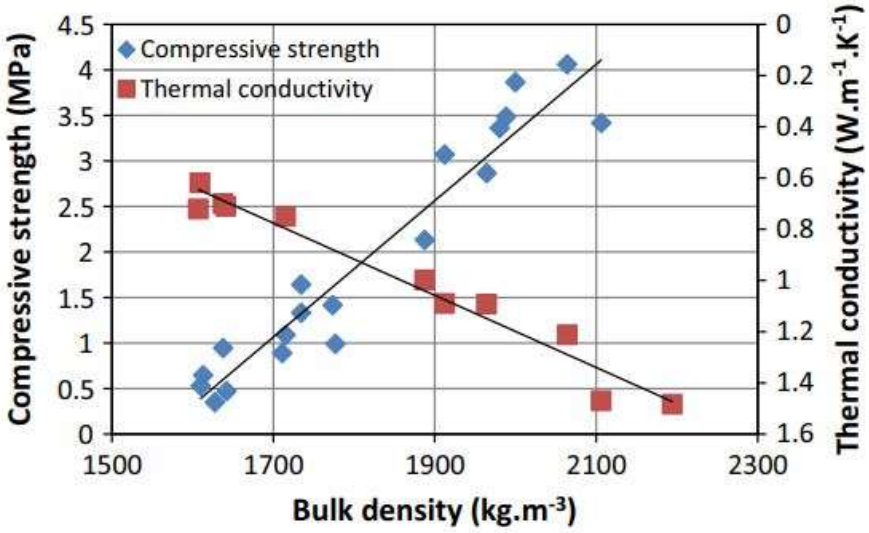

a)

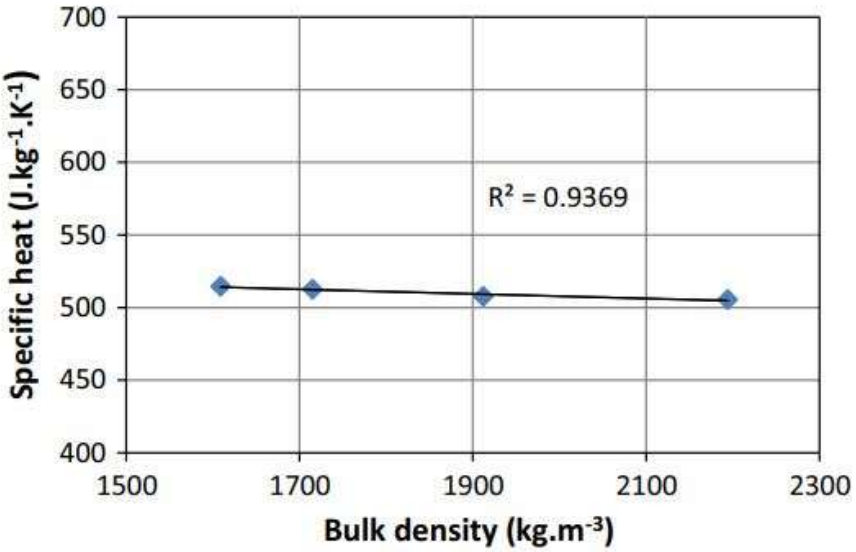

b)

Figure 21: Influence of bulk density on: a) compressive strength and thermal conductivity; b) specific heat; of CEBs at 20ºC [38].

Even that bulk density is directly correlated to the porosity of the blocks, Mansour *et al* also present influences of the porosity on the thermal conductivity of CEBs for ambient temperature (Figure 22).

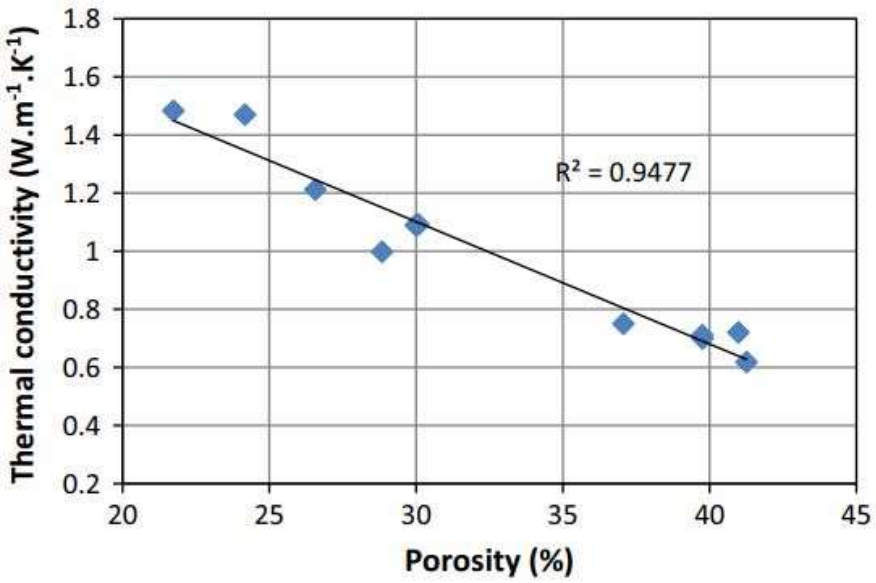

Figure 22: Influence of porosity on thermal conductivity of CEBs at 20ºC [51].

Besides porosity and bulk density, Zhang *et al* (2017) have also investigated the influence of the percentage of cement in the CEBs in the thermal conductivity of the blocks. The work concluded that, although cement additions caused small variations in the thermal conductivity, there is no obvious trend connecting the cement percentage and thermal conductivity (the analysed cement contents varied from 0% to 9% of the total weight). According to the authors, this might be due to the similarity between thermal conductivity of both cement and soil, and since the measures of cement are not too large (maximum of 9%) it is not possible to see significant effects on the property of the blocks. Confirming the results obtained by Mansour *et al*, they also concluded bulk density and porosity as key factors in thermal conductivity values. The authors explain this fact due to the biphasic composition of the blocks (solid and gas phases), and since the thermal conductivities of the air and soil are very different, variations on their proportions may cause large differences in the thermal conductivity of the blocks. Figure 23 shows the thermal conductivity values obtained by Zhang for different percentages of cement and bulk densities [51], [52].

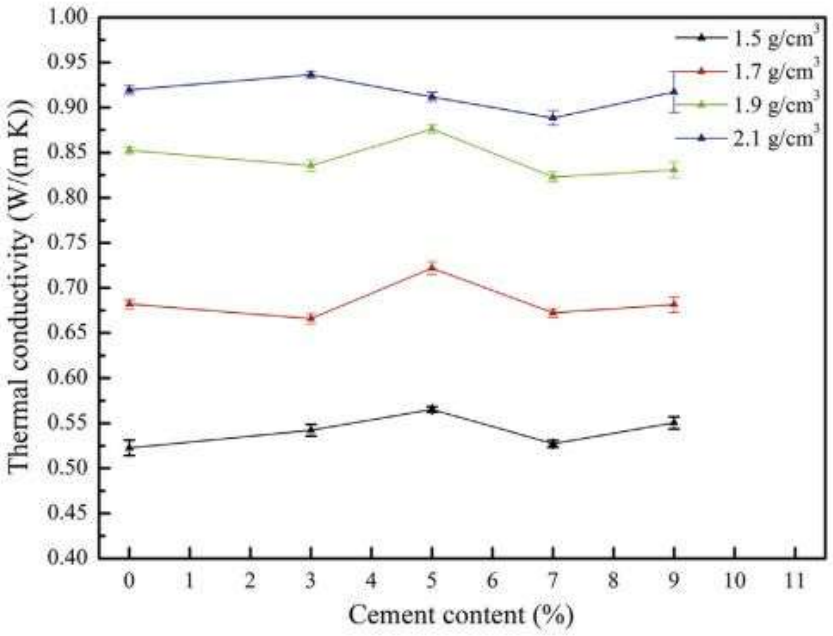

Figure 23: Influence of cement content on the thermal conductivity of CEBs at 20ºC for different bulk densities [52].

Although in the work of Zhang *et al* no trend was observed for the thermal conductivity with the increase of the cement content, Saidi *et al* (2018) have analysed the influence of the quantity of stabilizer compound on thermal conductivity of CEBs. In the work, the authors investigated how different percentages (0%, 5%, 8%, 10% and 12% of the dry soil weight) of cement and lime influence on the thermal conductivity of the blocks. All the analysed samples were made with similar bulk densities (approximately 1750 kg/m^3). The results showed that increasing the amount of stabilizer, thermal conductivity also increases, as presented on Figure 24 [53].

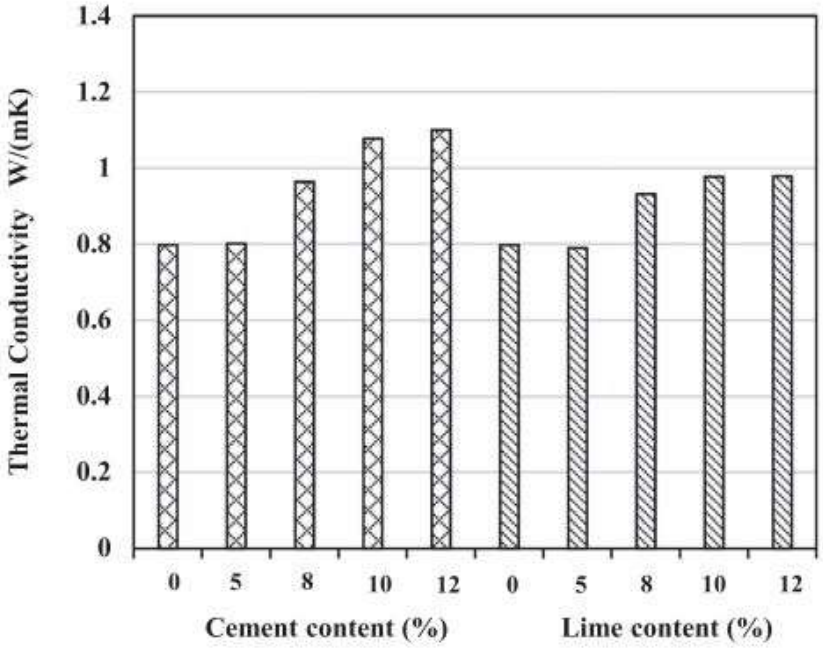

Figure 24: Influence of stabilizer content on thermal conductivity of CEBs at 20ºC [53].

2.5.2 Thermogravimetric Analysis

According to the International Union of Pure and Applied Chemistry (IUPAC), thermogravimetry can be defined as "A technique in which the mass of a substance (and/or its reaction product(s)) is measured as a function of temperature, while the substance is subjected to a controlled temperature program" [54]. Commonly, data evaluation is based on determination of fractions using derivative thermogravimetric curves (DTG). Thermogravimetric analysis can be used both to determine kinetics of reactions and also to predict a materials behaviour when submitted to high temperatures [55].

No thermogravimetric analyses were found for compressed earth blocks during the bibliometric research. However, thermogravimetric results for cement and artificial soil (sand + kaolin) are available, which can be useful for comparative purposes.

2.5.2.1 Artificial Soil

Ondruska *et al* (2020) have investigated kaolin-quartz mixtures during heating through thermogravimetric analyses. The work tested 6 different compositions made of kaolin, quartz and grog (which is a raw material rich in silica and alumina, and normally used for

making ceramics). Since the work is focused on ceramics industry, to obtain a plastic mass, all the compositions were mixed with 35% mass of distilled water. Figure 25 presents the results obtained by the authors in the thermogravimetric analyses [56].

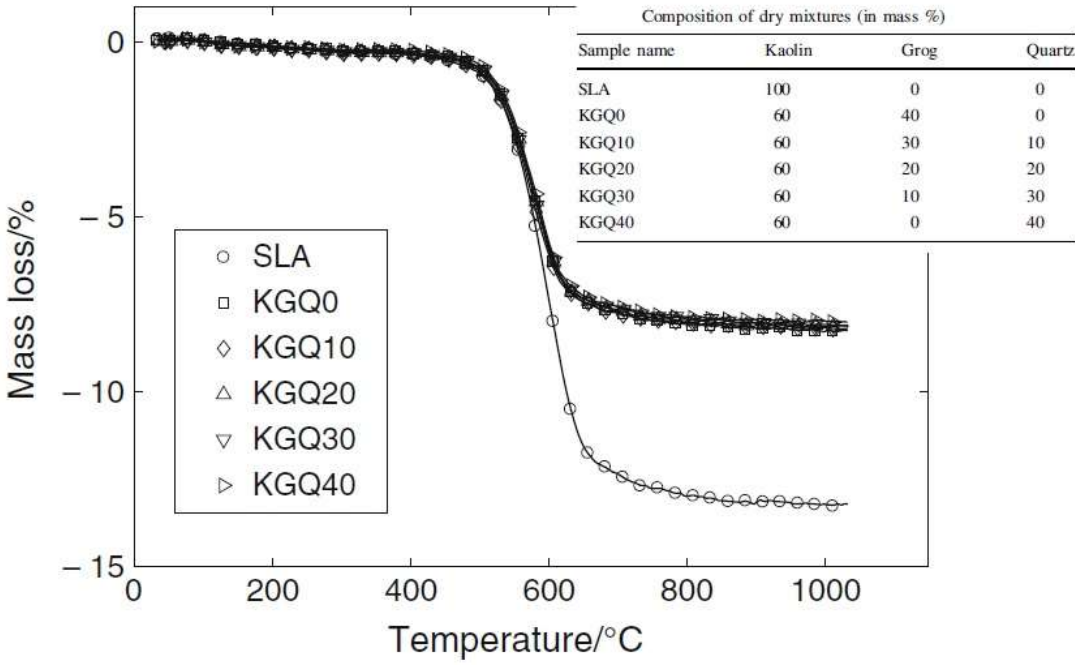

Composition of dry mixtures (in mass %)

Sample name	Kaolin	Grog	Quartz
SLA	100	0	0
KGQ0	60	40	0
KGQ10	60	30	10
KGQ20	60	20	20
KGQ30	60	10	30
KGQ40	60	0	40

Figure 25: Thermogravimetry (TG) results for kaolin-quartz mixtures [56].

As described by the authors, the main changes were identified in the interval from 500 ºC to 650 ºC, region where the kaolinite dehydroxylation occurs. The changes in the peak of the compositions is due to the reduced amount of kaolinite in the mixtures (KGQ0-KGQ40) when compared to the 100% kaolin specimen (SLA). Even that in this same range of temperature there is the transition of α-quartz to β-quartz, this phenomenon is superimposed by the kaolinite dehydroxylation. The peak reported around 950ºC corresponds to the transformation of metakaolinite to Al-Si spinel [56].

2.5.2.2 Cement

Dweck *et al* (2016) investigated the hydration kinetics of Portland cement pastes by thermogravimetry (TG) and differential thermogravimetry (DTG). The authors have analysed samples with different periods of hydration (1 hour, 24 hours, 7 days, 14 days and 28 days). The pastes were executed with a water/cement ratio of 0.5. All the tests were performed with a constant heating rate of 10ºC/min in a range of temperature from 35ºC to 1000ºC, with an initial isothermal step of 35ºC for 1 hour to eliminate residual

non-combined free water. Nitrogen was used as purge gas in a 100 mL/min flow. Figure 26 presents the obtained results for the TG and DTG analyses for the different aged samples [57].

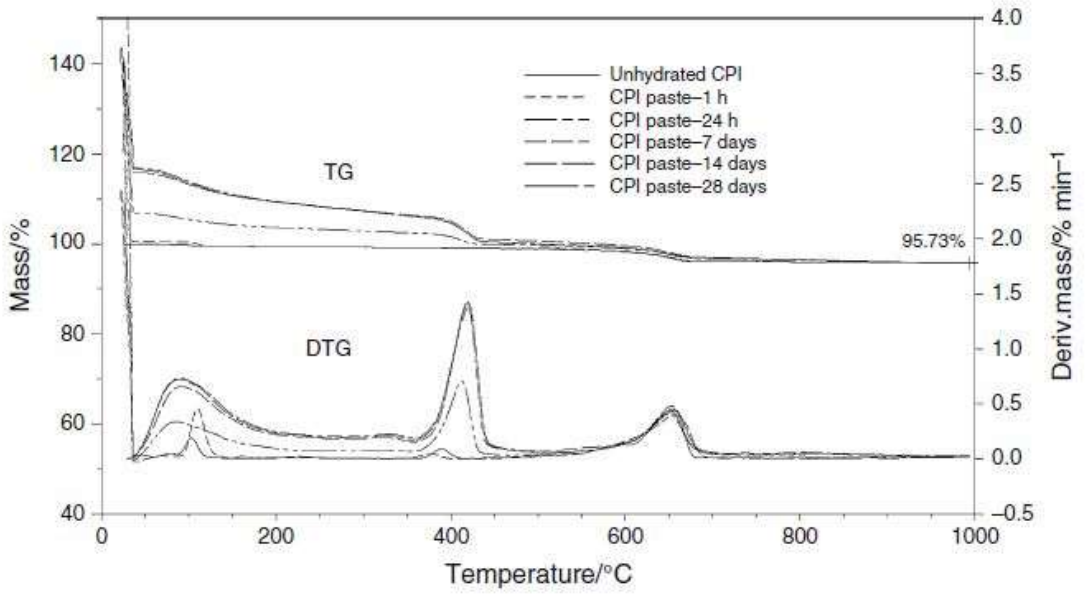

Figure 26: Thermogravimetry (TG) and differential thermogravimetry (DTG) for cement pastes with different ages on calcinated mass basis [57].

In order to compare the results obtained for cement pastes with different ages, the TG and DTG curves were converted from initial cement mass basis to calcined mass basis. This conversion is made considering that every paste made only of cement and water will present the same chemical composition at the end of a thermogravimetric analysis with the same operating conditions. Then, all the results are normalized in function of the mass of the sample at the end of the tests (calcinated mass) [57].

The first peak on the TG curves represents the mass loss due to the release of free water at the isothermal step at 35ºC. Between 35ºC and 200ºC there is a continuous mass loss which refers to the combined water released from dehydration of tobermorite and ettringite phases. Simultaneously, from 100ºC to 150ºC occurs the dehydration of the gypsum phase (the samples with more than 24 hours of curing already had their gypsum content totally consumed). From 350ºC to 500ºC occurs the dehydroxylation of the calcium hydroxide. From 500ºC to 750ºC the main reaction is the decomposition of calcium carbonate, aggregated to the clinker during cement manufacture [57].

CHAPTER 3

MANUFACTURE AND PROPERTIES OF THE CEBs

3.1 Materials used on the Manufacture of the CEBs

To understand the behaviour of CEBs is of key importance to know the materials used on its manufacture and their properties. Since the blocks are made of soil, and soil is a very heterogeneous material, a description of the used soil is fundamental to characterize the blocks. This section aims to present the materials used on the CEBs production and their properties.

3.1.1 Soil

To minimize the influence of soils heterogeneity in the analysis, it was decided to use an artificial soil on the experimental program. The soil composition was based on the work of Nepomuceno [46], made of a 70% mass proportion of sand and 30% of kaolin. Properties of these materials are presented below.

3.1.1.1 Sand

The used sand was acquired in the region and consists of a conventional sand destinated for general constructions use. It was stored in dry and covered place, in order to be protected from humidity. Before used, the sand was dried. The volumetric mass of the sand was determined according to NP 954 and resulted in 2.58 g/cm^3 [58].

3.1.1.2 Kaolin

The kaolin was acquired from the company MIBAL – Minas de Barqueiros, in pressed, granulated and powder form. The product is commercialized in 20 kgs bags. The physical and chemical properties presented in the technical file of the product are shown on Table 4 and Table 5, respectively.

Table 4: Physical Properties of kaolin (adapted from [59]).

Properties	Value	Unit
Moisture	<2	%
Density	2.4 to 2.7	g/cm³
Granulometric distribution		
<30 μm	99 ± 3	%
<10 μm	92 ± 3	%
<5 μm	81 ± 3	%
<2 μm	68 ± 3	%

Table 5: Chemical properties of kaolin (adapted from [59]).

Element / Property	Symbol	Value	Unit
Silicon dioxide	SiO_2	46.43	%
Aluminum oxide	Al_2O_3	35.66	%
Iron (III) oxide	FeO_3	1.02	%
Calcium oxide / Quicklime	CaO	0.04	%
Magnesium oxide	MgO	0.12	%
Sodium oxide	Na_2O	0.06	%
Potassium oxide	K_2O	1.22	%
Titanium dioxide	TiO_2	0.26	%
Loss on ignition	L.O.I.	15.00	%
Potential of hydrogen	pH	5 to 8	-

3.1.1.3 Soil Characterization

As described on section 2.4.3, the artificial soil used on the manufacture of the blocks followed the same composition as used by Nepomuceno [46]. Hence, the soil limits of plasticity and liquidity, maximum dry unit weight, optimum water content and the granulometry are the same as those obtained by the author. These results, obtained for an artificial soil composed by 70% of sand and 30% of kaolin (in weight), are presented below on Figure 27 and Table 6.

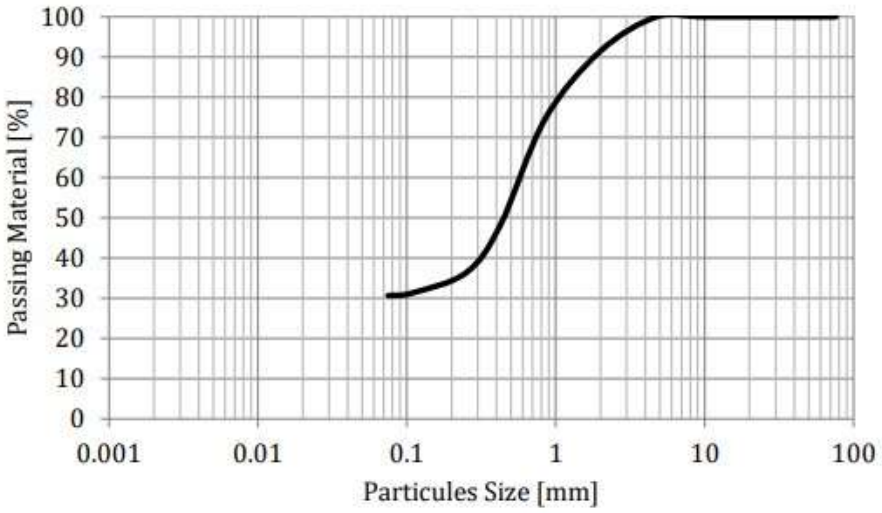

Figure 27: Artificial soil grain curve [46].

Table 6: Consistency Limits of the artificial soil (adapted from [46]).

Consistency Limits	Value	Unit
Liquid Limit	43.5	%
Plastic Limit	25.8	%
Plasticity Index	17.1	%

The granulometric curve of the soil was obtained by wet sieving according to LNEC E 239 [60]. The consistency limits were calculated as described by NP EN 143 [61]. Through the analysis, the artificial soil presents properties of a Clayey Sand (SC), according to the unified classification of soils ASTM D 2487 and can be classified as A2-7 according to the classification of AASHTO M 145-91 [62], [63]. Figure 28 shows the proctor compaction of the artificial soil. The maximum dry unit weight (γ_d) and optimum water content (ω) were obtained according to LNEC E 197 [46], [64].

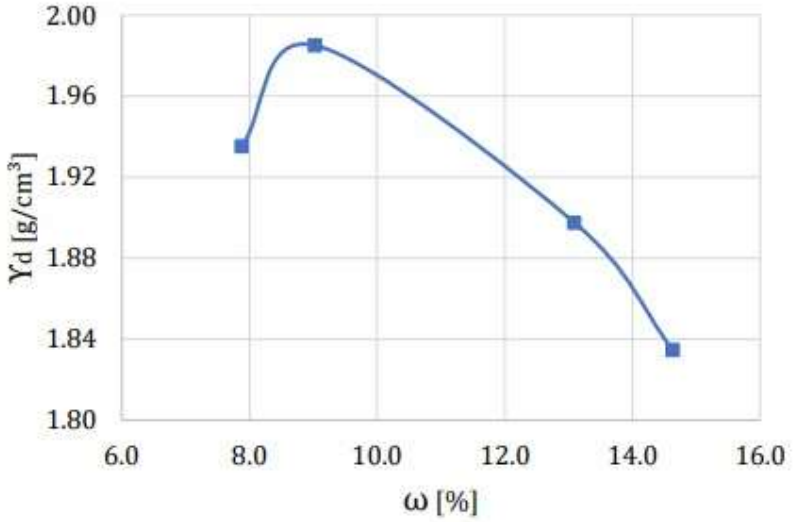

Figure 28: Proctor compaction of the artificial soil [46].

3.1.2 Cement

The used cement was from SECIL brand, type CEM II / B-L 32.5 N. The characteristics presented in the technical file of the product are shown in Table 7.

Table 7: Cement characteristics [65].

Item	Specified Value	Performance	Unit
Composition			
Clinker	65 to 79	-	%
Limestone	21 to 35	-	%
Other constituents	0 to 5	-	%
Chemical Properties			
SO_3 content	≤ 3.50	Conform	%
Chloride content	≤ 0.10	Conform	%
Physical Properties			
Initial setting	≥ 75	Conform	min
Expandability	≤ 10	Conform	min

3.1.3 Municipal Waste

The municipal waste incorporated into the CEBs during the research were provided by the company Resíduos do Nordeste, located in Mirandela, Portugal. The material consists of an organic compound of class IIA quality, normally used for arboreal and shrubby agricultural crops and results from the biological treatment of municipal solid waste (as shown on Figure 29). This waste is collected in the Northeast Trás-os-Montes region and

data show an average production of 140 tons/day. The composition of the waste is presented on Table 8.

Table 8: Municipal waste composition (supplied by the company Resíduos do Nordeste).

Component	Value	Unit
Humidity	29.6	%
Organic matter	48.8	%
Organic carbon	27.1	%
Nitrogen (N)	1.3	%
Phosphorus (P_2O_5)	1.1	%
Potassium (K_2O)	1.4	%
Calcium (Ca)	4.9	%
Magnesium (Mg)	0.8	%
Sulfur (S)	0.6	%
Boron (B)	43.4	mg/kg
Cadmium (Cd)	0.9	mg/kg
Chromium (Cr)	130	mg/kg
Copper (Cu)	209.7	mg/kg
Mercury (Hg)	0.4	mg/kg
Nickel (Ni)	49	mg/kg
Lead (Pb)	110	mg/kg
Zinc (Zn)	453	mg/kg
Salmonella spp. (Fresh matter, 25g)	Absent	-
Escherichia coli (Fresh matter)	460	nº/g
Weed plants (Fresh matter)	0	-
Anthropogenic inerts	0.7	%
C/N ratio	20.9	-
Density	0.45	g/cm³
Electrical conductivity (Fresh matter)	2.5	mS/cm
pH (Fresh matter)	8.0	-

Figure 29: Municipal waste to be incorporated into the CEBs.

3.1.4 Water

The water supplied for the public network of Bragança, Portugal, was used in the blocks manufacture.

3.2 Manufacture of the CEBs

As presented on section 2.4.3, this work is a continuation of the work made by Nepomuceno to analyse the viability of municipal organic wastes incorporation on CEBs [46]. Since the only specimens tested by Nepomuceno that met all the evaluated criteria were $SC_{10}R_{20}$ (see compositions on Table 1) the blocks were manufactured following the proportions used on this composition. Each block was manufactured with a total amount of 3820 grams of material. The amount of water used on the blocks was stablished according to the optimum water content presented on Figure 28. The quantity of materials per block is presented on Table 9. The geometry of the blocks is shown on Figure 30.

Table 9: Quantity of each material per block.

Material	Weight (g)	Percentage of the total weight
Sand	2004.44	52.47%
Kaolin	1073.82	28.11%
Cement	316.56	8.29%
Waste	87.41	2.29%
Water	337.78	8.84%
Total	**3820.00**	**100.00%**

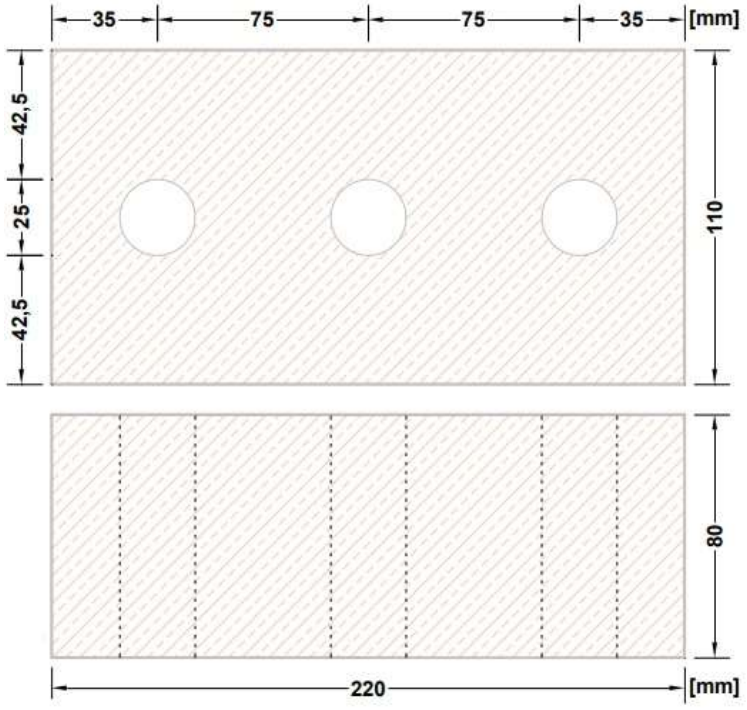

Figure 30: Geometry of the blocks.

To manufacture the blocks, the proportion of the dry materials was weighted and mixed manually. Then, the amount of water was added and the material was mixed in a mortar mixer (Figure 31).

Figure 31: Materials prepared to be mixed in a mortar mixer.

With the homogeneous mixture, each block was individually moulded and compacted. At this stage, the material was inserted into the mould and compacted in a mechanical press (model Instron® series 4485) using its final displacement as a stopping criterion. After compaction, the mechanical press is again used to demould the block by applying forces on the metal sides of the mould to separate it from the block. Figure 32 shows steps of the blocks manufacture. The compaction pressure applied on each block is presented on ANNEX A.

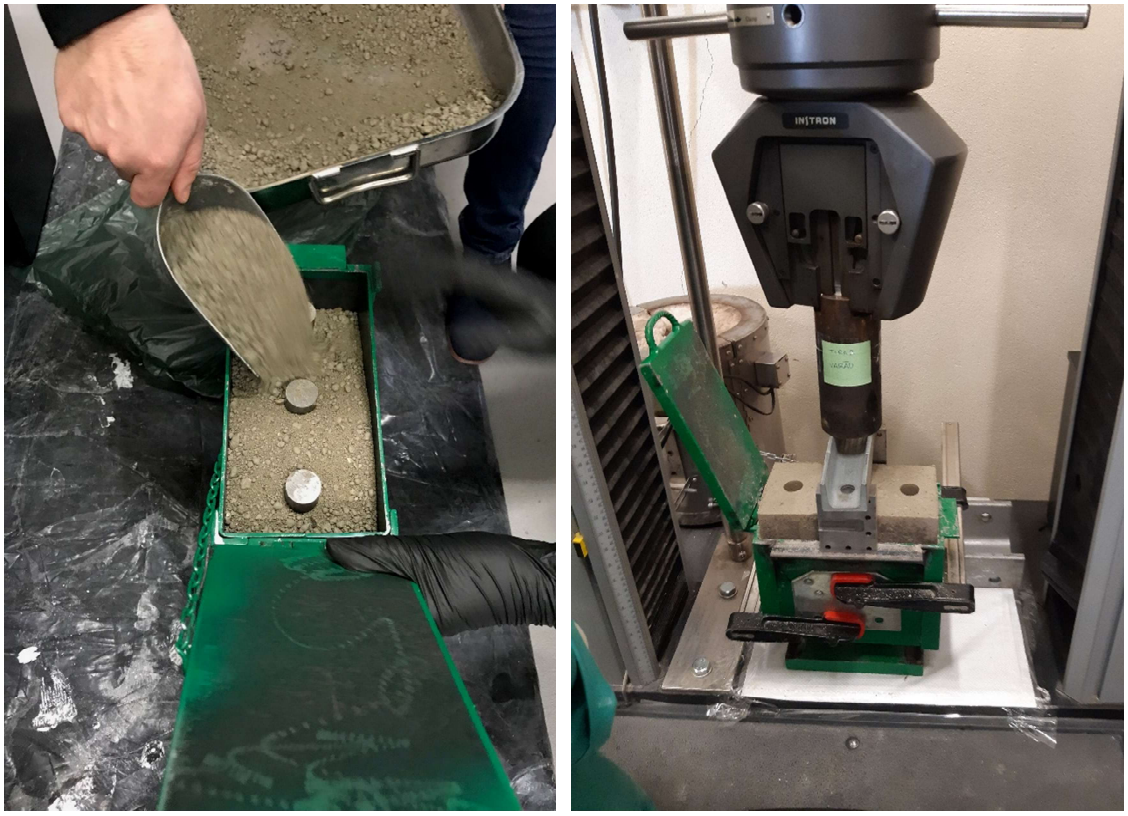

a) b)

Figure 32: a) Material being inserted in the mould. b) Mechanical press being used to demould a block.

After the manufacture, the blocks were transferred to a humid chamber to guarantee their curing process at a temperature of ± 20 ºC and constant humidity of 95% (Figure 33).

Figure 33: Blocks during the cure process in humid chamber.

3.3 Manufacture of Prism Specimens

To assess the thermal behaviour of the CEBs, prism specimens were manufactured using the same composition as the blocks described on section 3.2. Besides, in order to evaluate the influence of the municipal waste on the blocks, specimens without the incorporated waste were also fabricated. Table 10 presents the amount of each material used on the manufacture of the prism specimens.

Table 10: Quantity of each material per prism specimen.

Specimen	**Weight (g)**				
	Artificial Soil	Cement	Waste	Water	**Total**
With waste	1513	156	43	166	**1878**
Without waste	1556	156	0	166	**1878**

The specimens were fabricated using a metallic mould with 150x150 [mm^2], and with 40 mm width. In a similar procedure as the CEBs, the proportion of the dry materials was weighted and mixed manually. Then, the amount of water was added, and the material was mixed in a mortar mixer. With the homogeneous mixture, each specimen was individually moulded and compacted. At this stage, the material was inserted into the metallic mould, then a metal plate was placed above the mixture and the assemble was compacted in the same mechanical press (model Instron® series 4485) as the blocks, but

using the applied force as stopping criterion (the maximum applied force was calculated so the specimens would have been compacted with the same compaction pressure as the average value for the blocks). After compaction, the specimens were demoulded by disassemble of the metallic mould and then transferred to a humid chamber to guarantee their curing process at a temperature of ± 20 ºC and constant humidity of 95%. Figure 34 presents the stages of compaction and demoulding of the manufacture of the prism specimens.

a) b)

Figure 34: Manufacture of the prism specimen: a) compaction; b) demoulding.

3.4 Porosity and Bulk Density of the CEBs

3.4.1 Le Chatelier Flask

Porosity and bulk density of the CEBs were determined using a Le Chatelier flask (Figure 35), according to the Chinese Standard GB/T-208 [66] and American Society for Testing and Materials ASTM C188 [67]. The tests were carried out on the Laboratory of Chemical Process of the IPB.

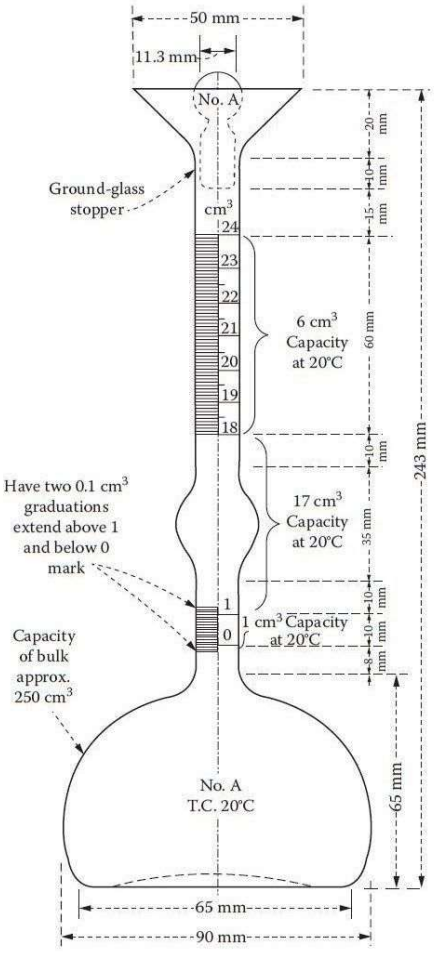

Figure 35: Le Chatelier flask for density and porosity test [67].

To perform the tests, two of the prism specimens (one with and one without waste incorporation) were weighted (M_{ceb}) and measured ($V_{ceb)}$ (to allow the calculation of their densities) and then smashed and milled using a basic analytical mill. The powders were kept in an oven at constant temperature of 105ºC for 24 hours to assure the complete evaporation of the non-combined water, and then put into a desiccant dryer to avoid atmospheric humidity absorptions. Three tests were performed for each specimen.

As prescribed on the ASTM C188 standard, a reference test using anhydrous kerosene was performed for both compositions. The standard allows the substitution of the kerosene for another liquid if verified that a single operator can obtain results within ± 30 kg/m^3 when compared to the kerosene ones. As reported by Helsel *et al* (2016), when measuring density of cement powders, kerosene is often replaced by isopropyl alcohol (IPA) or another readily available organic chemical. Helsel also reports that for density tests, IPA results in the lowest standard deviation, smallest average percent error, and

minimal temperature sensitivity when compared to the anhydrous kerosene. Hence, the two complementary tests for each composition were performed using IPA [67], [68].

At the beginning of the test, the liquid is poured into the flask until it reaches between 0 and 1 on the lower graduation scale. Then, the flask is stuffed by cap and put into thermostatic water bath (20 ºC) for 30 minutes. At the end of this period, the liquid volume (V_1) is denoted and a mass (m) of the dried powder is added into the flask using a funnel to prevent the material from sticking into the sides. To completely release the air from the liquid, the flask is wobbled and posteriorly stuffed by cap. Then, the flask is put into thermostatic water bath for another 30 minutes and the level (V_2) is denoted at the end of this period. Afterwards, the porosity (ε) and the bulk density (ρ) of the material can be calculated through the following relations:

$$\rho_{powder} = \frac{m}{V_{2-}V_1}, \qquad \rho_{CSEB} = \frac{m}{V_{CEB}}, \qquad \varepsilon = 1 - \frac{\rho_{CSEB}}{\rho_{powder}}$$

Figure 36 shows the steps of the Le Chatelier flask test.

a) Powders on desiccant drier;

b) Flasks on thermostatic water bath;

c) Mass being added to the flask;

d) Flask at the end of the test.

Figure 36: Le Chatelier flask test.

3.4.2 Picnometer Tests

To determine the density of the dry powder of the CEBs used on the Le Chatelier Flask method, Picnometer tests were also performed (Figure 37). At the beginning of the test, the 100 mL capacity picnometer flask is weighted and then filled with distilled water until it reaches its reference volume, then it is weighted once again. To assure the temperature of the water, it was kept for 30 minutes on thermostatic water bath (20ºC) before the test. From the ratio between the water mass and the picnometer volume, the density of the distilled water can thus be calculated. Then, the water is discarded and a mass (m) of the powder is put into the picnometer. Hence, the flask is filled with distilled water until it reaches its reference volume. From the mass of water on the picnometer, its volume can be calculated. Thus, the remaining volume of the flask represents the volume of the powder. Therefore, the bulk density of the dry powder can be assessed through the ratio between its mass (m) and its volume. The tests were performed for each composition and were carried out at the Laboratory of Chemical Process of IPB.

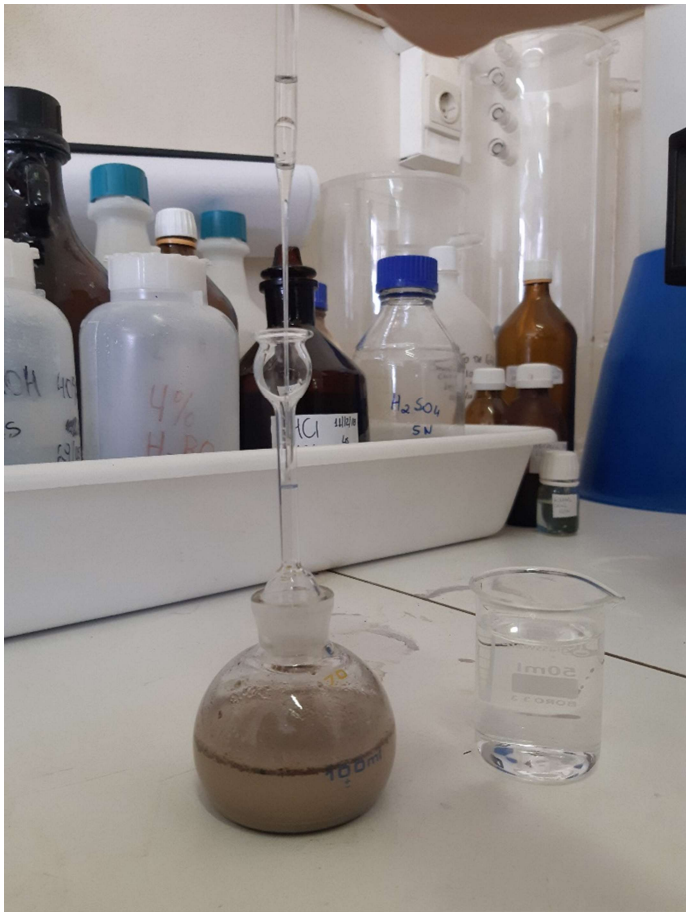

Figure 37: Picnometer test.

3.5 Thermal Properties of the CEBs

As presented on section 2.5, bibliographic researches evidenced a real lack of CEBs materials thermal properties in function of temperature. In order to overcome this problem, experimental tests were conducted to provide a background about CEBs thermal properties varying with temperature. Information about the performed tests are following presented.

3.5.1 Thermogravimetry

Thermogravimetric and differential thermogravimetric analyses were conducted to the artificial soil, the cement, the municipal waste and for two compositions of CEB (with and without waste).

Different samples of cement and artificial soil were prepared dehydrated and moistened with the same water/soil mass ratio as the CEB blocks described on section 3.2. The samples were kept in humid chamber with constant temperature of ± 20 ºC and constant humidity of 95%.

The waste sample was prepared by milling the material in a basic analytical mill. Figure 38 shows the aspect of the waste after milling.

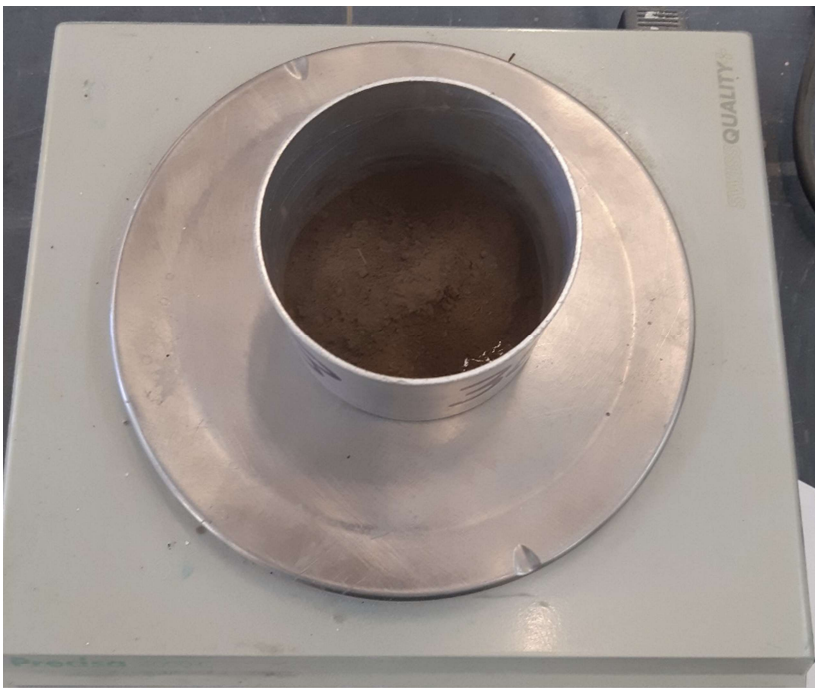

Figure 38: Aspect of the waste after milling.

To execute the CEBs hydrated samples, two of the specimens described on section 3.3 were used (one with and one without incorporated waste). First, the specimens were cut into four similar parts with 7.5x7.5x4.0 [cm^3] each. One of these four parts were posteriorly smashed with a hammer and milled in the same basic analytical mill as the cement and soil samples (Figure 39).

Figure 39: Basic analytic mill used for milling the waste and CEBs samples.

All the thermogravimetries were performed in TG/DTG Instrument Netzsch TG 209 F3 Tarsus® from the Laboratory of Applied Chemistry of the IPB (Figure 40). Tests were executed at a constant heat rating of 10ºC/min, in a temperature range from 20ºC to 800ºC. Nitrogen was used as purge gas in a flow of 40 mL/min. Before the execution of the tests, all the samples were kept for one day on a vacuum chamber to eliminate the residual non-combined free water (Figure 41).

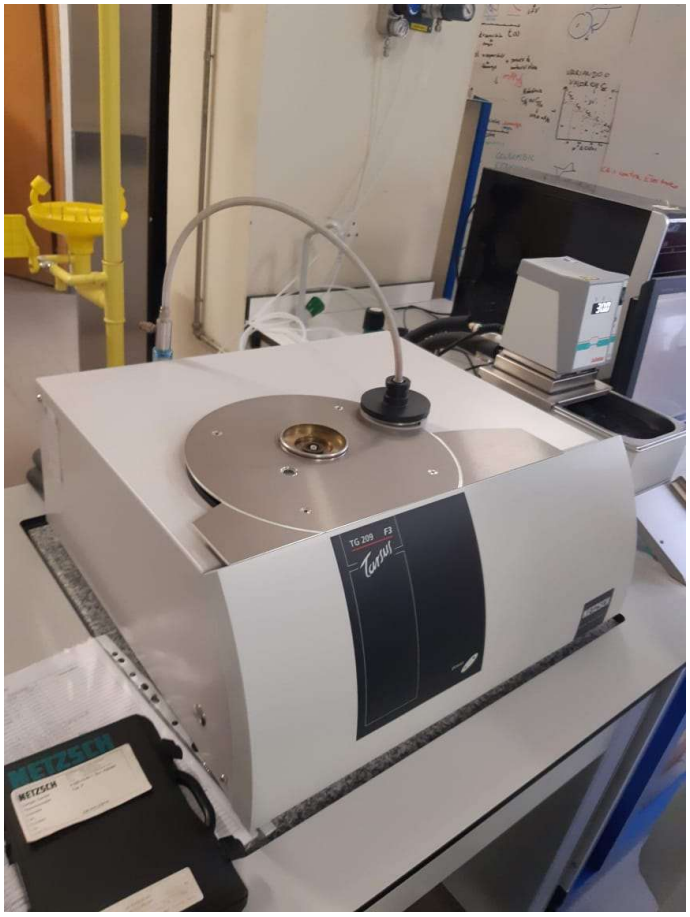

Figure 40: TG/DTG instrument Netzsch TG 209 F3 Tarsus.

Figure 41: Samples on vacuum chamber before thermogravimetry tests.

3.5.2 Transient Plane Source (TPS) Analyses

Transient plane source (TPS) techniques for measure thermal transport properties of materials arose in the decade of 1960s, developed by a Swedish physicist named Gustafsson. The aims of this techniques are to cover large ranges of transport properties and at the same time be applicable to a large number of different materials. This method is based on a transient plane source element, which is used both as a heat source and as a temperature sensor. The element consists of a pattern of thin layer of an electrically conducting material placed between two sample pieces, which its increase of temperature can be precisely deduced from a record of its resistance. The tests provide accurate data for the specific heat, the thermal diffusivity and the thermal conductivity of the material [78].

At the beginning of a TPS measure, the temperature of the specimen is stabilized and uniform, then a small disturbance in form of a heat pulse is applied to the specimen in the form of a stepwise function. From time response of temperature to this heat disturbance, thermophysical properties of the material are calculated based on a theoretical model that assumes the specimen as a semi-infinitum medium. Thus, the dimensions of the tested sample must be related to the depth of heat penetration of the heat pulse. Besides, the time of the transient recording must be chosen so the outer boundaries of the sample may not influence the temperature increase of the specimen to any measurable extent [79], [80].

To perform the test, the prism specimens described on section 3.3 were utilized. The remaining three cut parts of the specimens used for the Thermogravimetry analyses (described on section 3.5.1) were used. Additionally, two other specimens (one with and one without incorporated waste) were also cut into four similar parts with 7.5x7.5x4.0 [cm^3] to be used on the tests.

The TPS analyses were performed in Thermal Constant Analyzer - Hot Disk® TPS 2500S from Brigantia Ecopark (Figure 43). The temperature on the laboratory were controlled during all tests and kept constant at 20 ºC. The tests were conducted using a Kapton-insulated sensor (reference C5501, with 6.403 mm radius, as shown on Figure 42).

Figure 42: Kapton-insulated sensor used on TPS analyses [81].

To guarantee maximum homogeneity, the two samples pieces used at each run of the test were cut parts from the same prism specimen (described on section 3.3). The output heating power used on the tests was 100mW and the selected measure time was 20s.

Figure 43: Specimens during TPS analysis.

3.5.3 Guarded Hot Plate (GHP) Tests

Despite transient methods prominence has substantially increased over last years, steady state methods are still the most used to determine the thermal conductivity of insulating materials. Among the steady state measuring apparatus, the Guarded Hot Plate (GHP) is the most wildly used for this purpose. The equipment measurement is made based on the establishment of a steady state temperature gradient of a material with known cross-sectional area and width caused by a heat flux between two plates. The method is based on the assumption of an unidimensional conduction in which the temperature on each point of the system does not depends on the time. The experiments can be performed according to different international standards, such as ISO 8302, EN 1946-2, ENI12667, EN 12664, ENI12939, ASTM C177 and DIN 52612 [82], [83].

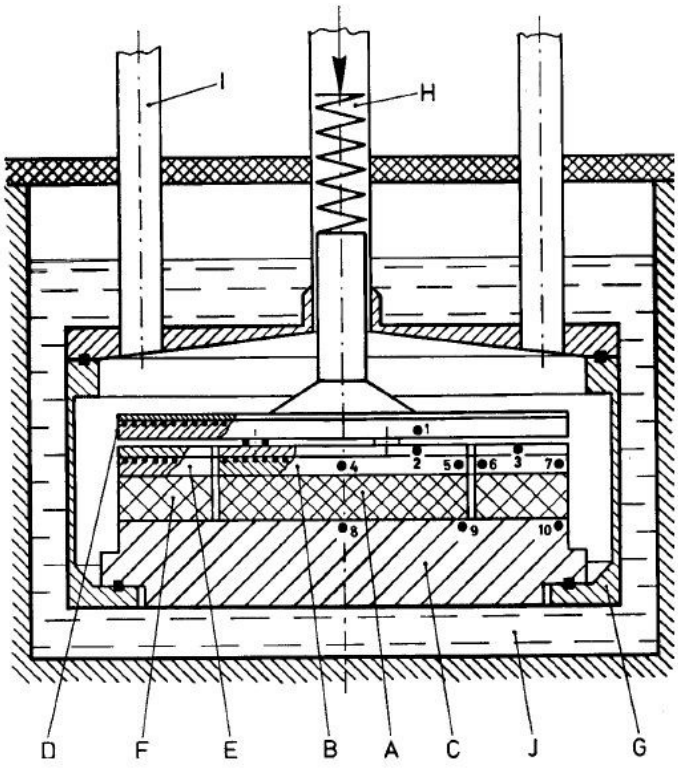

Figure 44: Schematic of a Guarded Hot Plate apparatus [83].

As shown on Figure 44, a Guarded Hot Plate apparatus consists on a stack accommodated in an evacuable casing (G). A prismatic solid sample (A) is placed between the upper electric hot plate (B) and the lower thermostated cold plate (C), with its lateral faces surrounded by edge insulation (F). A guard plate (D) and a guard ring (E) surround the hot plate to assure the establishment of a unidirectional and uniform heat flow. A push rod (H), which can be adjusted from the outside is used to ensure that the stack remains

tightly packed without the compression of the sample. The whole apparatus is immerged in a bath thermostat (J) [83].

To perform the test, the prism specimens described on section 3.3 were utilized. The analyses were performed in Lambda-Messtechnik® λ-Meter EP500e from Brigantia Ecopark (Figure 45). The tests were conducted for the temperatures of -10ºC, 0ºC, 10ºC, 20º, 30ºC, 40ºC and 50ºC, using a variation of less than 1% of the thermal conductivity measured value over a time of 180 minutes as stopping criterion.

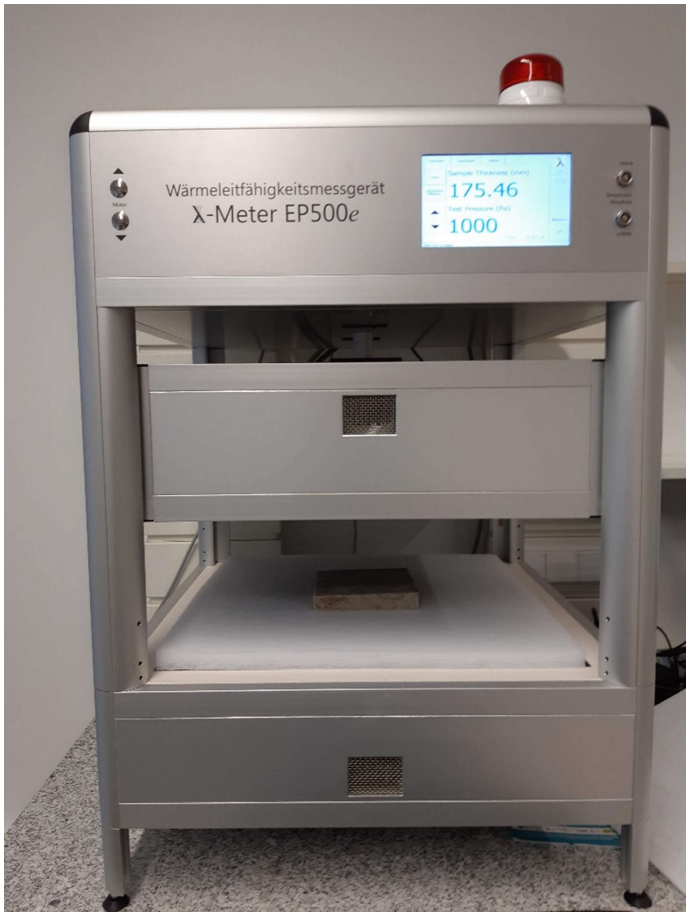

Figure 45: Lambda-Messtechnik® λ-Meter EP500e Guarded Hot Plate apparatus.

CHAPTER 4

PANEL FIRE RESISTANCE TEST - PRESCRIPTIONS

4.1 Manufacture of the CEBs panel

The panel was built internally in a metal frame suitable for fire tests, covered with refractory mortar. The dimensions of the wall follow the internal dimensions of the frame, being 1000 x 1000 [mm^2]. The panel was made in 11 interspersed rows in 3 different arrangements, being two of them with four entire blocks and a 60 mm cut block at opposite edges. The third kind of row consisted of 140 mm cut blocks at each extremity with three entire blocks in between. All horizontal and vertical joints between blocks were filled with a mortar layer of 10 mm of thickness. To ensure wall adhesion to the metal frame, the entire wall/frame interface was also filled with a layer of 10 mm thick mortar. To guarantee vertical and horizontal alignment, each block was positioned using a plumb line and a level. Wooden bars were also used to help ensuring the alignment between different rows of the wall. In order to avoid shrinkage effects, all the blocks were moistened before being layed. Figure 46 shows steps of the manufacture of the CEBs panel.

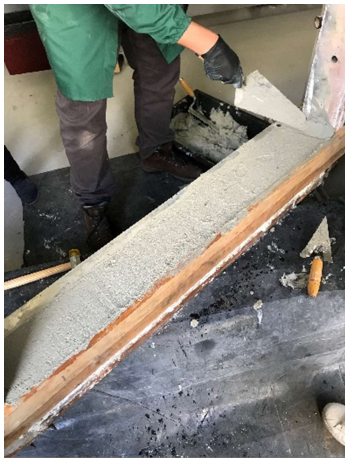

a) First mortar layer on the metal frame;

b) Moistening the blocks;

c) Aligning the rows;

d) Cleaning the panel;

Figure 46: CEBs panel during its execution.

4.2 Mortar

The mortar used to lay the CEBs was made with the same materials as the block (except for the waste). In order to enhance plasticity and workability of the material, a higher amount of water was used. The dry mass was made in a proportion of 90% artificial soil and 10% cement. Then, an amount of water equivalent to 35.7% of the dry weight was mixed to the material. To assess the mortar compressive resistance, six test specimens were moulded during the manufacture of the panel (Figure 47).

a) During moulding; b) After demoulded;

Figure 47: Mortar test specimens moulded during panel manufacture.

4.3 Instrumentation of the Panel

The instrumentation of the CEBs panel was performed in accordance with the provisions of the European Standards EN 1363-1 and EN 1364-1 [69], [70]. Five disc-thermocouples were set to the unexposed face of the wall (named as TDs), one of them being located at the central point of the panel and the others at the centre of each of the four quadrants formed from the first fixation. To monitor the temperature inside the blocks, six K-type thermocouples were set into drilling holes, being two of them at a depth of 27.5 mm, two at a depth of 55.0 mm and the remaining two at a depth 82.5 mm from the unexposed face (named as TBs). In addition to these, another five K-type thermocouples were set inside the central holes of the blocks (named as THs). To measure the temperature in the mortar, five K-type thermocouples (named as TMs) were inserted at the horizontal joints of the panel in a depth of 55 mm. Figure 48 presents the thermocouples position on the panel.

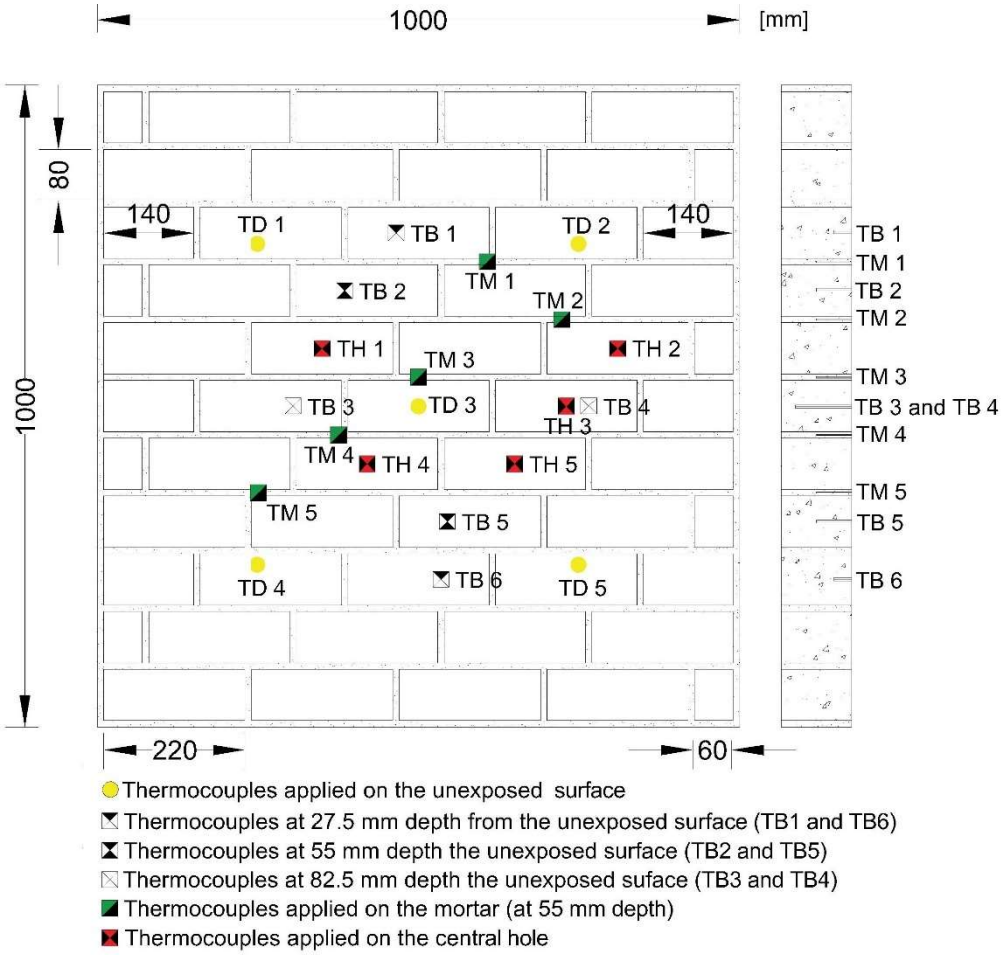

Figure 48: Position of the thermocouples on the panel.

The thermocouples inserted into the central holes of the blocks (TH) and the thermocouples placed in the mortar (TM) were positioned during the panel assemblage, as shown in Figure 49.

a) b)

Figure 49: a) TH thermocouple placed inside the hole of the block; b) TM thermocouple positioned to monitor mortar temperatures.

To ensure their protection, thermocouples positioned on the unexposed face of the panel (TDs) were welded to copper plates and overlaid by plasterboard. The blocks that were drilled for thermocouple insertion had their holes filled with mortar after their placement, as shown in Figure 50.

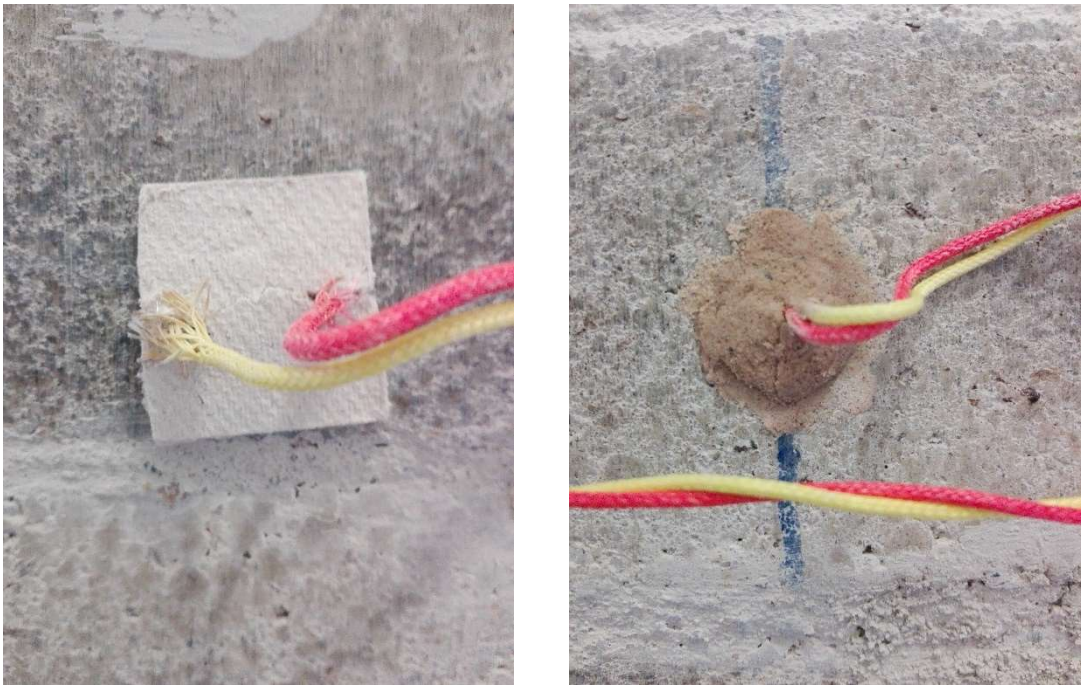

a) b)

Figure 50: a) TD thermocouple overlaid with plasterboard; b) TB thermocouple inserted in a drilling hole and filled with mortar

Figure 51 presents the panel seen from its unexposed surface with all the thermocouples properly positioned and instrumentalized.

Figure 51: View of the instrumentalized panel from its unexposed surface.

4.4 Data Acquisition System

The Laboratory of Structures and Materials Resistance of the IPB presents a MGC Plus data acquisition system, with 23 available channels (Figure 52). Each of the 21 thermocouples instrumented in the panel were connected to a channel of the system. The two remaining channels were used to monitor the ambient temperature and the temperature inside the furnace.

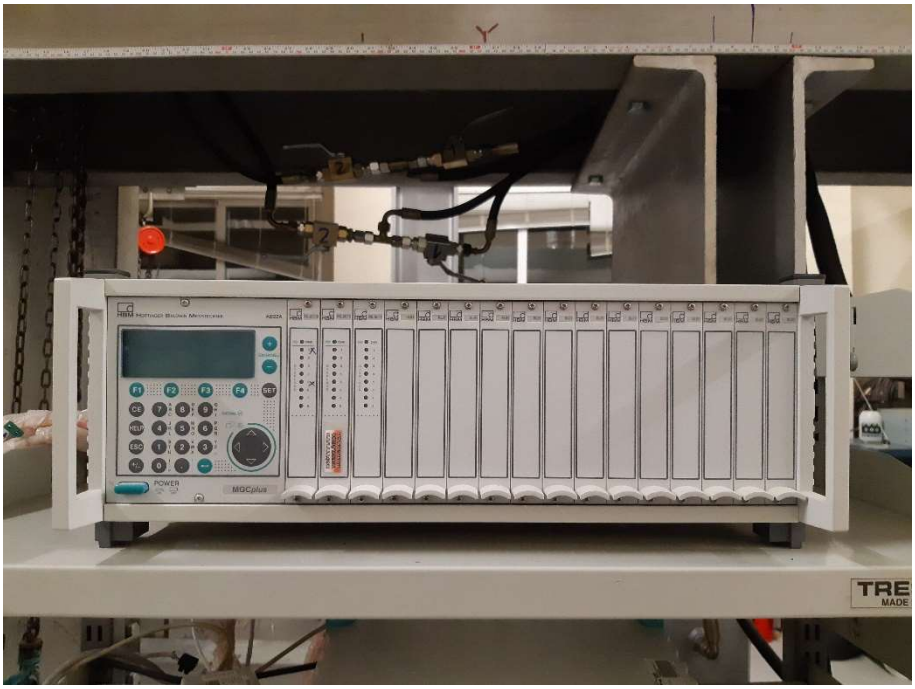

Figure 52: Data Acquisition System used to monitor temperatures during fire test.

4.5 Temperature of the Furnace

The temperature of the furnace during the test was programmed according to the prescriptions of ISO 834-1 standard (Figure 53) [71].

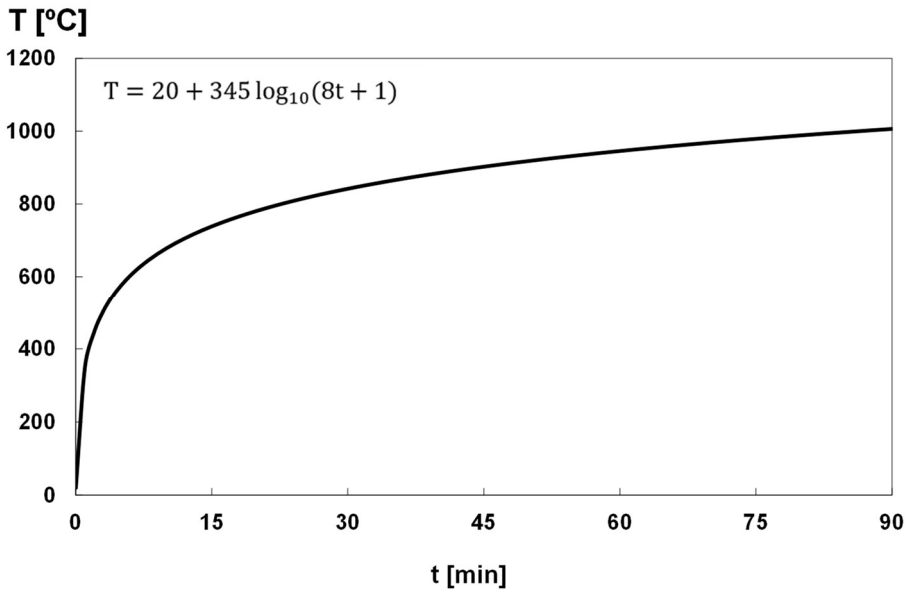

Figure 53: ISO 834-1 curve [71].

4.6 Test Prescriptions

The fire resistance test was conducted following the prescription of the European Standards EN 1363-1 and. EN 1364:1. According to these standards, two performance criteria were evaluated: the insulation and the integrity criteria. Fire insulation criterion is the time, in completed minutes, for which the test specimen continues to maintain its separating function during the test without developing temperatures on its unexposed side which increase the average temperature above the initial average temperature: i) by more than 140 °C (fire insulation criterion 1), ii) or increase more than 180 °C at any location of the unexposed side above the initial average temperature (fire insulation criterion 2). The fire integrity is the ability to prevent the fire and the smoke transmission through the element. The integrity criterion was verified throughout the experiments by employing a cotton wool pad saturated in ethyl alcohol [69], [70]. Throughout the test, the ambient temperature of the laboratory was monitored at a distance of 1 m horizontally away of the unexposed surface of the panel, such as the sensor is not affected by the thermal radiation emitted during the test (Figure 54).

Figure 54: Thermocouple installed to monitor the ambient temperature at the laboratory during fire test.

The test was performed over a period of 90 min corresponding to a maximum real temperature in the furnace of 1000 ºC. In order to evaluate insulation criterion, temperatures at the unexposed side of the panel were continuously monitored through

infrared thermography (instrument Infrared Detector – FLIR SC7000 – Picture in Picture), as shown on Figure 55.

Figure 55: Infrared Camera monitoring the temperature of the unexposed surface of the panel.

4.7 Compressive Resistance of the Blocks

To assess the mechanical behaviour of the CEBs with incorporated waste when submitted to high temperatures, compressive resistance tests were conducted on blocks after the fire resistance test. In order to evaluate the influence of heating, reference blocks with and without waste incorporation, which were not submitted to high temperatures, were tested as well. The tests were conducted at the Laboratory of Structures and Materials Resistance of the IPB, using a mechanical press model Instron® series 4485 (the same used to manufacture the blocks and presented on Figure 32).

CHAPTER 5

EXPERIMENTAL RESULTS

Experimental results of the tests described on Chapter 3 and Chapter 4 are following presented.

5.1 Le Chatelier Flask

As presented on section 3.4.1, the first step to execute the Le Chatelier Flask tests consisted on the determination of the bulk density of the prism specimens. Table 11 shows the calculated bulk density for each specimen. All the dimensions were measured using a digital calliper and the masses using a scale with 0.01g precision.

Table 11: Bulk density of the prism specimens.

Specimen	Dimensions (cm)			Volume (cm^3)	Mass (g)	Bulk Density (g/cm^3)
	Side 1	Side 2	Width			
Without Waste	15.335	15.214	4.051	945.125	1861.86	1.970
With Waste	15.343	15.171	3.936	916.177	1852.63	2.022

The following step to perform the tests consisted on smashing and milling the specimens. Then, the bulk density presented on Table 11 was used to determine the volume of the powder added on the flask during the tests. In this stage, the masses of the material were determined using a scale with 0.0001g precision. Results obtained in each of the tests are shown on Table 12.

Table 12: Results of the Le Chatelier Flask tests.

	Without Waste			With Waste		
	Test 1	Test 2	Test 3	Test 1	Test 2	Test 3
Liquid:	Kerosene	IPA	IPA	Kerosene	IPA	IPA
V_1 (cm^3):	0.3	0.0	0.0	0.9	0.0	0.0
m_1 (g):	57.0084	60.0264	60.0456	60.8897	59.9840	60.0757
V_2 (cm^3):	22.0	22.8	23.0	23.2	21.9	21.9
ρ_{powder} (g/cm^3):	2.627	2.633	2.611	2.730	2.739	2.743
Porosity:	25.01%	25.17%	24.54%	25.94%	26.17%	26.29%

From Table 12, one can see that the results obtained for the isopropyl alcohol (IPA) comply with the prescriptions of the ASTM C188 standard, once the density of the

powder do not differ more than ±0.3 g/cm^3 when compared to the ones obtained with the anhydrous kerosene [67]. Table 13 synthetizes the results obtained on the tests and presents the average values for the bulk density of the powders and the porosity of the specimens.

Table 13: Average values obtained on Le Chatelier flask tests.

	Without Waste	With Waste
ρ_{powder} (g/cm³):	2.624	2.738
Porosity:	24.91%	26.13%

The porosity values obtained on the Le Chatelier flask tests comply with the results obtained by Zhang et al (2017), which stablish that CEBs with a 9% mass content of cement (slightly smaller than the used on this research) and bulk density around 2.00 g/cm^3 present porosity values around 24% [52].

5.2 Picnometer Tests

Picnometer tests were conducted as described on section 3.4.2. The first procedure to perform the tests was the determination of the density of the distilled water (at a constant temperature of 20 ºC). Table 14 shows the results obtained on this stage.

Table 14: Density of distilled water

Description	**Value**
Mass of water (g):	105.343
Volume of the Picnometer (cm³):	100
Density (g/cm³):	1.053

Afterwards, once the density of the distilled was known, the tests to determine the density of the powders were performed. All the masses presented on this section were measured on a scale with 0.0001g precision. Table 15 presents the results obtained on these tests.

Table 15: Density of the powders determined through picnometer tests.

Description	Without waste	With Waste
Mass of powder (g):	10.7500	10.8020
Mass of water (g):	101.0550	101.1417
Volume of water (cm^3):	95.929	96.012
Volume of powder (cm^3):	4.071	3.988
Density of powder(g/cm^3):	2.641	2.708

From Table 15 one can see the obtained results comply with the values obtained on Le Chatelier Flask tests, presented on section 5.

5.3 Thermogravimetric Results

The results obtained on the Thermogravimetric analyses described on section 3.5.1 are following presented.

5.3.1 Artificial Soil

Figure 56 presents the thermogravimetric analysis of the artificial soil. As presented on section 3.1.1, the artificial soil was composed by a mixture of sand and kaolin.

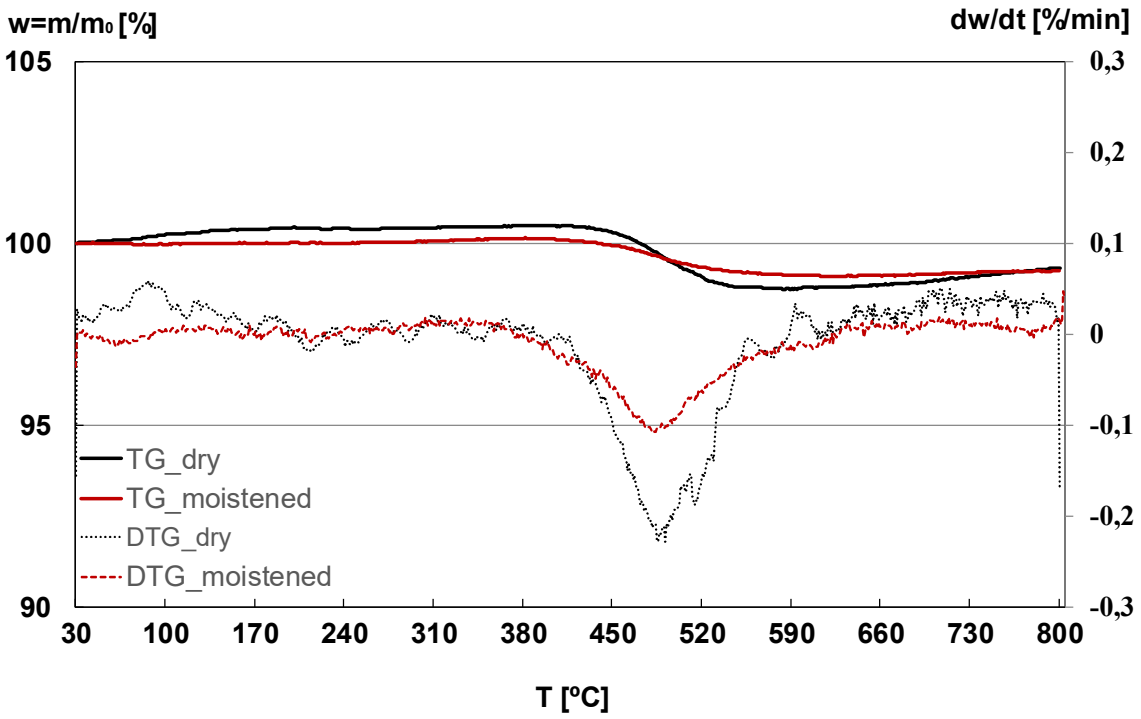

Figure 56: Thermogravimetric analysis of the artificial soil.

From Figure 56 analysis one can see that until 400 ºC there is an increase on the mass of the sample. This is due to reaction between the artificial soil and the oxidative atmosphere used on the test. Then, major changes are reported from 400 ºC to 600 ºC, interval in which the kaolinite dehydroxylation takes place. During this reaction, occurs the thermal decomposition of the kaolinite lattice and the chemically bounds OH groups are removed, resulting in the formation of an amorphous metakaolinite phase. In this same interval, more precisely at 573 ºC, occurs the transition of α-quartz to β-quartz particles of the sand. However, this transition is superimposed by the described dehydroxylation of the kaolinite due to the difference between the enthalpy of these reactions (220 kJ mol^{-1} for the dehydroxylation and 45 kJ mol^{-1} for the transition). Thus, the results are in accordance to the reported by Ondruska *et al* (2020), evidencing that the overall mass change during the analysis is more affected by the kaolinite content than the quartz particles of the sand [56], [72], [73].

5.3.2 Cement

Figure 57 presents the thermogravimetric analysis of the cement.

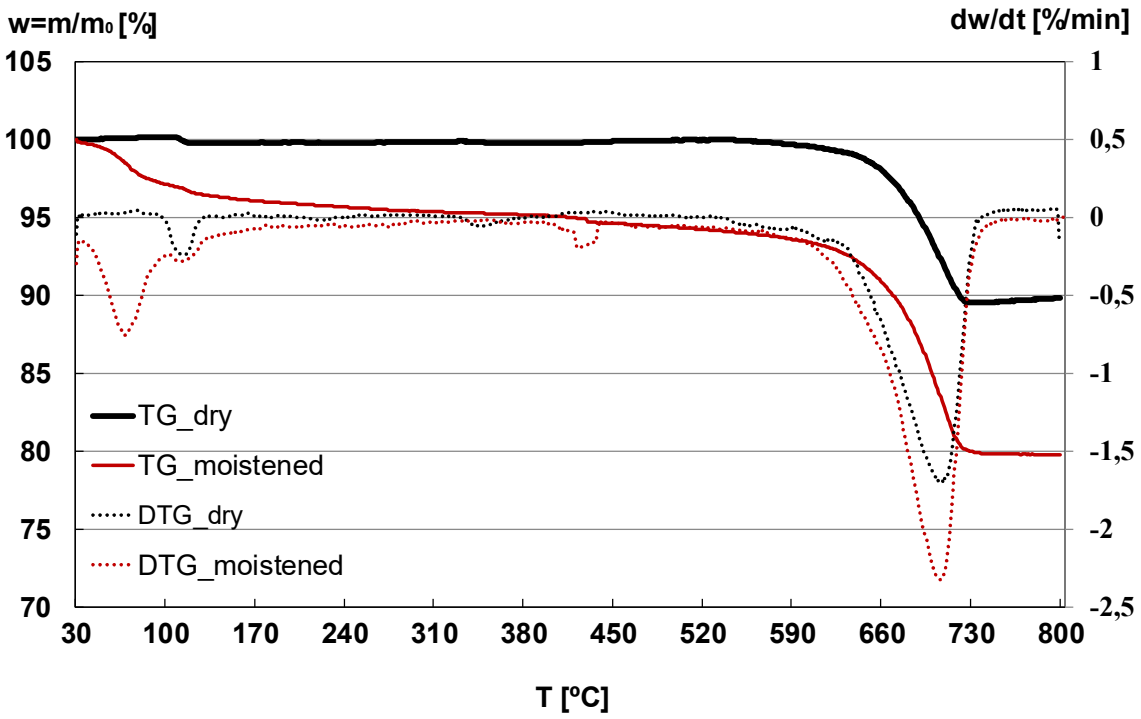

Figure 57: Thermogravimetric analysis of the cement.

From Figure 57 analysis, two peaks of DTG values are reported. The first one occurs between 50 ºC to 150 ºC, interval in which the dehydration of di-hydrated calcium sulphate takes place. This peak is slighter in the dry specimen once it was not hydrated, however it is still noticeable since Portland cement may content calcium sulphates from its manufacture (in anhydrous, mono- and di-hydrated phases), used to retard the setting time of the cement. The second peak, which takes place between 550 ºC and 730 ºC, corresponds to the decarbonation of the calcium carbonate which was aggregated to the clinker during cement manufacture [57], [74]–[76] .

5.3.3 Municipal Waste

Figure 58 presents the thermogravimetric analysis of the municipal waste.

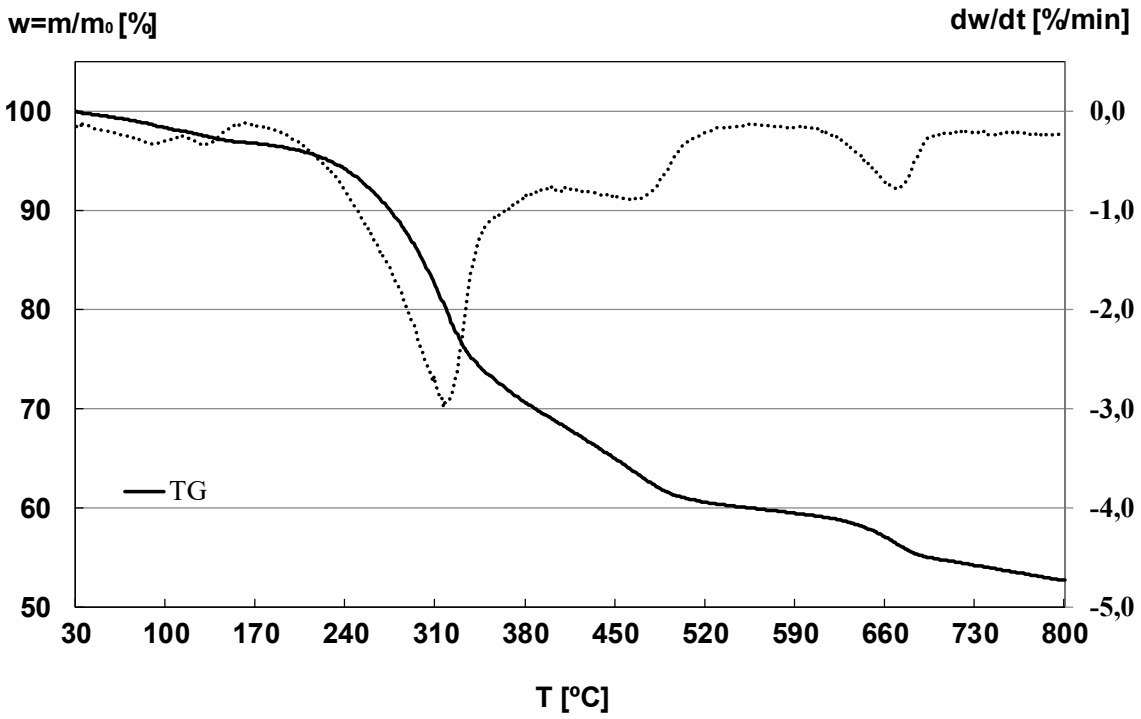

Figure 58: Thermogravimetric analysis of the municipal organic waste.

As described on section 3.1.3, the waste incorporated into the CEBs consists of an organic compound resulted from the biological treatment of municipal solid waste. Therefore, due to the high heterogeneity of the material and for the purposes of the present research, no further analysis of the reactions in function of the temperature intervals on the waste were evaluated. However, the obtained results are in accordance to the waste composition provided by the company *Resíduos do Nordeste*, which stablished a 48.8% amount of organic matter. At the end of the thermogravimetric analysis the residual mass of the sample was of 52.69% of the initial mass, in consonance to the amount of organic matter (which was expected to entirely degrade during the TG analysis).

5.3.4 Compressed Earth Blocks

Figure 59 presents the thermogravimetric analysis of the CEBs with and without incorporated waste.

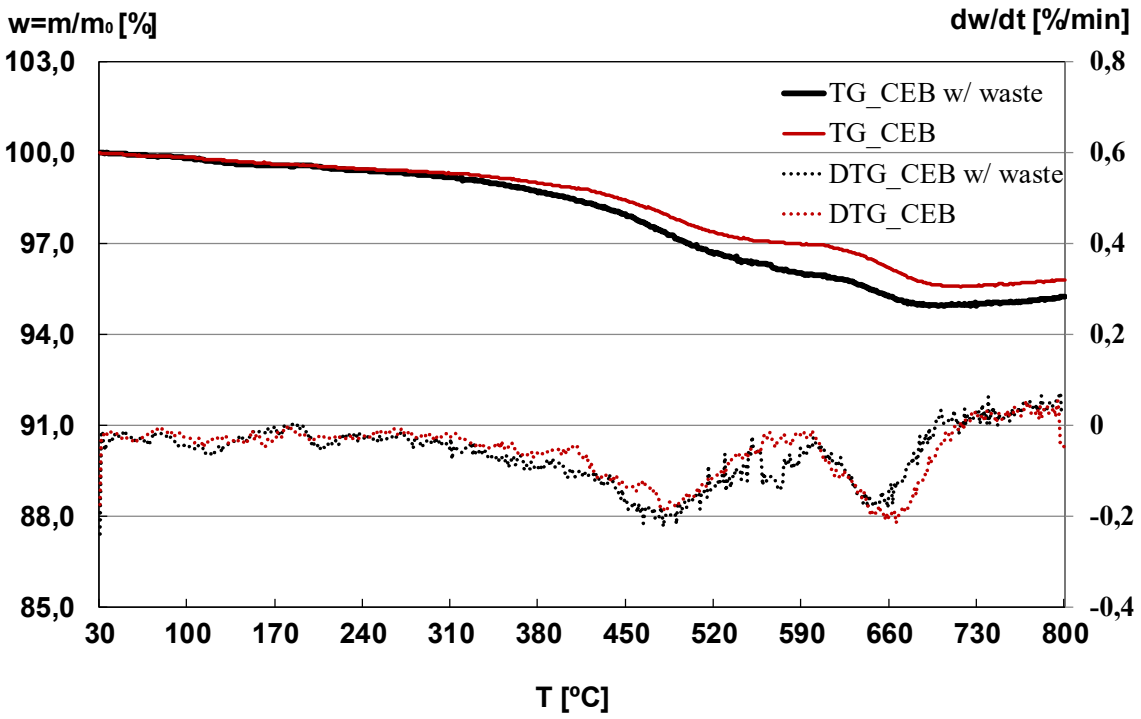

Figure 59: Thermogravimetric analyses of the CEBs with and without incorporated waste.

Figure 59 analyses can be assessed through the cement and artificial soil reactions. As described on section 5.3.2, from 100 ºC to 150 ºC occurs the dehydration of di-hydrated calcium sulphates on the cement. Simultaneously, from 30 ºC to 200ºC takes place the dehydration of the tobermorite and ettringite phases formed during the hydration of the blocks. Between 200 ºC and 350 ºC a slow decrease in the sample's mass is noticed due to the decomposition of other cement hydrated phases. From 350 ºC to 450 ºC occurs a dehydroxylation phenomenon due to the decomposition of the cement's calcium hydroxide. The end of this reaction is superimposed by the kaolinite dehydroxylation described on section 5.3.1, which takes place between 400 ºC and 600ºC. From 550 ºC to 730ºC a DTG peak is noticed, which corresponds to the decarbonation of calcium carbonate on the cement content of the blocks [57], [72], [73], [75]–[77].

At the end of the tests, the CEB sample with waste incorporation presented a residual mass of 95.23% of the initial mass. This value for the sample without waste was 95.79%. The difference between these values (0.56%) may explained by the degradation of the organic matter present in the waste.

5.4 Transient Plane Source (TPS) Results

As described on section 3.5.2, twenty-seven TPS tests were conducted for the specimens with incorporated waste and twenty-seven for the specimens without the waste. The entire results are presented individually on ANNEX B. Table 16 shows the average and standard deviations obtained on these tests. TPS results provide data for thermal conductivity, thermal diffusivity and volumetric specific heat for the tests. The specific heat per unit mass was calculated by the ratio of the volumetric specific heat and the bulk density of the specimens (calculated by Le Chatelier flask tests and presented on Table 13).

Table 16: TPS analyses results.

Specimen	**Thermal Conductivity [W/mK]**		**Thermal Diffusivity [mm²/s]**		**Volumetric Specific Heat [MJ/m³K]**		**Specific Heat per unit mass [J/KgK]**
	Average	Standard Deviation	Average	Standard Deviation	Average	Standard Deviation	
Without Waste	1.774	0.077	1.202	0.068	1.482	0.115	752.274
With Waste	1.380	0.070	1.074	0.065	1.291	0.115	638.542

The obtained results comply with the thermal properties data found on bibliographic research about compressed earth blocks. According to Mansour *et al* (2016), CEBs with 25% porosity present thermal conductivity values around 1.35 W/mK (see Figure 22 on section 2.5.1). Even that the thermal conductivity obtained for the CEBs without incorporated waste is higher than this value, this might be explained by the higher compaction pressure and higher percentage of cement content on the blocks, which according to Saidi *et al* (2018) influence on their thermal properties. Another aspect which interferes on the measured values is the use of an artificial soil instead of natural ones, as used on the other researches [51], [53].

According to Mansour *et al*, CEBs with bulk density around 2.00 g/cm^3 present thermal diffusivity of 1.2 mm^2/s, which also complies with the values obtained on the TPS tests. For the specific heat per unit mass, the obtained values are higher than those found by Mansour *et al* (around 520 J/KgK, for CEBs with bulk density of 2.00g/cm^3), which may be explained by the same reasons as the higher thermal conductivity values described on the paragraph above [51].

5.5 Guarded Hot Plate (GHP) Results

Guarded Hot Plate (GHP) tests were conducted as described on section 3.5.3. The entire results are presented individually on ANNEX C. Figure 60 presents the average obtained results for each temperature for the specimens with and without incorporated waste. From Figure 60 analysis, one can see that the obtained thermal conductivity results differ significantly when compared to the TPS ones and to those found on the bibliographic research (presented on section 2.5.1). This significant difference leads to conclude that the obtained results were inaccurate. This inaccuracy may be a consequence of the irregularity of the specimens. According to Hammerschmidt (2002), to obtain accurate GHP results, the plane parallelism of the top and the bottom surfaces of the specimens should not exceed ±0.1mm, however, due to the roughness of specimens this aspect was not attained [83].

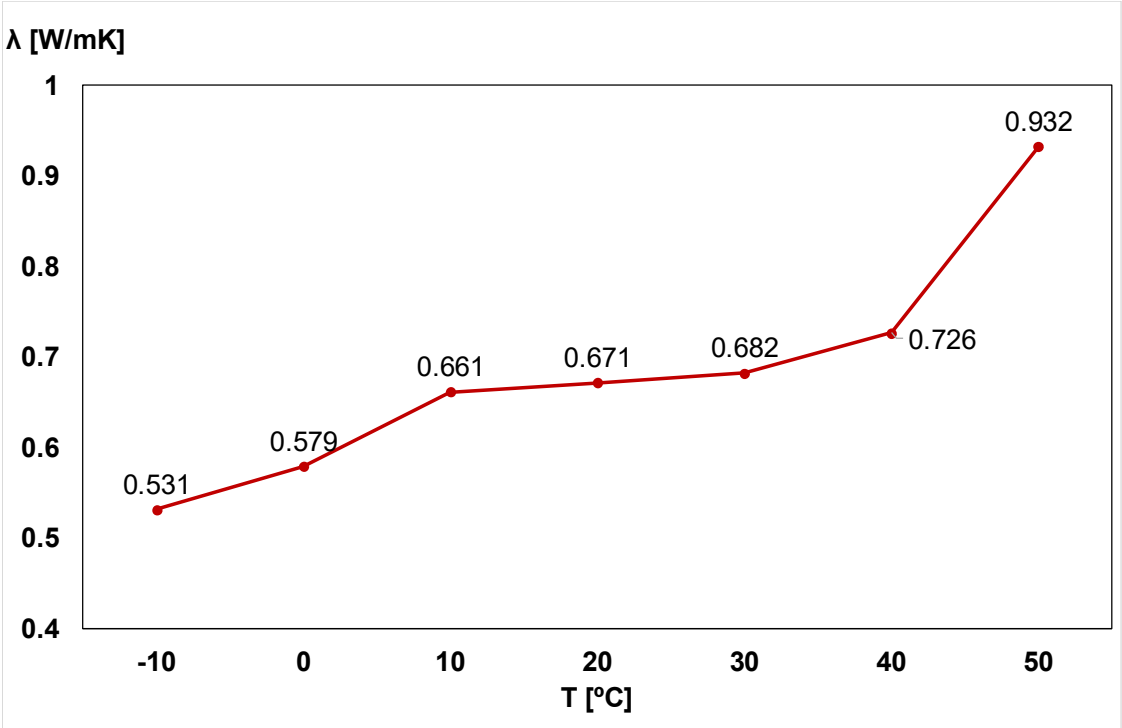

a)

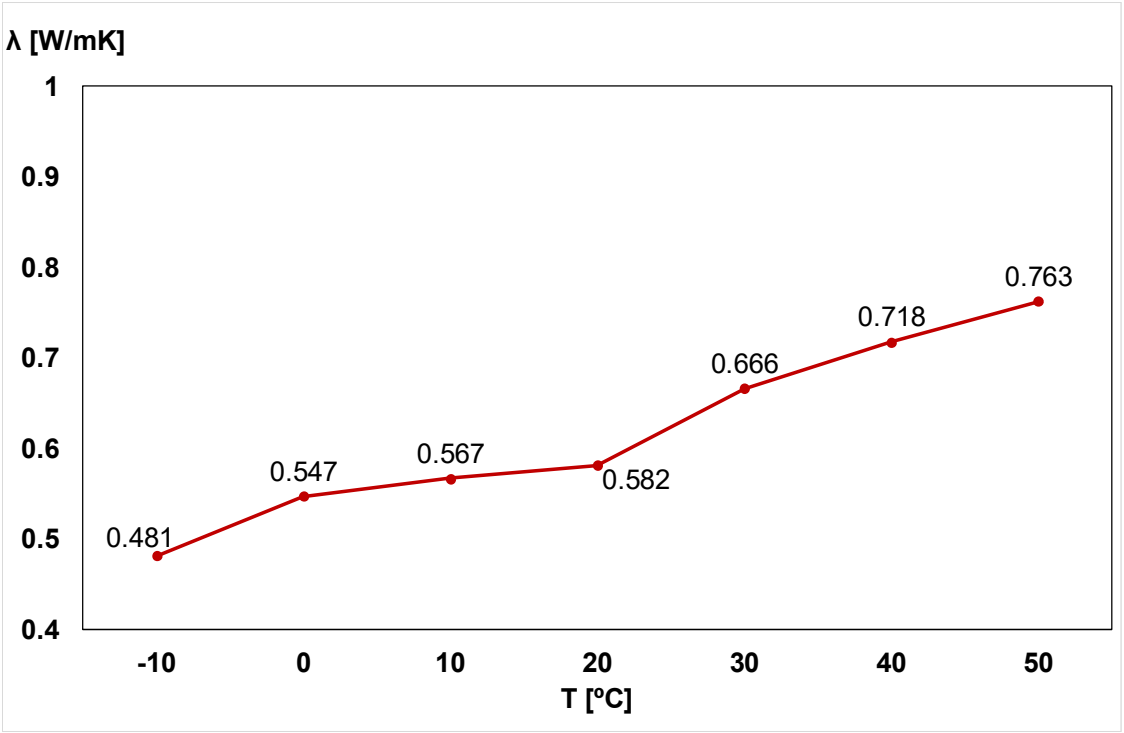

b)

Figure 60: Average GHP results: a) specimens without waste; b) specimens with waste.

5.6 CEBs Panel - Thermocouples Analyses

The temperatures measured in each of the thermocouples were monitored throughout the test. Integrity criterion was evaluated using a cotton wool pad saturated in ethyl alcohol, as described on section 4.6. Since no flames or ignition were identified on the cotton wool pad, the panel attained the integrity criterion prescriptions during the entire test. The insulation criterion was evaluated through the evolution of the temperature on the unexposed surface of the panel (Figure 61).

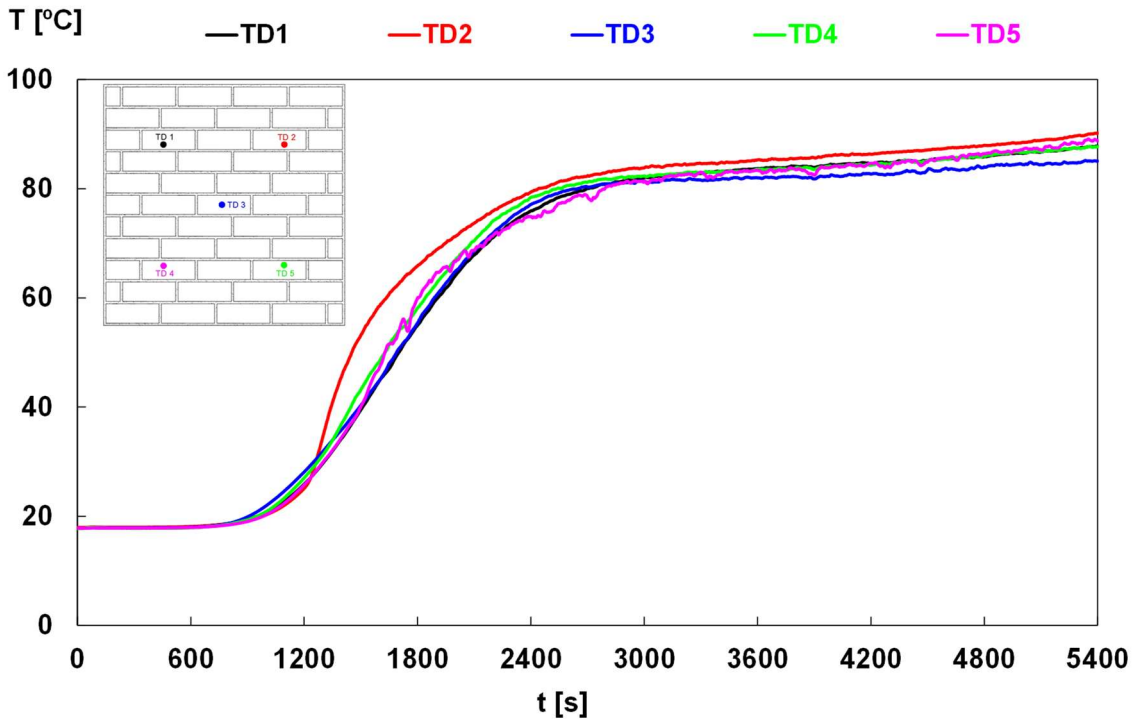

Figure 61: Time-temperature evolution on the unexposed surface of the panel (TDs).

From Figure 61 analysis one can see that the temperatures on the unexposed surface reached ±90 °C in all thermocouples. Therefore, the panel attained the insulation criterion (described on section 4.6) during the entire test. However, a smoke release from burning CEBs was noticed since middle of the test.

Figure 62 presents the time-temperature evolution measured inside the blocks.

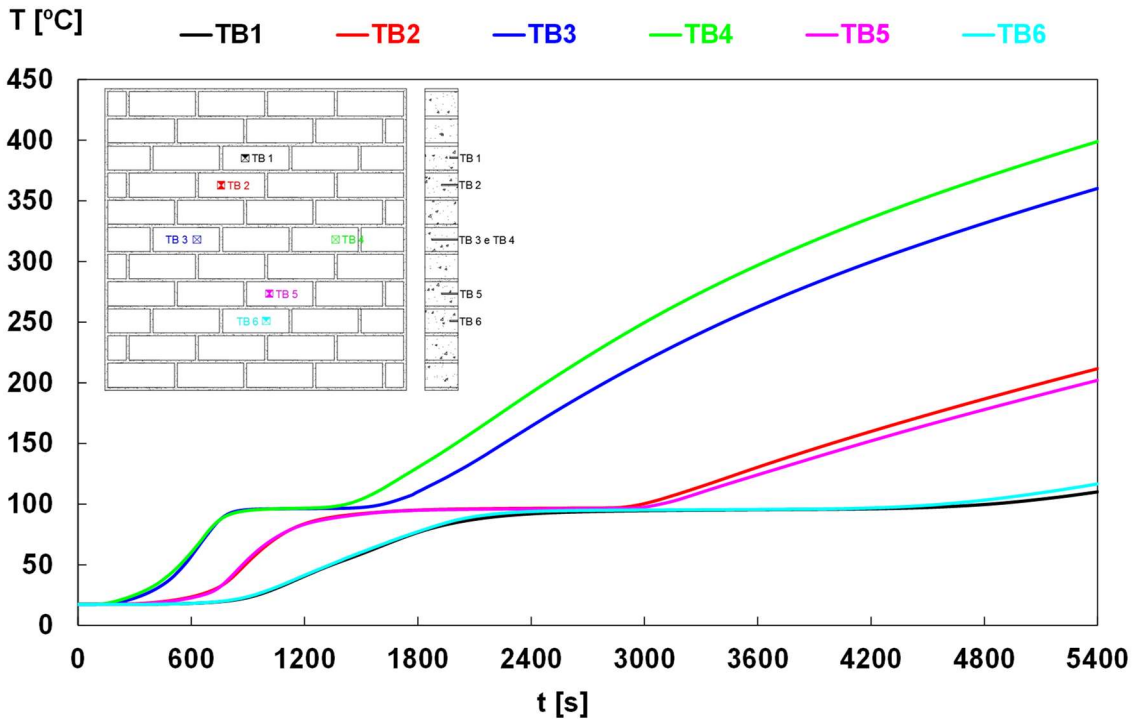

Figure 62: Time-temperature evolution inside the blocks (TBs).

From Figure 62 it can be seen that thermocouples TB3 and TB4 (which are placed in the block at 82.5 mm depth from the unexposed fire surface) recorded the highest temperatures of approximately 400 °C. Thermocouples TB2 and TB5, located at 55.0 mm depth from the unexposed surface (which represents the middle of the panel depth) recorded maximum temperatures of approximately 220 ºC at the end of the test. Concerning the thermocouples TB1 and TB6 located near the unexposed surface (27.5 mm deep), the maximum temperature was approximately 115 ºC.

Figure 63 and Figure 64 presents the time-temperature inside the holes of the blocks and in the mortar, respectively.

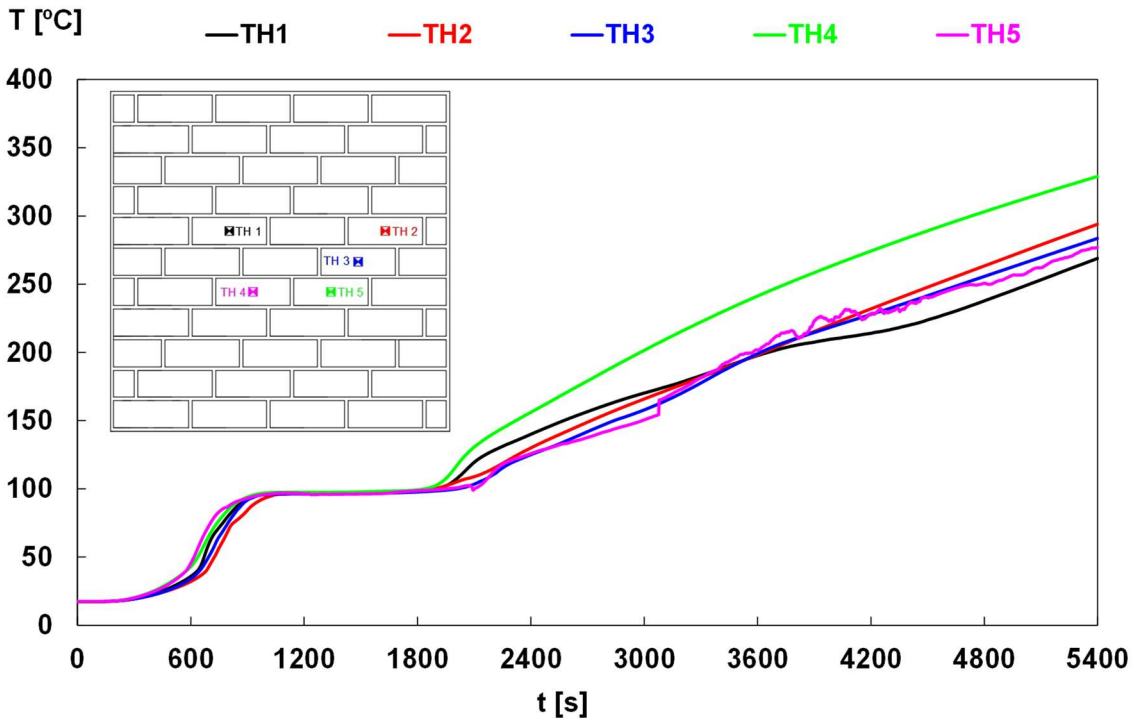

Figure 63: Time-temperature evolution inside the block holes (THs).

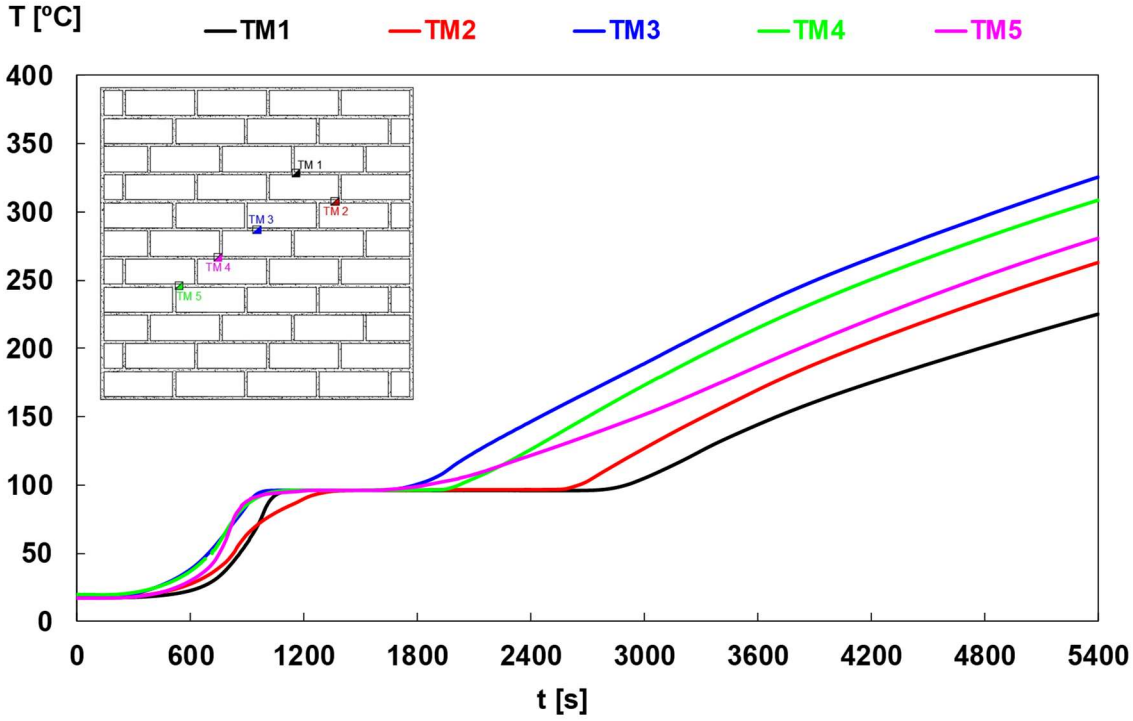

Figure 64: Time-temperature evolution in the mortar (TM).

From Figure 62, Figure 63 and Figure 64 analysis a plateau is noticed around the temperature of 100 ºC. This plateau represents the evaporation of the non-combined water of the materials. During this isothermal step, the materials accumulate energy in an endothermic process. When the amount of non-combined water is entirely evaporated the measured temperatures increase again, following a similar slope than the initial behaviour.

5.7 Infrared Thermography (IR)

Figure 65 shows the infrared (IR) thermography diagrams at different testing stages. The results of the IR thermography complement the thermocouple temperature analyses since the temperatures of the entire unexposed surface of the panel can be assessed. In contrast, thermocouples measured temperatures locally. This field measurement is of great importance to define the position of thermocouples used to find maximum temperature events in future tests. The figure presents the evolution of temperatures seen from the unexposed surface of CEBs wall panel. According to the IR thermography, the increasing of temperature was noticed after 30 min and ranged to a maximum of 90 °C. Comparing the respective time temperature evolution obtained by the thermocouples placed on the unexposed surface and using infrared thermography, it is possible to figure out that there is an adequate accordance.

Also, from Figure 65 one can see that from times of 45 min until 75 min the higher temperatures obtained on the unexposed side of the panel occurred on the mortar. This may be a consequence of its smaller thermal conductivity when compared to the blocks (due to their higher percentage of water). At the end of the test (90 min), it is possible to perceive a higher homogeneity on the colour of the blocks which reveal a similar final temperature both for the mortar and the blocks.

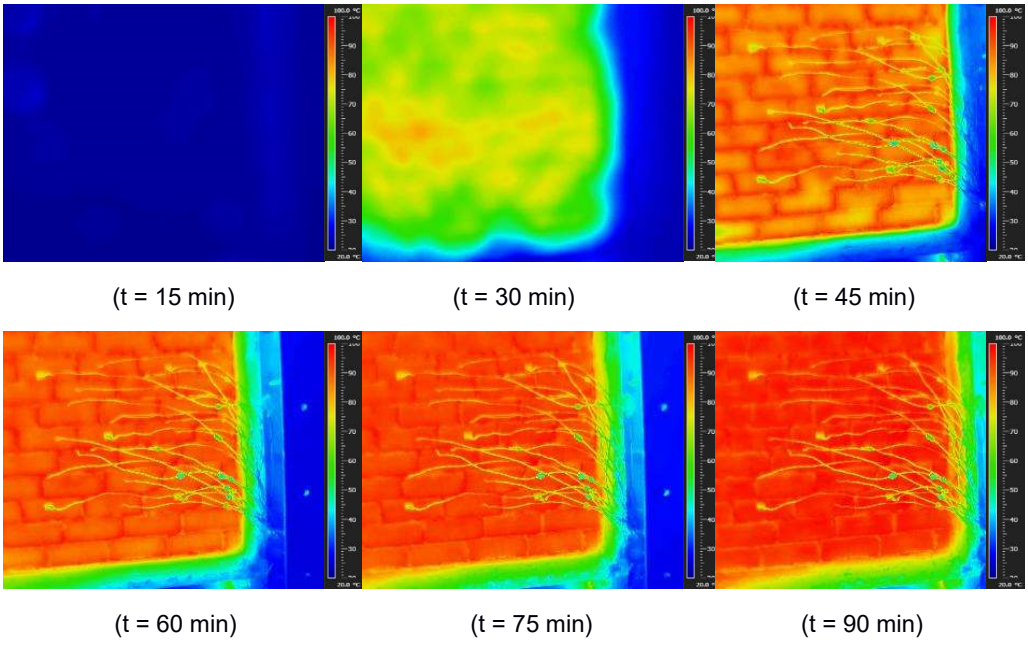

Figure 65: Infrared thermograph diagrams of CEBs wall panel.

5.8 Compressive Resistance of the Blocks

Table 17 shows the obtained values on the compressive resistance tests of the CEBs. The results presented are the average of maximum stress obtained in 10 blocks tested in compression. One can observe that the results obtained in the blocks subjected to fire were higher than the results for the blocks without fire exposure, which is due to the cooking effect of the blocks. It is also observed that the non-waste blocks have a higher resistant capacity than the blocks with waste incorporation, in accordance with the previous results obtained by Nepomuceno *et al* (2018) on the mechanical characterization tests of the soil–cement samples [1], [46].

Table 17: Compressive resistance of the blocks.

	Blocks without waste	**Blocks with waste**	
	Blocks without fire exposure	**Blocks without fire exposure**	**Blocks with fire exposure**
Average results (MPa):	7.89	4.67	11.49
Coefficient of variation:	0.02	0.11	0.12

CHAPTER 6

NUMERICAL ANALYSIS

To enhance the comprehension towards the heating process of the CEBs panels, numerical analyses of the phenomenon were developed as well. Ansys® was the chosen software to perform the simulations [84]. Ansys consists on a finite-element method software worldwide used to describe thermomechanical phenomena. Among its main purposes, simulations involving finite element analysis, computational fluid dynamics, electronics and semiconductors can be highlighted.

6.1 3D Analysis of the CEBs Panel

The panel was analysed numerically using a nonlinear transient heat transfer analysis by the finite element method, using the software Ansys® [84]. The complete panel, CEBs and mortar, were modelled by 3D Solid90 finite elements (Figure 66). This element is a high order element with 20 nodes and with temperatures as a single degree of freedom. On this simulation, the internal holes of the blocks were modelled as cavities, hence allowing only radiation phenomenon. The simulation was carried out for 5400s, with an initial time step of 10s and minimum and maximum time steps of 1s and 60s, respectively.

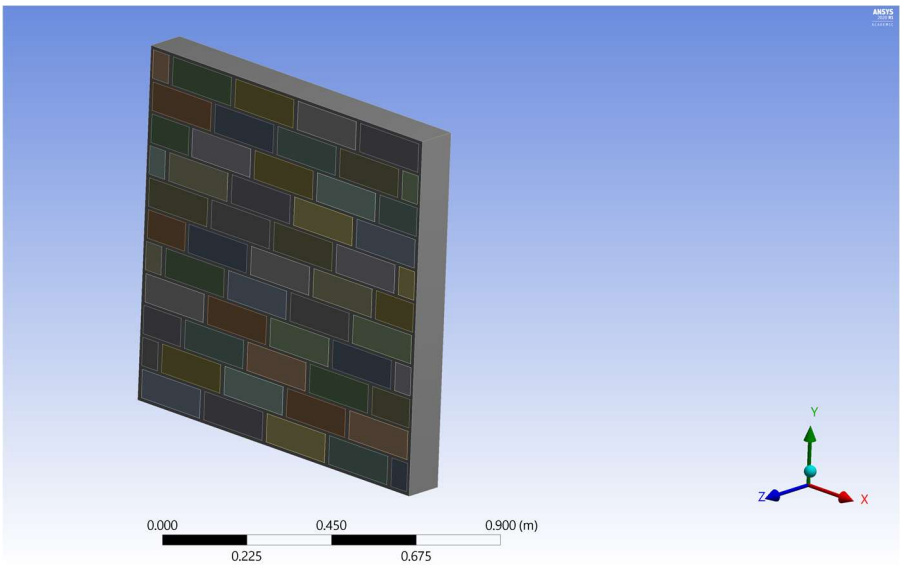

Figure 66: 3D CEBs panel model on Ansys

The temperature field is determined accordingly to the energy equation (Equation 1), considering the solid material thermal capacitance and the conduction heat flux. For the solution a heat convergence criterion based on the norm of the Newton-Raphson load with a tolerance of $1e^{-3}$ and a minimum reference value of $1e^{-6}$ were used [1].

$$\frac{d}{dt}\left(\rho(T).c_p(T).T\right) = \frac{d}{dx}\left(k(T).\frac{dT}{dx}\right) + \frac{d}{dy}\left(k(T).\frac{dT}{dy}\right) + \frac{d}{dz}\left(k(T).\frac{dT}{dz}\right)$$

Equation 1

Convection and radiation were considered in the exposed and unexposed surfaces, taking into account the boundary condition represented in Equation 2.

$$k(T)\frac{dT}{dn} = h_c.(T_s - T_\infty) + \varepsilon.\sigma_{sb}.(T_s^4 - T_\infty^4)$$

Equation 2

where k(T), ρ(T) and c_p(T), are the thermal conductivity, the specific mass and the specific heat for CEBs and mortar. h_c is the convection heat transfer coefficient, which was defined according to the prescriptions of the EN1992-1-2 Eurocode 2 and, hence, considered as 25 W/m^{2}K for the exposed surface and 4 W/m^{2}K for the unexposed outside surface of the panel [1], [85]. Radiation phenomenon was also considered on both surfaces, and defined by an emissivity equal to 0.85 to CEBs and mortar, and the Stefan-Boltzmann constant σ_{sb}. T_∞ represents the air temperature in contact to the surface, at temperature T_s, being defined by the standard fire curve ISO834 and the ambient temperature, for the exposed and unexposed faces, respectively. Figure 67 presents the boundary conditions applied on the 3D panel [71], [86].

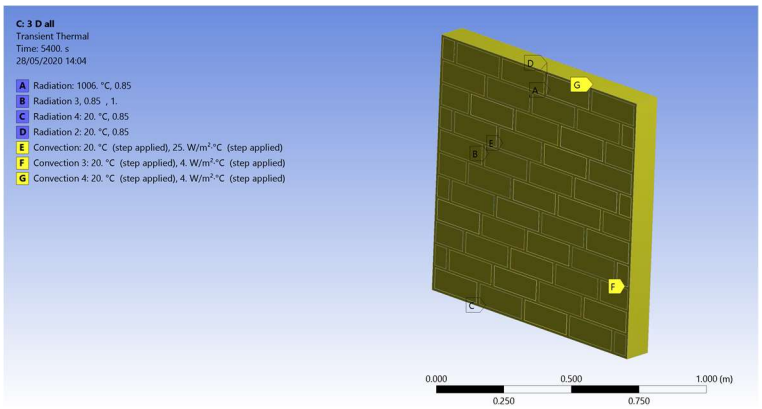

Figure 67: Boundary conditions applied on the 3D panel simulation.

In this simulation, Eurocode EN 1992-1-2 prescriptions were used to determine the solid specific mass and the specific heat values of the CEBs and mortar, both properties varying with the temperature. This Eurocode was also used to establish the thermal conductivity temperature variation, according to the moisture of mortar. For the CEBs the Eurocode was also used, but to allow for the heat consumed during water evaporation, a specific heat peak was calculated from the measured moisture content and water latent heat of vaporisation (2260 kJ/kg), assuming that water vaporization occur between 100 ºC and 200 ºC, giving a peak value at 150 ºC equal to 1170 + 3977,6 = 5147,6 J/kgK [1], [85].

The effective thermal conductivity of the CEBs was calculated according to the Russel model, which considers the average porosity (φ) as well as solid (k_s) and gas (k_g) thermal conductivities (Equation 3) [1], [87].

$$k_{eff} = k_s \frac{\varphi^{2/3} + \left(\frac{k_s}{k_g}\right)\left(1 - \varphi^{2/3}\right)}{\left(\varphi^{2/3} - \varphi\right) + \left(\frac{k_s}{k_g}\right)\left(1 - \varphi^{2/3} + \varphi\right)}$$

Equation 3

The gas thermal conductivity includes the conductive term given by the air conduction heat transfer coefficient (presented in Equation 4), and by an irradiative component [88].

$$k_g = -1{,}881 \times 10^{-8} T^2 + 8{,}38 \times 10^{-5} T + 0{,}002244$$

Equation 4

Radiation inside porous material was modelled as a series of parallel opaque planes with separation equal to the cell size, providing a irradiative contribution to the total effective conductivity which, according to Glicksman (1994), can be calculated according to Equation 5 [89].

$$k_r = 4\frac{\epsilon}{2-\varepsilon}\sigma d T^3$$

Equation 5

Where ε is the wall emissivity, considered as 0,85, σ is the Stefan-Boltzmann constant and d the pore diameter, considered equal to 160 μm, based on Zhang's work and expected increase in porous size during fire action. Russell model was applied after water dehydration due the increased importance of porosity. In order to approximate experimental and numerical results, an increase variation between 50 ºC and 100 ºC was used. Figure 68 shows the thermal properties of the CEBs and mortar used on the 3D simulations [1], [52], [87].

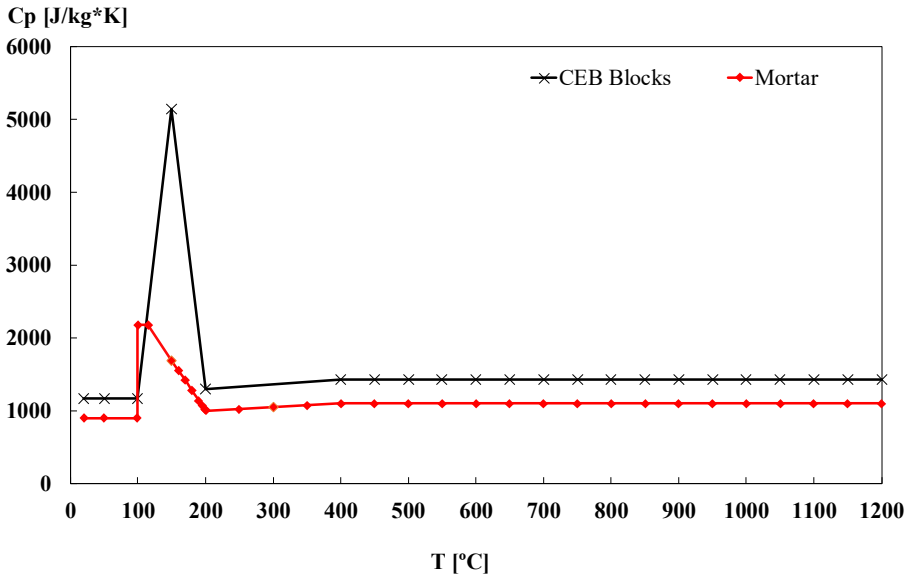

a)

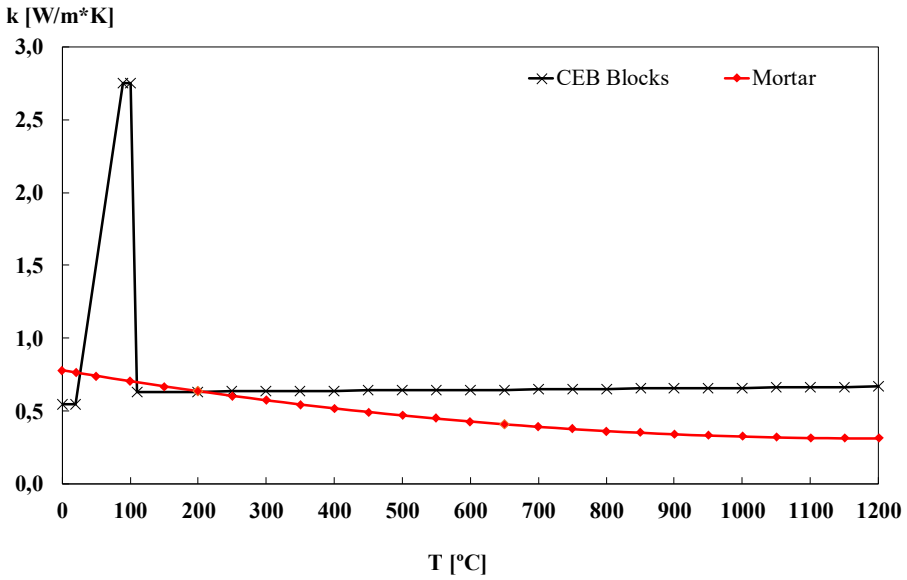

b)

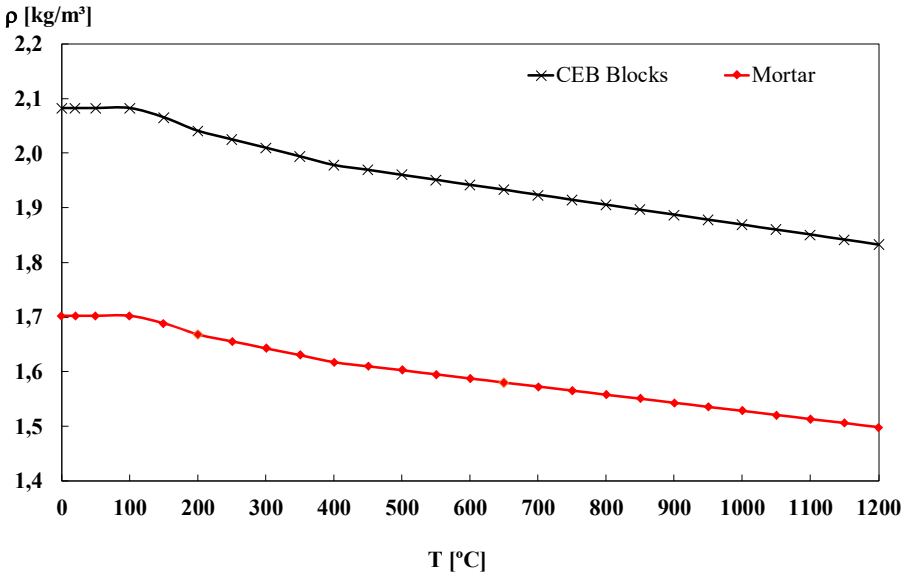

c)

Figure 68: Thermal properties of the CEBs and mortar used on 3D simulations: a) specific heat; b) thermal conductivity; c) specific mass [1].

The results obtained on the simulation are shown on Figure 69, with the exposed surface presented towards. The temperature gradient across the wall is similar for the CEBs and for the mortar elements. This is mainly due to the assumed perfect thermal contact between both materials, neglecting any thermal conductance between both surfaces. Additionally, CEBs holes were modelled as cavities, allowing radiation between surfaces.

However, due to the temperature levels, no temperature gradient around the holes was noticed in comparison to the solid CEBs section [1].

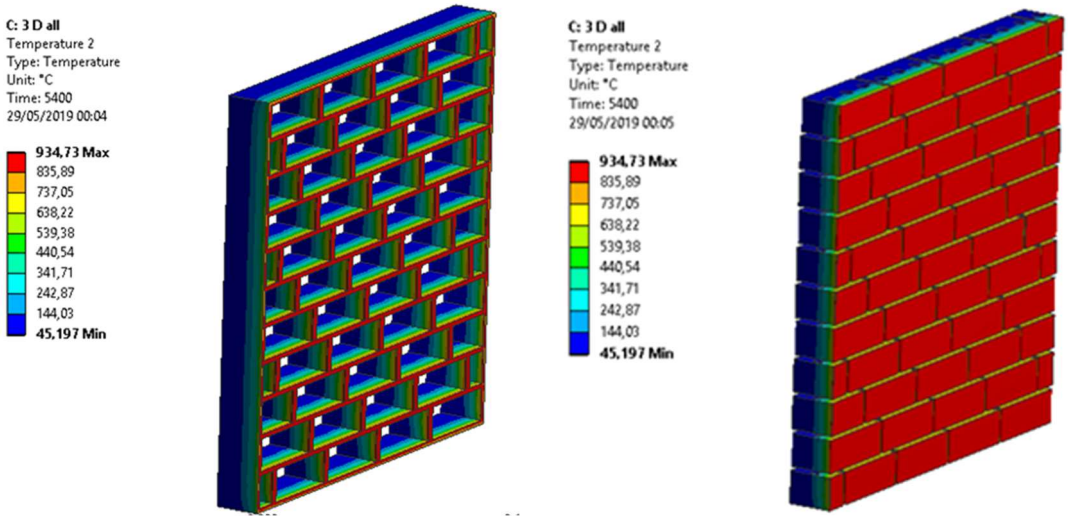

Figure 69: Gradients of temperature obtained on 3D simulation [1].

In order to evaluate the results obtained on the numerical model, the evolution of the temperature on a depth of 27.5 mm, 55.0 mm and 82.5 mm inside the blocks were developed. These depths correspond to the TB thermocouples analysed on the experimental panel (presented on section 5.6). Figure 70 shows the comparison between the results obtained on the experimental and numerical analyses. TB1-Num, TB2-Num and TB3-Num correspond to the temperature evolution at a depth of 27.5 mm, 55.0 mm and 82.5 mm from the unexposed surface, respectively.

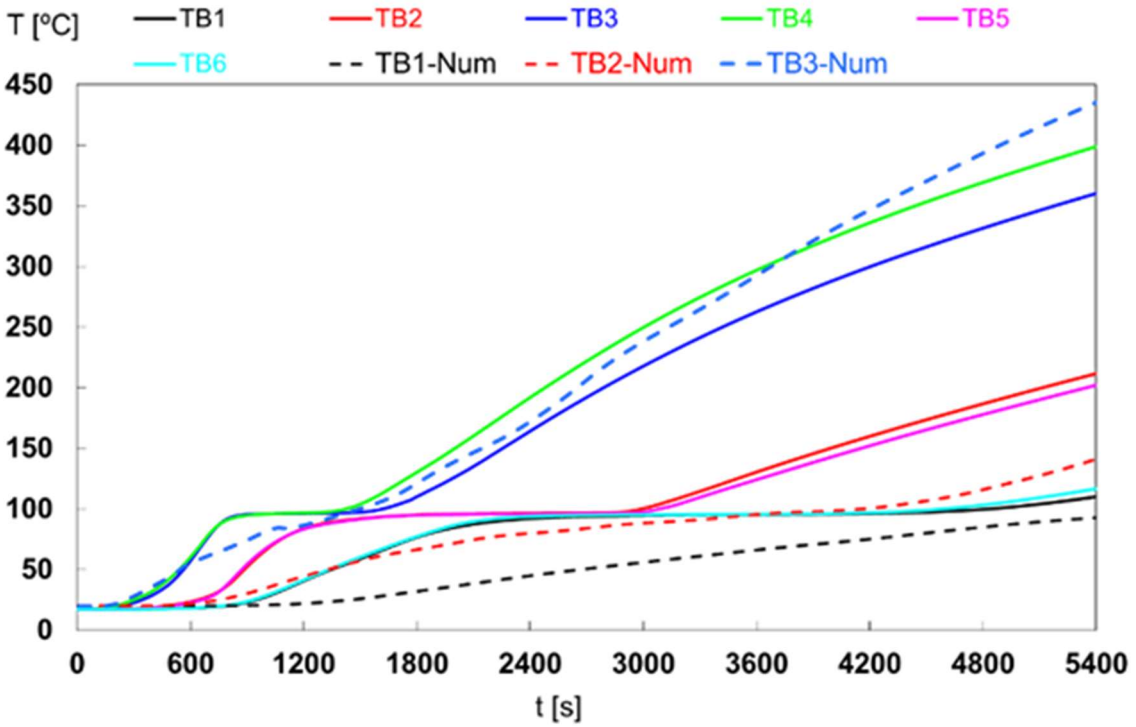

Figure 70: Comparison between the results obtained on the experimental and 3D numerical models of the panel [1].

The difference between numerical and experimental temperatures increases from the exposed to the unexposed wall face. Being noticed a higher difference for the TB1 position, which numerically stays below the 100 ºC. Even the dehydration experimental plateau is remarkably higher than the numerical, giving some evidence to a better definition of the thermal conductivity and specific heat in function of temperatures and water content. During the manufacture of the experimental CEBs panel, water was poured onto the blocks to avoid shrinkage on the mortar layers (which is a common civil engineering practice). This aspect may as well influence on the difference noticed between the dehydration plateau on the experimental and numerical results, once it affects the moisture content on the blocks [1].

6.2 2D Analysis of the CEBs

As described on section 6.1, on the 3D simulation the block holes were modelled as cavities, hence considering an absence of materials which allows only radiation phenomenon in their interior. However, on the experimental model these holes are fulfilled with air (and may also present remnants of the mortar used to lay the blocks). To

evaluate the influence of the presence of air inside the holes, a 2D model of a block was modelled on Ansys. To perform this simulation, a transient thermal analysis was developed for a single block. The entire three-dimensional block (Figure 71) was designed on the software and set for a bidimensional analysis [84].

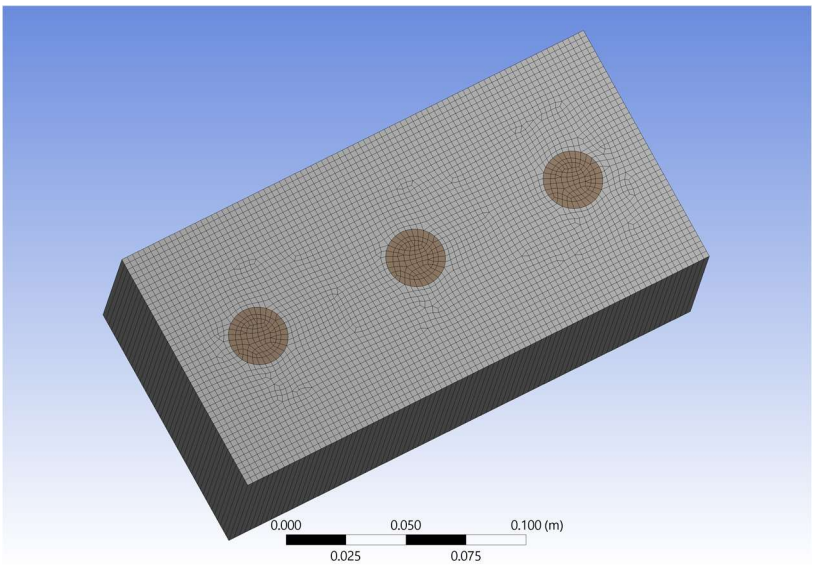

Figure 71: 3D sketch of the block designed for the 2D simulations.

The finite element used on the simulation was Plane 77, a high order bidimensional 8 nodes thermal solid element with temperature as single degree of freedom. The transient thermal solution is based on the energy equation (presented on Equation 1 described on section 6.1), neglecting the spatial Z component terms, once the simulation is bidimensional. For the solution, a heat convergence criterion based on the norm of the Newton-Raphson load with a tolerance of 1e-3 and a minimum reference value of 1e-6 were used, in the same way as for the 3D simulation. The simulation was also carried out for 5400s, with an initial time step of 10s and minimum and maximum time steps of 1s and 60s, respectively. The boundary conditions applied on the block were the same presented on section 6.1. Figure 72 shows a bidimensional view of the block with the applied boundary conditions.

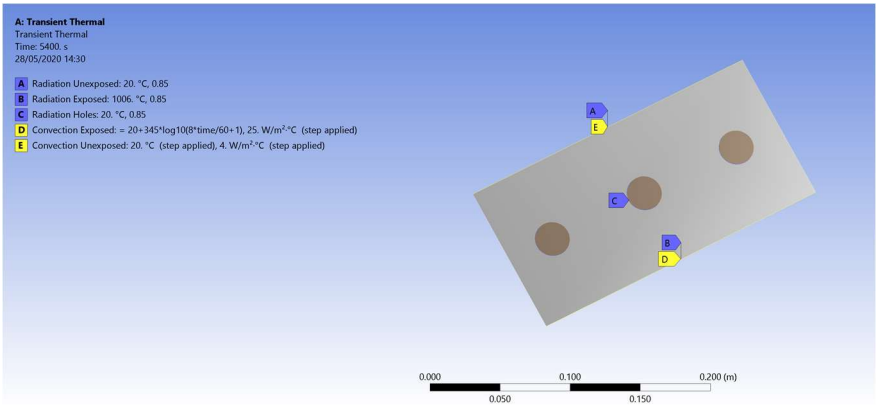

Figure 72: Boundary conditions used on the 2D transient thermal simulation.

The thermal properties used for the block were the same presented on Figure 68. The thermal properties of the air were set according to Capitelli *et al* (2000), and are shown on Figure 73 [90].

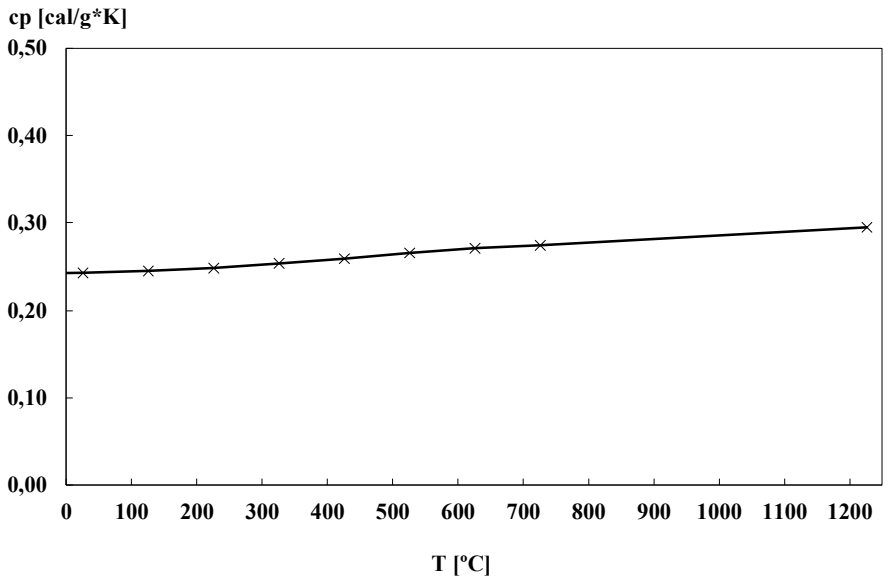

a)

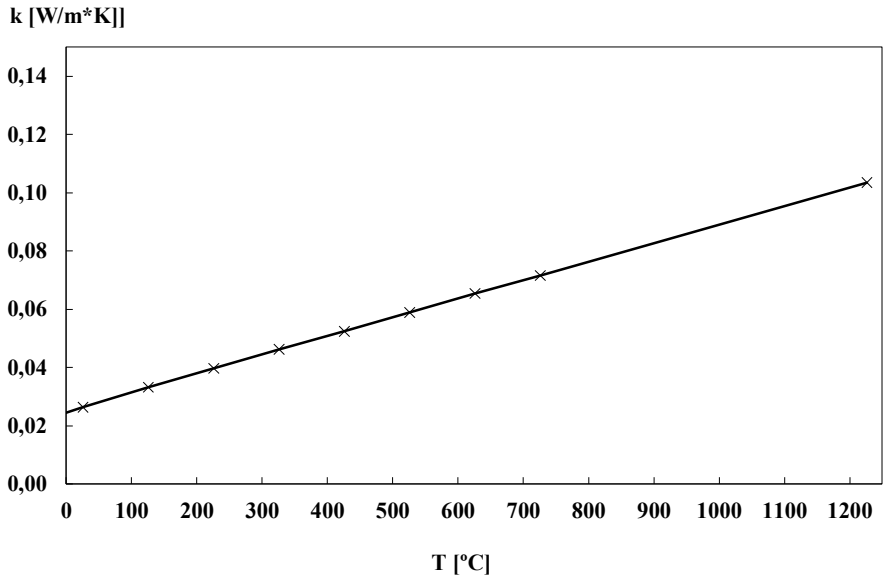

b)

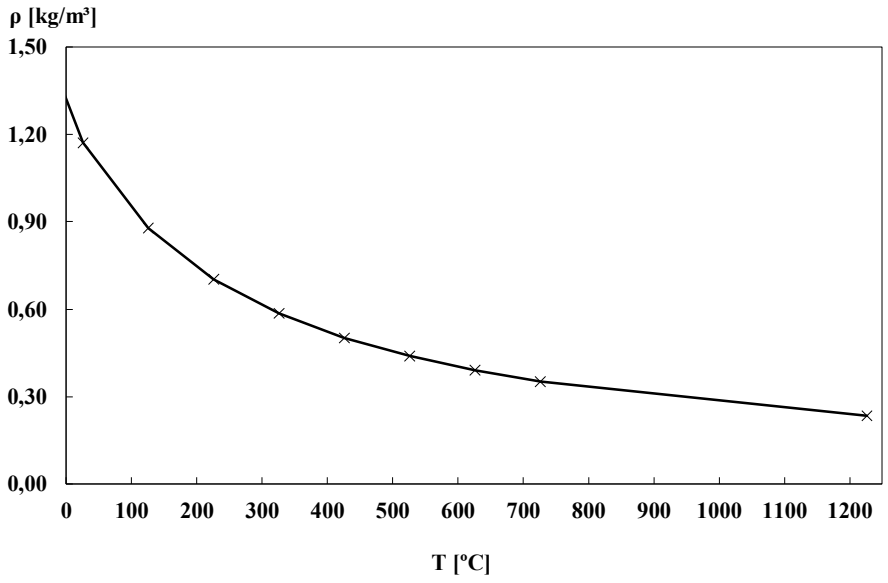

c)

Figure 73: Thermal properties of the air used on 2D simulations: a) specific heat; b) thermal conductivity; c) specific mass [90].

Figure 74 presents a comparison between the results obtained on the 2D simulation and the experimental ones. From Figure 74 analysis, one can see that no major changes were reported when compared to the results obtained on the 3D simulation, which were shown on Figure 70. Once again, the difference between the experimental and numerical curves

increases in the parts of the panel which attained higher temperatures, suggesting that an improvement is required on the thermal properties of the material at high temperatures.

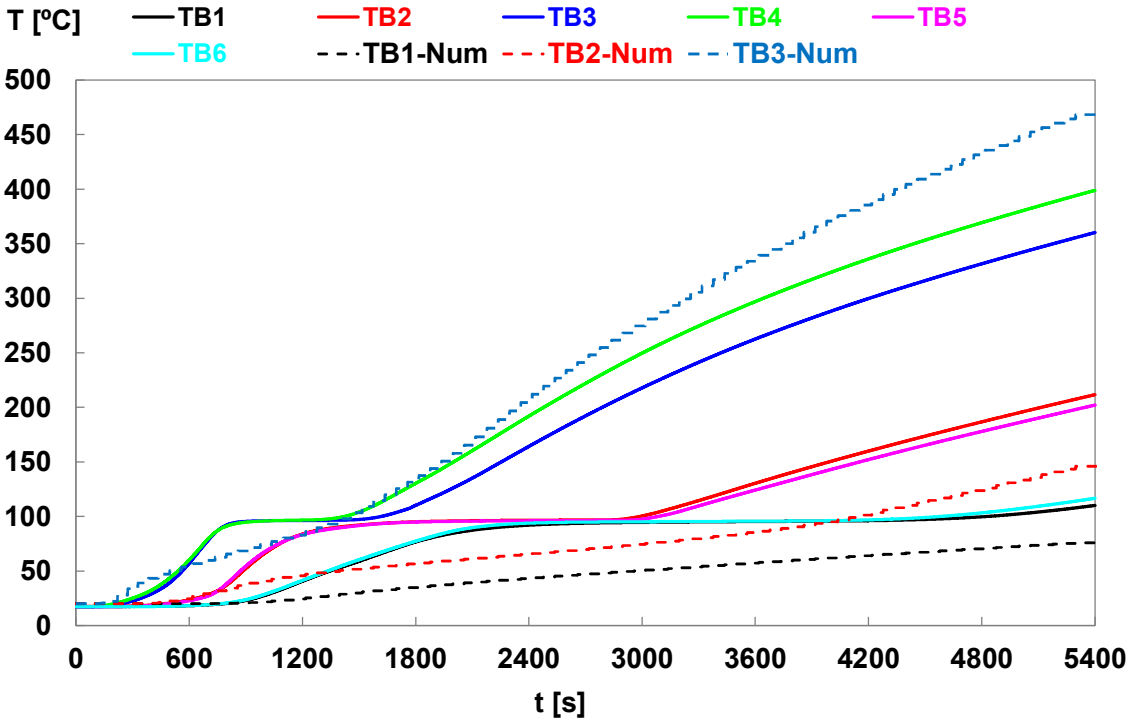

Figure 74: Comparison between the results obtained on the experimental and 3D numerical models of the panel.

Once the main goal of the 2D simulation was to evaluate the temperature gradient on the holes and their adjacencies, special attention was given to this part of the block (as shown on Figure 75). From Figure 75 analysis, one can see a slightly greater increase on the temperatures inside the holes, mainly due to the higher variation of the specific mass and thermal conductivity of the air when compared to the CEBs. On the other hand, the borders of the holes present slightly lower temperatures than the other parts of the block which are at a same width. This is due to the absence of conduction phenomenon between the air and the solid material.

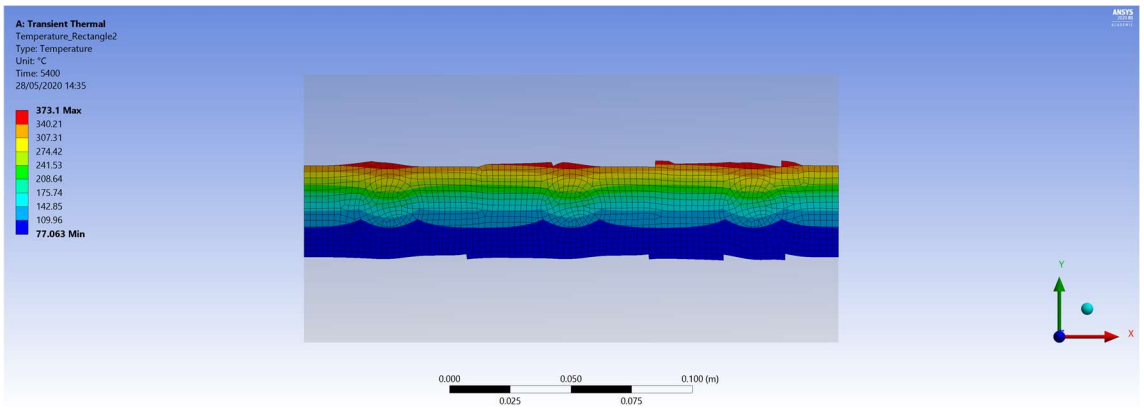

Figure 75: Temperature gradient on the adjacencies of the block holes on the 2D simulation.

6.3 CFD Analysis of the CEBs

On section 6.2, an analysis of the CEBs considering the holes fulfilled with air was presented. However, this simulation was developed as an Ansys transient thermal simulation, and therefore, does not evaluates the convection currents that occur on the fluid. In order to enhance the investigation towards this phenomenon, a Computational Fluid Dynamics (CFD) Ansys Fluent analysis was also performed [91].

Ansys Fluent consists on a software which relies on the finite volume method and contains the broad, physical modelling capabilities needed to model flow, turbulence, heat transfer and reactions for industrial applications. The software employs the finite volume method to solve the three kinds of equations which govern fluid dynamics and thermal analysis, namely the Nanvier-Stokes equations (which represent conservation of momentum), continuity equations (which represent the conservation of mass) and the first law of thermodynamics (which represent the conservation of energy). To solve transient phenomena, Fluent also applies the energy equation (Equation 1, presented on section 6.1). The simulation was performed in 3D and double precision settings. To perform the simulation, a three-dimensional model of the CEB was sketched and then meshed (Figure 76) [92], [93].

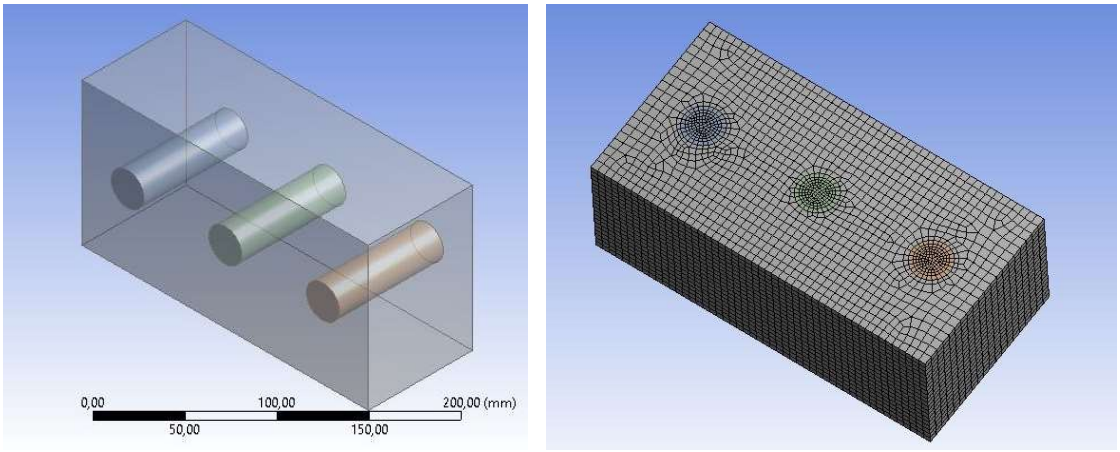

a) Model b) Mesh

Figure 76: CEB model and mesh sketched for CFD simulation.

The thermal properties applied for the CEB and for the air were the same used on transient thermal simulations (presented on Figure 68 and Figure 73, respectively).Similarly, the same boundary conditions used for the previous simulations were applied on the CFD analysis. The simulation was carried out with an initial pressure gauge of 101325 Pa (pressure equivalent to 1 atm) and gravity of 9.81 m/s^2. The available pressure-based solver was used on the simulation. Convergence criteria were set as 1e-4 for the residuals of continuity and velocity (for each one of the x, y and z components) and as 1e-6 for the energy.

From Figure 77 to Figure 79 the obtained gradients of temperature and currents of convection inside the CEB holes at, 1800s, 3600s and 5400s of simulation are presented. As can be seen, with the evolution of time the average values of velocity and the currents of convection (represented by the arrows) increase due to the enlargement of the gradient of temperature inside the holes. The circular pattern observed on the air flow is due to the buoyancy phenomenon. The magnitude of the velocities demonstrate that the air behaviour inside the holes is governed by a laminar flow [93].

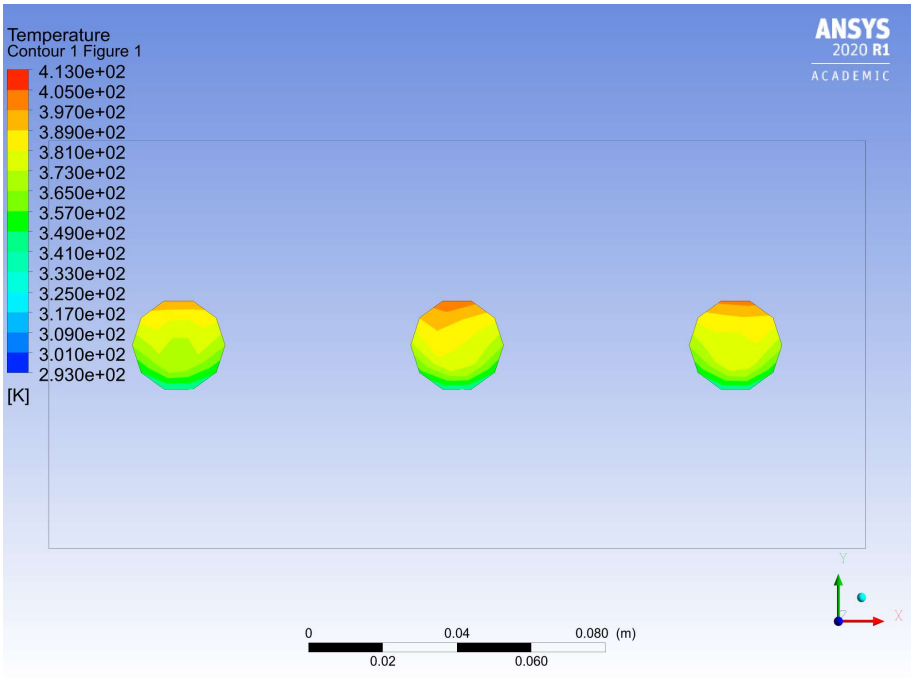

a)

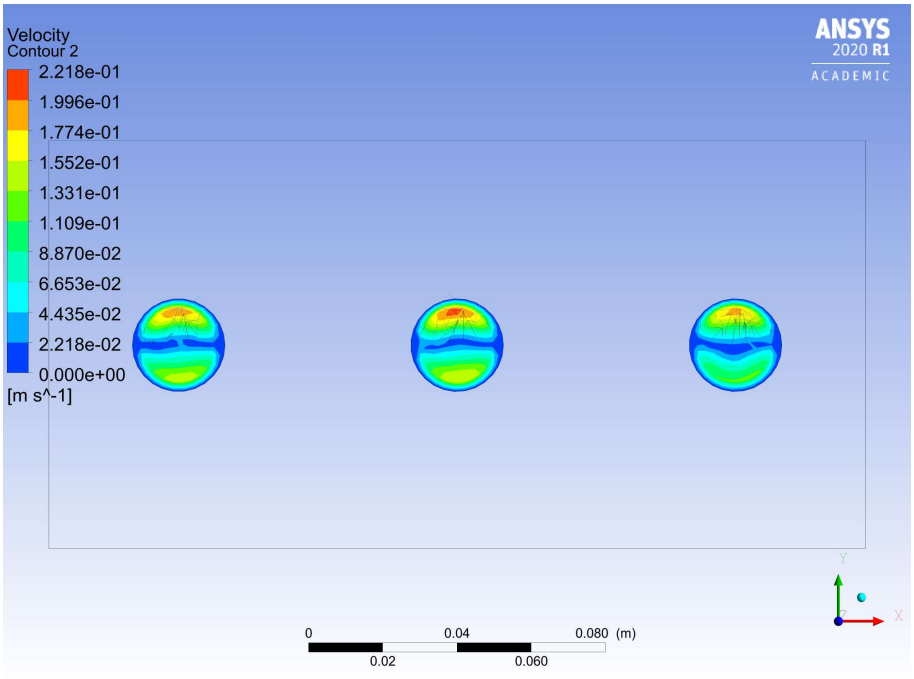

b)

Figure 77: Gradient of temperature (a) and current of convection (b) inside the CEB holes at 1800s.

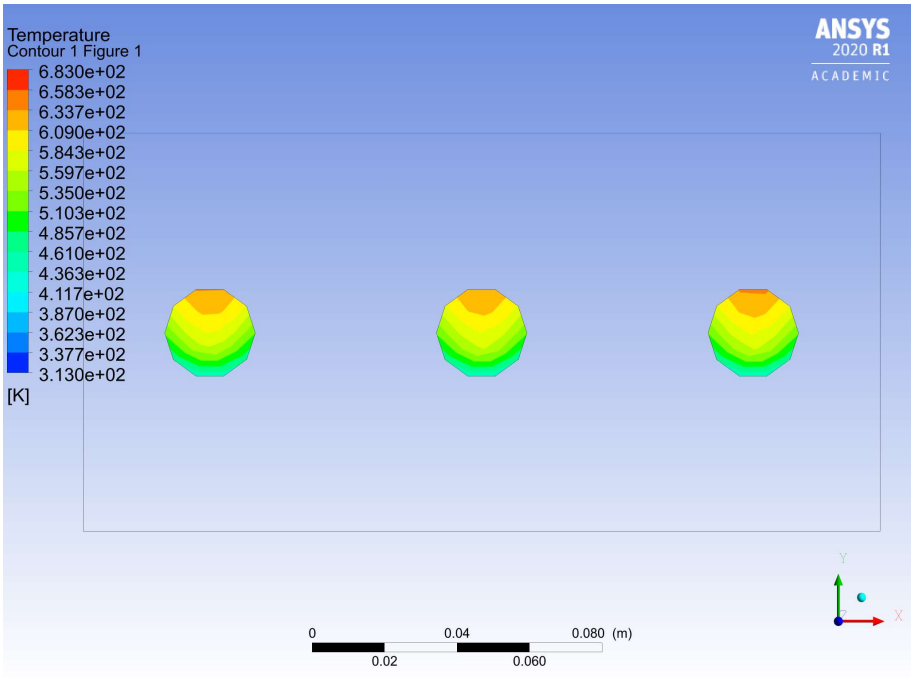

a)

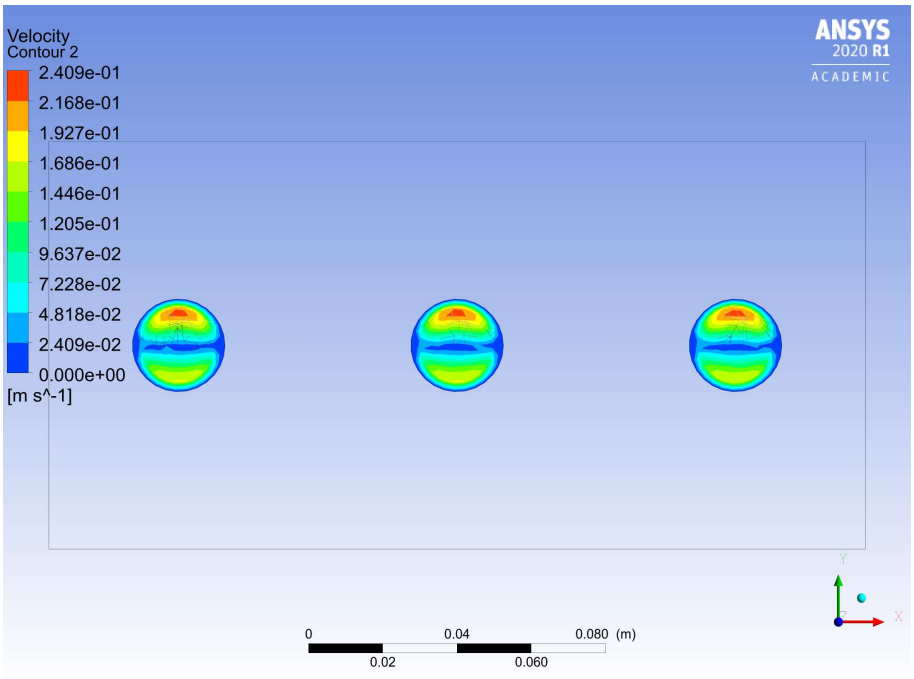

b)

Figure 78: Gradient of temperature (a) and current of convection (b) inside the CEB holes at 3600s.

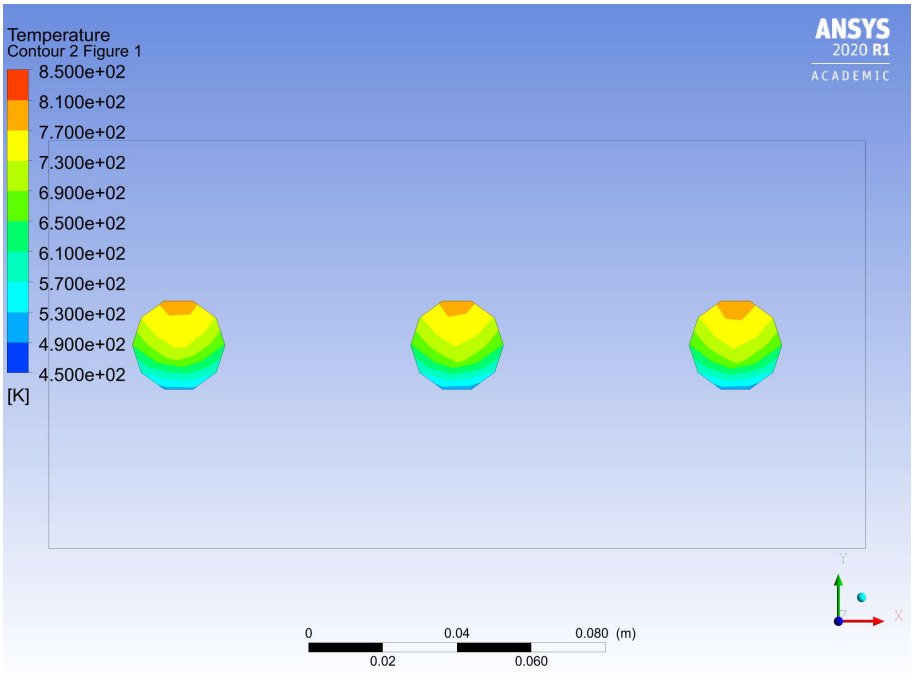

a)

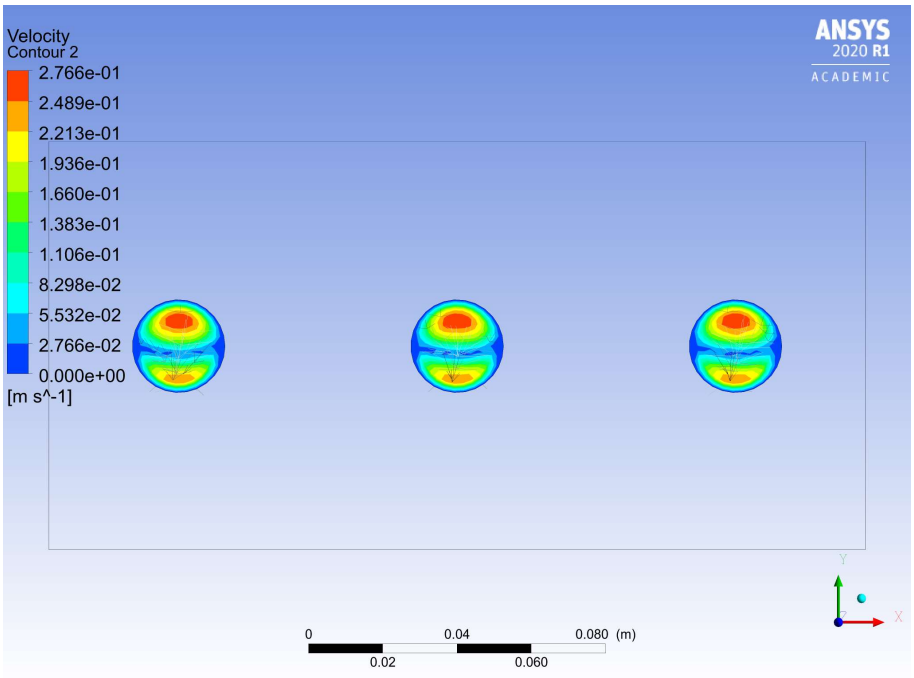

b)

Figure 79: Gradient of temperature (a) and current of convection (b) inside the CEB holes at 5400s.

As expected, once the CFD simulation also relies on the energy equation to solve transient phenomena and the thermal properties used were the same, the obtained gradient of temperature (Figure 80) complies with the obtained on the transient thermal simulations.

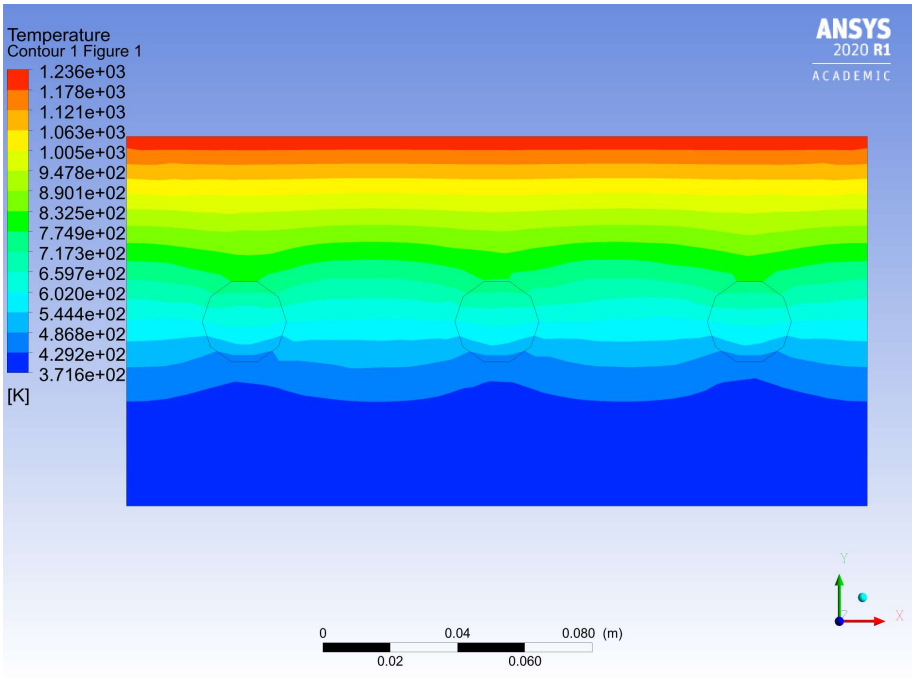

Figure 80: Gradient of temperature at the end of the CFD simulation.

CHAPTER 7

CONCLUSIONS AND FUTURE WORKS

The present work has evaluated the feasibility of the incorporation of the organic fraction of municipal waste on the manufacture of compressed earth blocks. Previous researches had already proven preliminary the potential of the incorporation at a mechanical point of view. Evaluating the thermal properties of the incorporated CEBs, the waste incorporation shown an enhancement on their behaviour, once the blocks still accomplish the prescriptions of several international standards and also reduced their thermal conductivity in 22.2%, which can lead to a reduction on the heat transfer through building envelopes. This aspect may be a consequence of the increase on the porosity of the blocks (the porosity of the CEBs with waste rose 1.22% when compared to the CEBs without waste), which previous researches evidenced to cause reductions of the thermal conductivity of the CEBs. The thermogravimetric results did not reveal any major changes on the reactions on the blocks (despite the degradation of the organic fraction of the waste), suggesting that the incorporated waste does not causes modifications on the chemical behaviour of the CEBs when submitted to high temperatures.

The performance of the incorporated CEBs panel when subjected to fire situations was also satisfactory, since the CEBs panel attained criterion of integrity (once no flames or ignitions were observed on the cotton wool pad), however small cracks were identified in the mortar, which allowed a smoke release from the blocks, leading to burning and compound volatilization. The panel also attained the insulation criterion defined by the European standard, once the maximum temperature noticed on the unexposed side of the panel was of 92 ºC, value considerably smaller than the 140 ºC increase on the initial temperature of the panel (20 ºC) or 180 ºC (which are the prescriptions of the standard). On the test, the temperature evolutions on the panel were linear up to 100 ºC, and then a plateau corresponding to evaporation of the humidity of the blocks was noticed. After the moisture content in the panel had evaporated, the temperatures increase again with a similar slope as in the beginning.

Furthermore, both the CEBs with and without incorporated waste shown an increase on their mechanical resistance after submitted to high temperatures due to their cooking. However, negative modifications of materials after returning to room temperature may

cause a loss of resistance in the CEB. Therefore, caution is advised and a masonry strengthening strategy may be recommended.

Three models of numerical simulations of the CEBs panel submitted to fire resistance tests were performed, namely a 3D transient thermal of the entire panel (in which no material was considered on the interior of the block holes), a 2D transient thermal simulation of a single block considering the block holes fulfilled with air and a CFD simulation of a 3D single block also with its holes fulfilled with air. Comparisons between the obtained results on these tests and the experimental one shown considerable differences on the temperature evolutions inside the blocks, which reveals the necessity of clearly define the temperature variation of the thermal properties of the CEBs. The higher difference between the numerical and experimental results was observed on the unexposed side of the panel, which confirms the inconsistency of the thermal properties variation with temperature.

Recommendations for future work are:

- Evaluation of the incorporation of the organic fraction of municipal waste on CEBs made with natural soil, in order to enhance the sustainable feature of the blocks.
- Development of a full description of the CEBs properties variation with temperature.
- Development of numerical simulations considering the fluid phase inside the CEBs, in order to understand its influence on the thermomechanical properties of the blocks during heating phenomena.
- Performance of experimental tests on incorporated CEBs panels with the application of loads, in order to analyse the loadbearing capacity of the CEBs subjected fire situations.

BIBLIOGRAPHY

[1] D. M. Ferreira, E. Luso, M. L. Cruz, L. M. R. Mesquita, and G. Gontijo, "Fire behaviour of ecological soil–cement blocks with waste incorporation: Experimental and numerical analysis," *J. Fire Sci.*, p. 073490411989392, 2020.

[2] G. Minke, *Building with Earth*. Birkhäuser – Publishers for Architecture, 2006.

[3] B. Berge, *The Ecology of Building Materials*, 2nd ed. Elsevier Science, 2009.

[4] P. Torgal., R. Eires., and S. Jalali., *Construção em Terra*. 2016.

[5] P. A. Jaquin, C. E. Augarde, and C. M. Gerrard, "Chronological description of the spatial development of rammed Earth techniques," *Int. J. Archit. Herit.*, vol. 2, no. 4, pp. 377–400, 2008.

[6] ArcaTerra, "Muralha da China," 2012. [Online]. Available: https://arcaterrablog.files.wordpress.com/2012/07/25-tapial-muralha-da-china-e1490729915662.jpg. [Accessed: 30-Oct-2019].

[7] S. Torgal, F.; Jalali, "Considerações sobre a Sustentabilidade dos Materiais de Construção," *C. Mater.*, p. 2010, 2010.

[8] P. A. Jaquin, "Analysis of Historic Rammed Earth construction," Doctoral Thesis presented to Durhan University School of Engineering, 2008.

[9] C. M. M. Neves, "Resgate e Atualização do Construir com Terra: O Projeto Proterra." I Conferência Latino-Americana de Construção Sustentável X Encontro Nacional de Tecnologia do Meio Ambiente Construído, São Paulo, 2004.

[10] J. C. Reyes, L. E. Yamin, W. M. Hassan, J. D. Sandoval, C. D. Gonzalez, and F. A. Galvis, "Shear behavior of adobe and rammed earth walls of heritage structures," *Eng. Struct.*, vol. 174, no. 19, pp. 526–537, 2018.

[11] A. G. Araújo, "Comportamento ao Fogo de Paredes em Tabique," Master Thesis presented to Instituto Politecnico de Bragança, 2014.

[12] S. Cunha *et al.*, "A contribution for the improvement in thermal insulation of tabique walls coated with metal corrugated sheets," *Build. Serv. Eng. Res. Technol.*, vol. 36, no. 4, pp. 439–454, 2015.

[13] E. L. Krüger and M. D. Santos, “the Use of Earth As an Appropriate Building Material in Brazilian Low-Cost Housing.” 2013.

[14] T. M. P. Carvalho and W. G. R. Lopes, “A arquitetura de terra e o desenvolvimento sustentável na construção civil,” *VI Congr. Norte e Nord. Pesqui. e Inovação*, 2012.

[15] B. D. E. A. Negreiros, “Thermal Comfort Through Thermal Mass and Natural Ventilation in Social Housing in Northeast Brazil . A thesis submitted to the University of Manchester for the degree of Doctor of Philosophy in the Faculty of Science & Engineering 2018 SCHOOL OF MECHANICA,” Doctoral Thesis presented to University of Manchester, 2018.

[16] Portal do Instituto Brasileiro de Museus, “Museu da Inconfidência,” 2018. [Online]. Available: http://boletim.museus.gov.br/wp-content/uploads/2014/07/museu-da-inconfidencia.jpg. [Accessed: 02-Jul-2020].

[17] C. G. T. Silva, “Conceitos e Preconceitos relativos às Construções em Terra Crua,” *Fundação Oswaldo Cruz*, 2000.

[18] U. of S. Paulo, “As histórias de Ivaporunduva,” *Newspaper of the University of São Paulo*, 2007. [Online]. Available: http://www.usp.br/jorusp/arquivo/2007/jusp804/pag0405.htm. [Accessed: 02-Jul-2020].

[19] A. P. Bayer, “Proposta de diretrizes para o desenvolvimento da arquitetura em terra no Rio Grande do Sul, a partir da interpretação de estratégias uruguaias,” Master Thesis presented to Universidade Federal do Rio Grande do Sul, 2010.

[20] A. C. Villaça, “A atual tendência da construção no Brasil e seus reflexos para a arquitetura e construção com terra,” *Terra Bras. - IV Congr. Arquitetura e Construção com Terra no Bras.*, 2012.

[21] M. K. Nito and A. M. M. C. Amorim, “Sistemas construtivos em terra crua: panorama brasileiro e suas referências técnicas históricas,” *Terra Bras. - IIICongresso Arquitetura e Construção com Terra no Bras.*, 2010.

[22] V. Rigassi and CRATerre-EAG, *Compressed Earth Blocks: Manual Of Production*, vol. I. Deutsches Zentrum für Entwicklungstechnologien, 1985.

[23] J. V. Oliveira, “Comportamento mecânico de blocos de terra compactada ativados alcalinamente,” Master Thesis presented to Universidade do Minho, 2014.

[24] H. Ma, Q. Ma, and P. Gaire, “Development and mechanical evaluation of a new interlocking earth masonry block,” *Adv. Struct. Eng.*, 2019.

[25] M. C. N. Villamizar, V. S. Araque, C. A. R. Reyes, and R. S. Silva, “Effect of the addition of coal-ash and cassava peels on the engineering properties of compressed earth blocks,” *Constr. Build. Mater.*, vol. 36, pp. 276–286, 2012.

[26] D. Leitão, J. Barbosa, E. Soares, T. Miranda, N. Cristelo, and A. Briga-Sá, “Thermal performance assessment of masonry made of ICEB’s stabilised with alkali-activated fly ash,” *Energy Build.*, vol. 139, pp. 44–52, 2017.

[27] F. X. R. F. Lima, “Blocos de terra compactada de solo-cimento com resíduo de argamassa de assentamento e revestimento: caracterização para uso em edificações,” Doctoral Thesis presented to Universidade de Brasília, 2013.

[28] K. Park, D. Monitoring, T. Morton, F. Stevenson, B. Taylor, and N. C. Smith, *Low Cost Earth Brick Construction*. 2005.

[29] C. F. Oliveira, H. Varum, and J. Vargas, “Earthen Construction : Structural Vulnerabilities and Retrofit Solutions for Seismic Actions,” *15 Wcee*, pp. 1–9, 2012.

[30] K. Hadjri, M. Osmani, B. Baicha, and C. Chifunda, “Attitudes towards earth building for Zambian housing provision,” *Proc. Inst. Civ. Eng. Eng. Sustain.*, vol. 160, no. 3, pp. 141–149, 2007.

[31] E. A. Adam and A. R. A. Agib, “Compressed Stabilized Earth Block Manufacturing in Sudan,” *Organization*, p. 101, 2001.

[32] M. A. Buson, “Kraftterra- desenvolvimento e análise preliminar do desempenho técnico de componentes de terra com a incorporação de fibras de papel kraft provenientes da reciclagem de sacos de cimento para vedação vertical,” Doctoral Thesis presented to Universidade de Brasília, 2009.

[33] M. Buson, H. Varum, and R. M. Sposto, “Viability Analysis of Using Cellulose Pulp Recycled from Cement Sacks in The Production of Compressed Earth Blocks,” *37th IAHS world Congr. Hous. Sci.*, 2010.

[34] M. Buson, N. Lopes, H. Varum, R. M. Sposto, and P. Vila Real, “Fire Resistance of Walls Made of Soil-Cement and Kraftterra Compressed Earth Blocks,” *Fire Mater.*, 2012.

[35] B. Taallah, A. Guettala, S. Guettala, and A. Kriker, “Mechanical Properties and Hygroscopicity Behavior of Compressed Earth Blocks Filled by Date Palm Fibers,” *Constr. Build. Mater.*, vol. 59, pp. 161–168, 2014.

[36] M. Mostafa and N. Uddin, “Effect of banana fibers on the compressive and flexural strength of compressed earth blocks,” *Buildings*, vol. 5, no. 1, pp. 282–296, 2015.

[37] E. O. Gapuz and J. M. C. Ongpeng, “Optimizing compressed earth blocks mix design incorporating rice straw and cement using artificial neural network,” *HNICEM 2017 - 9th Int. Conf. Humanoid, Nanotechnology, Inf. Technol. Commun. Control. Environ. Manag.*, pp. 1–6, 2017.

[38] K. Q. Tran, T. Satomi, and H. Takahashi, “Improvement of mechanical behavior of cemented soil reinforced with waste cornsilk fibers,” *Constr. Build. Mater.*, vol. 178, pp. 204–210, 2018.

[39] W. Acchar, J. B. Silva, V. M. Silva, L. C. Góis, and A. M. Segadães, “Incorporation of fired ceramic waste into binary and ternary earth-binder(s) mixtures for compressed blocks,” *Mater. Sci. Forum*, vol. 798–799, pp. 498–502, 2014.

[40] C. K. Subramaniaprasad, B. M. Abraham, and E. K. K. Nambiar, “Sorption characteristics of stabilised soil blocks embedded with waste plastic fibres,” *Constr. Build. Mater.*, vol. 63, pp. 25–32, 2014.

[41] C. K. Subramaniaprasad, B. M. Abraham, and E. K. Kunhanandan Nambiar, “Influence of embedded waste-plastic fibers on the improvement of the tensile strength of stabilized mud masonry blocks,” *J. Mater. Civ. Eng.*, vol. 27, no. 7, pp. 1–7, 2015.

[42] H. B. Nagaraj and C. Shreyasvi, “Compressed Stabilized Earth Blocks Using Iron Mine Spoil Waste - An Explorative Study,” *Procedia Eng.*, vol. 180, pp. 1203–1212, 2017.

[43] B. O. I. Standards, *IS 3495-Part 1: Methods of Tests of Burnt Clay Building Bricks*. New Delhi, India, 1992.

[44] B. O. I. Standards, *IS 1725: Specification for Soil Based Blocks Used in General Building Construction*. New Delhi, India, 2013.

[45] B. R. França *et al.*, "Durability of soil-Cement blocks with the incorporation of limestone residues from the processing of marble," *Mater. Res.*, vol. 21, pp. 1–6, 2018.

[46] C. Nepomuceno, "Use of Municipal Waste to Build Ecological Blocks," Master Thesis presented to Instituto Politécnico de Bragança, 2018.

[47] ABNT, *NBR 8491: Tijolo de solo-cimento - requisitos*. Rio de Janeiro, Brazil, 2012.

[48] AENOR, *UNE 41410: Bloque de tierra comprimida para muros y tabiques: Definiciones, especificaciones y métodos de ensayo*. Madrid, España, 2008.

[49] NABau, *DIN 18945: Lehmsteine - begriffe, anforderungen, prüfverfahren*. Berlin, Germany, 2013.

[50] ABNT, *NBR 13554: Solo-cimento - ensaio de durabildade por molhagem e secagem - método de ensaio*. Rio de Janeiro, Brazil, 2012.

[51] M. Ben Mansour, A. Jelidi, A. S. Cherif, and S. Ben Jabrallah, "Optimizing thermal and mechanical performance of compressed earth blocks (CEB)," *Constr. Build. Mater.*, vol. 104, pp. 44–51, 2016.

[52] L. Zhang, A. Gustavsen, B. Petter, L. Yang, T. Gao, and Y. Wang, "Thermal conductivity of cement stabilized earth blocks," *Constr. Build. Mater.*, vol. 151, pp. 504–511, 2017.

[53] M. Saidi, A. Soukaina, B. Zeghmati, and E. Sediki, "Stabilization effects on the thermal conductivity and sorption behavior of earth bricks," *Constr. Build. Mater.*, vol. 167, pp. 566–577, 2018.

[54] IUPAC, *Compendium of chemical terminology*, 2nd ed. International Union of Pure and Applied Chemistry, 1997.

[55] J. Kucerik, "Thermogravimetry," in *Encyclopedia of Geochemistry*, W. M. White, Ed. Springer, Cham, 2018, pp. 1–4.

[56] J. Ondruska, S. Csáki, I. Stubna, and V. Trnovcova, "Investigation of kaolin – quartz mixtures during heating using thermodilatometry and DC

thermoconductometry," *J. Therm. Anal. Calorim.*, vol. 2, pp. 833–838, 2020.

[57] J. Dweck *et al.*, "A comparative study of hydration kinetics of different cements by thermogravimetry on calcined mass basis," *J. Therm. Anal. Calorim.*, 2016.

[58] NP, *EN 954: Inertes para argamassas e betões. Determinação das massas volúmicas e da absorção de água das areias*. Lisboa, Portugal, 1973.

[59] MIBAL, "Minas de Barqueiros: Caolino MIB - A," 2019. [Online]. Available: http://www.mibal.pt/en/mibal-group/. [Accessed: 10-Dec-2019].

[60] LNEC, *E 239: Solos - análise granulométrica por peneiração húmida*. Lisboa, Portugal, 1970.

[61] NP, *EN 143: Determinação dos limites de consistência*. Lisboa, Portugal, 1969.

[62] AASHTO, *M 145-91: Standard specification for classification of soils ans soil-aggregate mixtures for highway construction purposes*. 2017.

[63] ASTM, *D 2487: Classification of soils for engineering purposes (unified soil classification system)*. 2000.

[64] LNEC, *E 197: Solos. Ensaio de compactação*. Lisboa, Portugal, 1966.

[65] SECIL, "Ficha de Produto," 2017. [Online]. Available: https://secilpro.com/produtos/nossos_produtos/cimento/cimento-composto-cem-ii. [Accessed: 10-Dec-2019].

[66] Standardization Administration of the People's Republic of China, *GB/T 208- Test Method for Determinging Cement Density*. Beijing, China, 2004.

[67] American Society for Testing and Materials, *ASTM C188-14: Standard Test Method for Density of Hydraulic Cement*. West Conshohocken, 2014.

[68] M. Helsel, C. Ferraris, and D. Bentz, "Comparative Study of Methods to Measure the Density of Cementitious Powders," *J. Test. Eval.*, vol. 44, no. 6, pp. 2147–2154, 2016.

[69] CEN, *EN 1363-1: Fire resistance tests. Part 1: General Requirements*. Bruxelles, 1999.

[70] CEN, *EN 1364-1: Fire resistance tests for non-loadbearing elements. Part 1: Walls.* Bruxelles, 1999.

[71] ISO, *834-1- International Organization for Standardization*. 1999.

[72] P. Ptáček, F. Frajkorová, F. Šoukal, and T. Opravil, "Kinetics and mechanism of three stages of thermal transformation of kaolinite to metakaolinite," *Powder Technol.*, vol. 264, pp. 439–445, 2014.

[73] R. L. Frost and A. M. Vassallo, "The dehydroxylation of the kaolinite clay minerals using infrared emission spectroscopy," *Clays Clay Miner.*, vol. 44, no. 5, pp. 635–651, 1996.

[74] J. Dweck, M. B. M. Melchert, M. M. Viana, F. K. Cartledge, and P. M. Büchler, "Importance of quantitative thermogravimetry on initial cement mass basis to evaluate the hydration of cement pastes and mortars," *J. Therm. Anal. Calorim.*, vol. 113, no. 3, pp. 1481–1490, 2013.

[75] R. Sersale, *Aspects of the Chemistry of Additions*. Pergamon Press Ltd., 1983.

[76] H. F. W. Taylor, *Cement Chemistry*, 2nd ed. London: Thomas Telford, 1990.

[77] J. Dweck, A. L. Cherem Da Cunha, C. A. Pinto, J. Pereira Gonçalves, and P. M. Büchler, "Thermogravimetry on calcined mass basis - Hydrated cement phases and pozzolanic activity quantitative analysis," *J. Therm. Anal. Calorim.*, vol. 97, no. 1, pp. 85–89, 2009.

[78] S. E. Gustafsson, "Transient plane source techniques for thermal conductivity and thermal diffusivity measurements of solid materials," *Rev. Sci. Instrum.*, vol. 62, no. 3, pp. 797–804, 1991.

[79] P. Koniorczyk, J. Zmywaczyk, and M. Wielgosz, "Step-wise transient method for analysis of thermal properties of materials part 1. Theoretical considerations," *Thermochim. Acta*, vol. 682, no. August, p. 178429, 2019.

[80] V. Bohac, M. K. Gustavsson, L. Kubicar, and S. E. Gustafsson, "Parameter estimations for measurements of thermal transport properties with the hot disk thermal constants analyzer," *Rev. Sci. Instrum.*, vol. 71, no. 6, pp. 2452–2455, 2000.

[81] HotDisk, "Kapton Sensors2," 2020. [Online]. Available: https://www.hotdiskinstruments.com/products-services/sensors/kapton-sensors/. [Accessed: 17-Jan-2020].

[82] S. A. Al-Ajlan, “Measurements of thermal properties of insulation materials by using transient plane source technique,” *Appl. Therm. Eng.*, vol. 26, no. 17–18, pp. 2184–2191, 2006.

[83] U. Hammerschmidt, “Guarded Hot-Plate (GHP) Method: Uncertainty Assessment,” *Int. J. Thermophys.*, vol. 23, no. 6, pp. 1551–1570, 2002.

[84] “Ansys® Academic Research Mechanical, Release 20.1.” .

[85] CEN, *EN1992-1-2 Eurocode 2: Design of Concrete Structures. Part 1.2: General Rules, Structural Fire Design*. Belgium: European Committee for Standardization, 2010.

[86] D. M. Ferreira, A. Araújo, E. M. M. Fonseca, P. A. G. Piloto, and J. Pinto, “Behaviour of non-loadbearing tabique wall subjected to fire – Experimental and numerical analysis,” *J. Build. Eng.*, vol. 9, no. November 2016, pp. 164–176, 2017.

[87] H. W. Russel, “Principles of heat flow in porous insulators,” *J. Ceram. Soc.*, vol. 18, pp. 1–12, 1935.

[88] Y. Çengel, *Introduction to thermodynamics and heat transfer*. Boston: Irwin - McGraw - Hill, 1997.

[89] LR Glicksman, “Heat Transfer in foams,” in *Low density cellular plastics: Physical basis of beahviour*, Netherlands: Springer, 1994, pp. 104–152.

[90] M. Capitelli, G. Colonna, C. Gorse, and A. D ’angola, “Transport properties of high temperature air in local thermodynamic equilibrium,” *Eur. Phys. J. D*, vol. 11, pp. 279–289, 2000.

[91] “Ansys® Fluent, Release 20.1.” .

[92] *Ansys Fluent ® - User’s Guidebook Release 20.1*. 2020.

[93] M. Martínez, N. Huygen, J. Sanders, and S. Atamturktur, “Thermo-fluid dynamic analysis of concrete masonry units via experimental testing and numerical modeling,” *J. Build. Eng.*, vol. 19, no. April, pp. 80–90, 2018.

[94] H. D. Ab, “Hot Disk Thermal Constants Analyser Instruction Manual,” 2015. [Online]. Available: https://www.hotdiskinstruments.com/products-services/sensors/kapton-sensors/.

[95] H. D. Ab, “Hot Disk Thermal Constants Analyser Instruction Manual,” 2015.

ANNEX A – COMPACTION OF THE BLOCKS

The CEBs were manufactured as described on section 3.2. Table 18 presents the maximum load and the compaction pressure of each one of the blocks. The maximum load refers to the loading presented on the screen of the mechanical press at the moment the blocks attained the displacement used as stopping criterion. Then, the compaction pressure was calculated by the ratio between the maximum load and the surface area of the blocks (227.2738 cm^2).

Table 18: Compaction pressure of the CEBs.

Block Number	Maximum Load [kN]	Compaction Pressure [Mpa]
1	103	4.53
2	100	4.40
3	101	4.44
4	101	4.44
5	120	5.28
6	124	5.46
7	105	4.62
8	102	4.49
9	108	4.75
10	129	5.68
11	88	3.87
12	111	4.88
13	110	4.84
14	112	4.93
15	98	4.31
16	105	4.62
17	108	4.75
18	110	4.84
19	113	4.97
20	104	4.58
21	118	5.19
22	108	4.75
23	110	4.84
24	113	4.97
25	109	4.80
26	107	4.71
27	115	5.06
28	114	5.02
29	107	4.71
30	116	5.10
31	113	4.97
32	105	4.62
33	115	5.06
34	111	4.88
35	113	4.97
36	106	4.66
37	116	5.10
38	108	4.75
39	110	4.84
40	106	4.66
41	112	4.93
42	108	4.75
43	109	4.80
44	108	4.75
45	103	4.53
46	104	4.58
47	102	4.49
48	117	5.15
49	110	4.84
50	112	4.93
Average	**109.14**	**4.80**
Standard Deviation	**6.72**	**0.30**

ANNEX B – TPS Results

Table 19 and Table 20 present the complete results obtained on the Transient Plane Source tests. In order to obtain accurate results, as stablished on the Hot Disk Thermal Constants Analyzer Manual, the sensor used (Kepton sensor nº 5501) was chosen observing that the thermal penetration depth values shall be inside the interval of the radius (6.403 mm) and diameter (12.806 mm) of the sensor. The probing depth set on the tests consists on the minimum distance from the sensor to the boundary surfaces of the specimens, and shall never be smaller than the penetration depth of the heat flux [94]. These criteria were observed and attained on all the executed tests.

Other important aspects observed on the execution of the tests consisted on the Output Power and the Measurement Time used on the settings. These parameters are directly related to the total temperature increase on the specimens, which shall not be lower than 1 K and higher than 8 K, and also on the penetration depth of the heat flux mentioned above [79], [95]. Therefore, the Output Power used on all tests was of 0.1 W and the Measurement Time set for 20 s.

From Table 19 and Table 20, one can see that for each set of specimens three tests were conducted. The relaxation time (which means the time between repeated experiments) was determined according to the Hot Disk Thermal Constants Analyzer Manual, which stablishes that when the probing depth considerations are followed, it should be equal to 36 times the duration of the transient recording (20 s for this case), which resulted on 1200 s between repeated tests [95].

Table 19: Complete TPS results for specimens without incorporated waste.

Spec. Below	Spec. Upper	Test nº	*Th.Conduc. [W/mK]*	*Th.Diff. [mm²/s]*	*Spec.Heat [MJ/m³K]*	*Pr.Depth [mm]*	*Temp.Incr.*	*Total/Temp.Incr.*	*Total/Char.Time*	*Time Corr.*	*Mean Dev. [K]*	*Disk Resistance [Ω]*
SC03a	SC03b	Test1	1.934	1.157	1.671	9.20	0.235 K	1.85 K	0.516	0.0995 s	1.033E-4	12.527075
SC03a	SC03b	Test2	1.848	1.172	1.576	9.26	0.245 K	1.66 K	0.523	0.0982 s	9.570E-5	12.531493
SC03a	SC03b	Test3	1.915	1.131	1.693	9.30	0.228 K	2.00 K	0.526	0.0987 s	8.181E-5	12.519338
SC03a	SC03c	Test1	1.823	1.103	1.653	9.13	0.266 K	1.91 K	0.508	0.0979 s	8.554E-5	12.522533
SC03a	SC03c	Test2	1.848	1.151	1.606	9.33	0.263 K	1.91 K	0.530	0.0966 s	9.681E-5	12.523504
SC03a	SC03c	Test3	1.859	1.167	1.593	9.16	0.231 K	1.90 K	0.512	0.0967 s	8.643E-5	12.523185
SC03b	SC03c	Test1	1.804	1.173	1.538	9.32	0.267 K	1.68 K	0.529	0.0520 s	6.833E-5	12.527532
SC03b	SC03c	Test2	1.818	1.178	1.544	9.34	0.292 K	1.69 K	0.531	0.0976 s	7.933E-5	12.528411
SC03b	SC03c	Test3	1.817	1.182	1.536	9.30	0.261 K	1.67 K	0.527	0.0828 s	6.928E-5	12.527441
SC04a	SC04b	Test1	1.786	1.330	1.343	10.32	0.252 K	3.12 K	0.648	0.0974 s	1.125E-4	12.516603
SC04a	SC04b	Test2	1.784	1.280	1.394	10.07	0.215 K	3.11 K	0.617	0.0987 s	9.301E-5	12.516313
SC04a	SC04b	Test3	1.772	1.272	1.393	9.86	0.236 K	3.06 K	0.592	0.0995 s	1.280E-4	12.513487
SC04a	SC04c	Test1	1.760	1.229	1.432	9.69	0.221 K	3.07 K	0.572	0.1000 s	1.005E-4	12.512868
SC04a	SC04c	Test2	1.731	1.197	1.446	9.56	0.246 K	3.55 K	0.557	0.1000 s	1.636E-4	12.528189
SC04a	SC04c	Test3	1.727	1.201	1.438	9.58	0.246 K	3.52 K	0.559	0.0979 s	1.603E-4	12.531132
SC04a	SC04d	Test1	1.696	1.342	1.264	10.13	0.251 K	3.04 K	0.625	0.000192 s	2.540E-4	12.538154
SC04a	SC04d	Test2	1.728	1.239	1.395	9.73	0.242 K	3.06 K	0.577	0.0992 s	1.435E-4	12.538860
SC04a	SC04d	Test3	1.728	1.248	1.385	9.76	0.257 K	3.06 K	0.580	0.1000 s	1.145E-4	12.541703
SC04b	SC04c	Test1	1.609	1.161	1.386	9.64	0.270 K	4.57 K	0.566	0.1000 s	1.837E-4	12.555616
SC04b	SC04c	Test2	1.633	1.167	1.399	9.59	0.248 K	4.60 K	0.560	0.1000 s	1.427E-4	12.554919
SC04b	SC04c	Test3	1.633	1.176	1.388	9.46	0.241 K	4.65 K	0.545	0.0992 s	1.491E-4	12.556176
SC04b	SC04d	Test1	1.768	1.258	1.406	9.78	0.239 K	3.07 K	0.582	0.1000 s	1.619E-4	12.557173
SC04b	SC04d	Test2	1.777	1.292	1.375	9.91	0.241 K	3.10 K	0.598	0.0990 s	1.281E-4	12.559573
SC04b	SC04d	Test3	1.790	1.283	1.395	9.88	0.233 K	3.06 K	0.594	0.1000 s	1.449E-4	12.561916
SC04c	SC04d	Test1	1.759	1.099	1.601	9.14	0.281 K	2.15 K	0.509	0.0967 s	1.009E-4	12.578909
SC04c	SC04d	Test2	1.778	1.126	1.578	9.25	0.271 K	2.16 K	0.521	0.0992 s	7.664E-5	12.577958
SC04c	SC04d	Test3	1.784	1.124	1.588	9.24	0.282 K	2.16 K	0.520	0.1000 s	1.119E-4	12.579585
Average:			**1.774**	**1.202**	**1.482**							
Standard Deviation:			**0.077**	**0.068**	**0.115**							

Table 20: Complete TPS results for specimens with incorporated waste.

Spec. Below	Spec. Upper	Test nº	*Th.Conduc. [W/mK]*	*Th.Diff. [mm²/s]*	*Spec.Heat [MJ/m³K]*	*Pr.Depth [mm]*	*Temp.Incr.*	*Total/Temp.Incr.*	*Total/Char.Time*	*Time Corr.*	*Mean Dev. [K]*	*Disk Resistance [Ω]*
SCR01a	SCR01b	Test1	1.437	1.055	1.362	9.19	0.296 K	3.12 K	0.514	0.1000 s	1.211E-4	12.579439
SCR01a	SCR01b	Test2	1.444	1.059	1.364	9.20	0.311 K	3.13 K	0.516	0.1000 s	1.455E-4	12.581608
SCR01a	SCR01b	Test3	1.446	1.073	1.348	9.26	0.311 K	3.14 K	0.523	0.0962 s	1.216E-4	12.582762
SCR01b	SCR01c	Test1	1.370	1.045	1.310	9.15	0.264 K	6.10 K	0.509	0.1000 s	1.488E-4	12.583088
SCR01b	SCR01c	Test2	1.379	1.101	1.253	9.38	0.290 K	6.06 K	0.536	0.0984 s	2.347E-4	12.585825
SCR01b	SCR01c	Test3	1.378	1.091	1.263	9.34	0.278 K	6.06 K	0.532	0.0984 s	2.428E-4	12.585865
SCR01a	SCR01c	Test1	1.404	1.024	1.371	9.05	0.323 K	3.02 K	0.499	0.0987 s	1.316E-4	12.598548
SCR01a	SCR01c	Test2	1.416	1.034	1.369	9.09	0.292 K	3.03 K	0.504	0.1000 s	1.270E-4	12.599397
SCR01a	SCR01c	Test3	1.422	1.036	1.373	9.10	0.302 K	3.03 K	0.505	0.0984 s	1.151E-4	12.600924
SCR02a	SCR04b	Test1	1.463	0.972	1.506	8.82	0.298 K	3.13 K	0.474	0.0997 s	1.685E-4	12.549450
SCR02a	SCR04b	Test2	1.488	0.998	1.490	8.94	0.270 K	3.11 K	0.486	0.0997 s	1.227E-4	12.554274
SCR02a	SCR04b	Test3	1.492	1.007	1.481	8.98	0.262 K	3.11 K	0.491	0.0997 s	9.903E-5	12.556118
SCR02a	SCR04c	Test1	1.350	1.082	1.248	9.12	0.305 K	5.83 K	0.506	0.1000 s	2.277E-4	12.561338
SCR02a	SCR04c	Test2	1.244	1.073	1.159	8.96	0.321 K	5.33 K	0.489	0.0987 s	1.604E-4	12.564483
SCR02a	SCR04c	Test3	1.289	1.193	1.081	9.27	0.304 K	6.01 K	0.523	0.1000 s	1.539E-4	12.571764
SCR02a	SCR04d	Test1	1.434	1.082	1.326	9.30	0.299 K	5.30 K	0.527	0.097871 s	1.683E-4	12.577976
SCR02a	SCR04d	Test2	1.442	1.092	1.321	9.35	0.297 K	5.37 K	0.532	0.1000 s	1.874E-4	12.576009
SCR02a	SCR04d	Test3	1.451	1.073	1.352	9.27	0.268 K	5.37 K	0.523	0.0987 s	1.435E-4	12.578540
SCR02b	SCR04c	Test2	1.229	1.048	1.172	9.16	0.357 K	5.23 K	0.511	0.1000 s	1.111E-4	12.583677
SCR02b	SCR04c	Test2	1.318	1.288	1.023	10.15	0.367 K	5.36 K	0.628	0.0008 s	5.971E-4	12.585465
SCR02b	SCR04c	Test3	1.298	0.957	1.356	8.75	0.362 K	5.42 K	0.466	0.0000 s	4.425E-4	12.585513
SCR02b	SCR04d	Test1	1.334	1.077	1.238	9.28	0.317 K	5.36 K	0.525	0.1000 s	1.715E-4	12.590877
SCR02b	SCR04d	Test2	1.347	1.106	1.219	9.40	0.323 K	5.42 K	0.539	0.1000 s	1.442E-4	12.589975
SCR02b	SCR04d	Test3	1.342	1.106	1.214	9.29	0.332 K	5.40 K	0.525	0.1000 s	1.428E-4	12.590072
SCR02c	SCR04d	Test1	1.343	1.081	1.243	9.18	0.320 K	3.40 K	0.513	0.0992 s	1.380E-4	12.596131
SCR02c	SCR04d	Test2	1.355	1.120	1.210	9.35	0.346 K	3.42 K	0.532	0.1000 s	1.284E-4	12.596986
SCR02c	SCR04d	Test3	1.356	1.122	1.209	9.35	0.340 K	3.45 K	0.533	0.1000 s	1.280E-4	12.596448
Average:			**1.380**	**1.074**	**1.291**							
Standard Deviation:			**0.070**	**0.065**	**0.115**							

ANNEX C – GHP Results

Table 21 and Table 22 present the complete results obtained on the Guarded Hot Plate tests for the specimens with and without incorporated waste. As described on section 3.5.3, the obtained results do not comply with the data found on bibliographic research nor with the TPS results. In order to obtain accurate results, the specimens require more precision on their manufacture.

Table 21: Complete GHP results for specimens without incorporated waste.

Specimen/Test	Temp (ºC)	ΔT [ºC]	Thermal Conductivity [W/mK]
SC02_Test5	-10	10	0.5482
SC02-Test3	-10	15	0.5139
SC02-Test3	0	10	0.5440
SC02-Test4	0	10	0.6141
SC02-Test3	10	15	0.5717
SC02-Test4	10	15	0.6411
SC03-Test1	10	5	0.6673
SC04-Test1	10	5	0.7646
SC02_Test5	20	10	0.6341
SC02_Test1	20	15	0.5934
SC02_Test2	20	15	0.5852
SC02-Test4	20	15	0.6646
SC03-Test1	20	5	0.7293
SC04-Test1	20	5	0.8196
SC02_Test5	30	15	0.7341
SC02_Test2	30	15	0.6298
SC02_Test1	40	15	0.7024
SC02_Test2	40	15	0.7501
SC02_Test5	50	10	0.8000
SC04-Test1	50	5	1.0640

Table 22: Complete GHP results for specimens with incorporated waste.

Specimen/Test	Temp (ºC)	ΔT [ºC]	Thermal Conductivity [W/mK]
SCR01_Test1	-10	5	0.4761
SCR02_Test1	-10	5	0.4867
SCR03-Test2	0	10	0.6180
SCR04_Test1	0	15	0.4764
SCR03-Test1	10	15	0.6321
SCR04_Test1	10	15	0.5016
SCR01_Test1	20	5	0.5477
SCR02_Test1	20	5	0.5834
SCR03-Test1	20	15	0.6653
SCR04_Test1	20	15	0.5297
SCR03-Test1	30	15	0.7175
SCR04_Test2	30	15	0.5661
SCR05_Test1	30	15	0.7155
SCR03-Test2	40	15	0.7716
SCR04_Test2	40	15	0.6027
SCR05_Test1	40	15	0.7785
SCR01_Test1	50	5	0.7411
SCR02_Test1	50	5	0.7801
SCR03-Test2	50	15	0.8001
SCR04_Test2	50	15	0.6478
SCR05_Test1	50	15	0.8435